Exploring the Role of Electrolytes in High Energy Alkali Metal Batteries

by

Abhinandan Shyamsunder

A thesis

presented to the University of Waterloo

in fulfillment of the

thesis requirement for the degree of

Master of Science

in

Chemistry

Waterloo, Ontario, Canada, 2016

AUTHOR'S DECLARATION

I hereby declare that I am the sole author of this thesis. This is a true copy of the thesis, including any required final revisions, as accepted by my examiners.

I understand that my thesis may be made electronically available to the public.

_____

Abhinandan Shyamsunder

Abstract

With the increasing importance of electrified transport, the need for high energy density storage is also increasing. Possible candidates include Li-O_2, Na-O_2 and Li-S batteries. One of the major components of all three battery types described is the electrolyte. The electrolyte dictates many of the electrochemical properties. In this thesis, the role of electrolytes in these battery types are examined; modifications are introduced and the resulting properties are extensively studied.

In **Chapter 3**, the decomposition of glyme based electrolytes in Na-O_2 batteries is studied, and a mechanism for the formation of high amounts of sodium acetate that are observed in the cell is proposed. This mechanism is the first to provide a reasonable explanation for the presence of the acetate side product in higher order glyme solvents but not the monoglyme (1,2-dimethoxyethane).

In **Chapter 4**, the decomposition of commonly used electrolyte solvents for Li- and Na-O_2 batteries are studied, and new electrolyte solvents are synthesised with an approach directed at overcoming the various drawbacks that the previously investigated solvents exhibit.

In **Chapter 5**, the parasitic polysulphide shuttle in Li-S batteries which hinders their function through reduced coulombic efficiency is discussed, and a new approach based on combining a low-ion pairing salt and novel sulphonamide solvent is developed. Utilized-in a Li-S cell, this electrolyte system exhibits almost 100% coulombic efficiency in the absence of lithium nitrate as an additive, and capacities of 900 mAh/g at 50 ˚C are achieved.

Acknowledgements

I would like to extend my sincerest gratitude to my supervisors Dr. Linda Nazar and Dr. Graham Murphy for their guidance and support throughout the course of this masters program. I am also happy that I have had an opportunity to work with all members of the Nazar and Murphy labs both past and present. I would also like to thank my committee members Dr. Scott Taylor and Dr. Vivek Maheshwari for taking time to discuss my research and findings.

I would like to thank Dr. Robert Black for his guidance and providing me with a publication next to my name, and also for all the help with carrying out the mass spectrometry experiments mentioned in **Chapter 3**.

I extend my gratitude to Dr. J. Michael Chong who although was not on my committee, assisted me with the many questions and challenges pertaining to organic chemistry.

I would like to make a special mention to Jason Tao and Keith Coffey who helped me with many ideas when I was struggling to get a working electrolyte solvent for the Li-O_2 batteries.

I would like to thank the non-teaching and administrative staff of the chemistry department for helping me out whenever needed, and making my transition into a new country smooth.

I would also like to thank Richard Tran for helping me compile this thesis in a coherent manner.

Table of Contents

List of Figures

List of Tables and Schemes

Chapter 1: Introduction

1.1 Overview of rechargeable batteries:

The rapid increase of the earth's population has resulted in an increased demand for fossil fuel energy over the last few decades. Energy demands are projected to double in the next fifteen years as nations around the world strive for a common level of development and infrastructure.[1] Oil, coal and natural gas have been extensively used to power automobiles, power plants and factories, causing a dramatic build-up of greenhouse gases in the atmosphere.[2] Thus we need to adopt a transition from fossil fuels towards batteries, as it would be a big step towards saving our environment. Such a transition is underway with a more widespread incursion of hybrid electric vehicles into the marketplace and with plug-in hybrid and fully electric vehicles starting to make their mark.[3]

However, battery chemistry has not been able to match the energy requirements of pure electric vehicles. In order to make electric and hybrid electric vehicles more practical, the development of high energy density storage batteries is required. Battery chemistries that do not operate on the basis of intercalation chemistries (Li-ion batteries), such as lithium/sodium air batteries or lithium sulphur batteries are amongst those which offer the possibilities in achieving these goals.

1.2 Lithium air batteries

Lithium oxygen (Li-O_2) or lithium air (Li-air) batteries were first introduced in 1970 for automotive transportation, but have garnered more popularity only in the last ten years.[4-8] The increased attention derives from the high energy density of Li-O_2 batteries (up to 2-3 $kWhkg^{-1}$), which is theoretically much higher compared to that of other rechargeable systems. Furthermore its cell configuration uses oxygen as the reactant at the positive electrode (cathode), so only the product and conductive cathode support is housed on board.[9-15]

There are currently four types of Li-O_2 batteries under investigation designated by the type of electrolyte used. All four make use of a lithium metal anode and a porous oxygen diffusion cathode with lithium salts dissolved in: (i) non-aqueous aprotic solvents, (ii) aqueous solvents, or (iii) hybrid non-aqueous/aqueous solvents. A fourth configuration (iv) utilizes solid-state Li ion conducting electrolytes. The chemistry at the oxygen cathode differs depending on the electrolyte. The reactions in the aqueous and hybrid systems are identical since the cathode is exposed to aqueous electrolyte in both, and although not as widely studied, the solid-state type Li-O_2 battery functions similarly to the non-aqueous system. The work in this thesis is limited to the non-aqueous aprotic type of Li-O_2 battery.

The battery operates on two major processes, the ORR (oxygen reduction reaction) and the OER (oxygen evolution reaction). On discharge, oxygen from the atmosphere is reduced at the cathode and combines with Li^+ to form Li_2O_2 (the oxygen reduction reaction or ORR): $2Li^+ + O_2 \rightarrow Li_2O_2$ (**Figure 1.1**). The peroxide is stored within the voids of a porous carbon black (or other lightweight inert, conductive material) that act as a membrane and support.

On charge, the lithium peroxide is converted back to Li and O_2 (oxygen evolution reaction; OER). A recent report based on online electrochemical mass spectroscopy[16](OEMS) showing that O_2 is indeed released by oxidation of Li_2O_2 invoked more interest in the Li-O_2 battery studies.

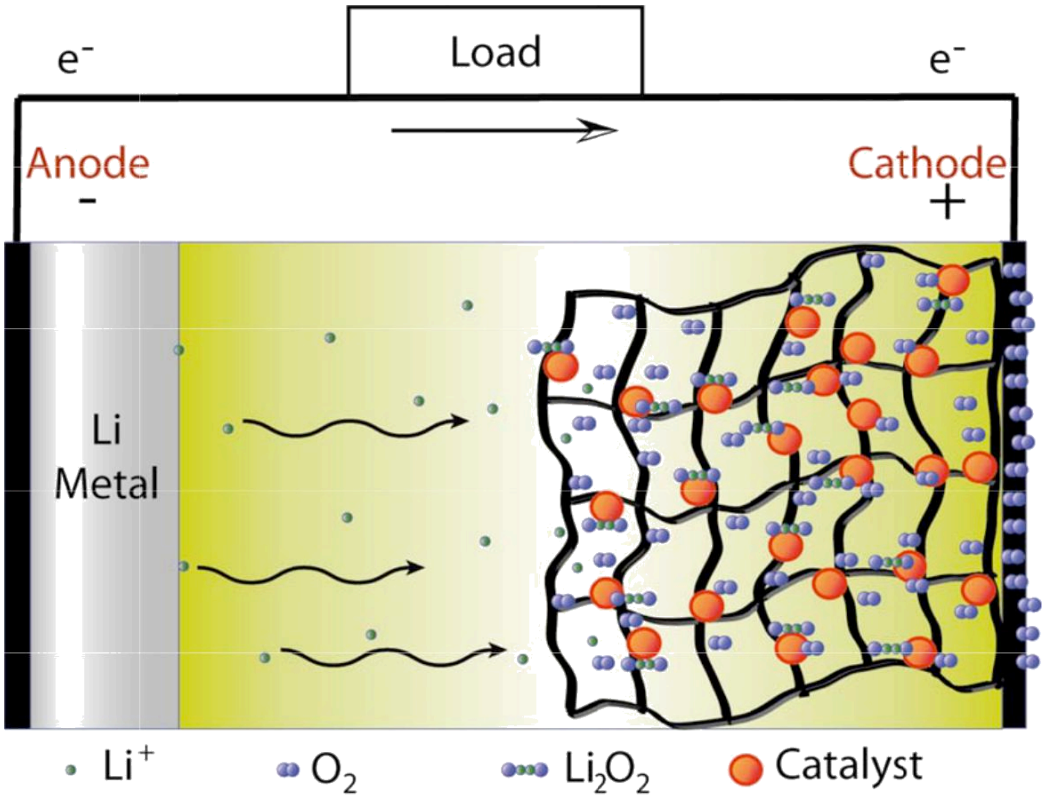

Figure 1.1 Systematic operation of the non-aqueous Li-O_2 cell during discharge.[4] The porous cathode is exposed to a source of oxygen and the spontaneous reaction of $2Li^+ + O_2 \rightarrow Li_2O_2$ occurs, accompanied by flow of electrons in the external circuit. The reverse occurs on charge.

1.2.1 ORR and OER Reactions in Non-Aqueous Media

The possible reactions in the non-aqueous Li-O_2 cell, which occur at the cathode via a series of oxygen reduction processes, are described below:[17]

$$O_2 + Li^+ + e^- \rightarrow LiO_2 \qquad (1\text{-}1)$$

$$2LiO_2 \rightarrow Li_2O_2 + O_2 \qquad \text{(Chemical Process)} \qquad (1\text{-}2)$$

$$LiO_2 + Li^+ + e^- \rightarrow Li_2O_2 \qquad (1\text{-}3)$$

$$Li_2O_2 + 2Li^+ + 2e^- \rightarrow 2Li_2O \qquad (1\text{-}4)$$

Theoretically speaking, Li_2O_2 ($E° = 2.96$ V) and Li_2O ($E° = 2.91$ V) are both possible discharge products of the Li-O_2 cell, but Li_2O_2 is the reaction product observed in practice for voltage cut-offs above 2.0V.[18-20] This product can be decomposed electrochemically ($Li_2O_2 \rightarrow 2Li^+ + 2e^- + O_2$), allowing for rechargeability of the non-aqueous Li-O_2 cell. However it will later be explained that the reactivity of the electrolyte will play a very important role in the impact of both OER and ORR.

OER refers to the electrochemical decomposition of solid lithium oxide products formed during discharge of the cell, and could be either four or two electron processes, or one that has as its first step the formation of "a superoxide-like species":

$$2Li_2O \rightarrow O_2 + 4Li^+ + 4e^- \qquad (1\text{-}5)$$

$$Li_2O_2 \rightarrow O_2 + 2Li^+ + 2e^- \qquad (1\text{-}6)$$

$$Li_2O_2 \rightarrow Li_{2-x}O_2 + xLi^+ + xe^- \qquad (1\text{-}7)$$

Li_2O has very rarely been observed,[18] with the main discharge product in a Li-O_2 cell being Li_2O_2,[21] which can be electrochemically decomposed. Reaction 1-6 (or 1-7) remains challenging and the exact mechanism is still up for debate, although it is most likely dependent on both solvent and the morphology of the solid Li_2O_2. Compared to the ORR process, OER for the Li-O_2 cell has not been studied as intensively.

The mechanisms of the Li-O_2 discharge and charge reactions were elucidated in acetonitrile on a gold electrode.[22] It was found that the discharge process occurs through an electrochemical-chemical (ECC) mechanism, with the initial electrochemical step ($O_2 + e^- \rightarrow O_2^{\bullet-}$) being followed by two chemical steps ($O_2^{\bullet-} + Li^+ \rightarrow LiO_2$ and $2LiO_2 \rightarrow Li_2O_2 + O_2$). The charge reaction was suggested to occur *via* direct electrochemical oxidation of Li_2O_2 (equation 1-6) because any formation of superoxide (reaction 1-7) was expected to decompose the propylene carbonate electrolyte that was used, however no decomposition was detected. In acetonitrile, the oxidation of LiO_2 occurs at approximately 3.5 V and Li_2O_2 at around 3.75 V vs. Li/Li^+, so LiO_2 is not expected to be an intermediate in the oxidation process of Li_2O_2 since it would be unstable at the higher potential. In contrast, theoretical calculations have determined that decomposition starts with the removal of lithium to form a superoxide, and that the kinetic rate of OER is highly dependent on surface orientation.[23] Based on this, a lithium deficient species could be an intermediate of the OER process by reaction (1-7).

1.2.2 Influence of electrolyte on the performance of the Li-O_2 battery

The choice of organic solvent is perhaps the most important factor in the performance and development of non-aqueous Li-O_2 cells. A good electrolyte should possess the

following qualities: good stability against $O_2^{\bullet-}$ attack; a wide potential window to withstand both high oxidation potentials and be stable to reaction with metallic lithium; low viscosity; low volatility; and high oxygen solubility.

Reaction with the highly reactive radical species ($O_2^{\bullet-}$, LiO_2) to form decomposition products is especially problematic for alkyl carbonate electrolytes. They are highly subject to nucleophilic attack of the superoxide radical ($O_2^{\bullet-}$),[21] the initial product formed from the oxygen reduction reaction (ORR). Their instability was made apparent by Mizuno *et al.*[24] and Freunberger *et al.*,[25] who demonstrated that the cycling performance associated with Li-O_2 cells utilizing carbonate based electrolytes were primarily due to oxidation of the decomposition products of the electrolyte on charge, and not Li_2O_2 (**Figure 1.2**). Experimental studies using chemically generated superoxide to probe its reactivity with different solvents confirm the high reactivity of propylene carbonate, and indicate that ethers are relatively stable.[26] This is also supported by theoretical studies using DFT that show that ethers are more stable to the oxygen reduction products,[27,28] however, behaviour in an actual cell, especially on charge at high potential in the presence of lithium peroxide, may be different and further investigation is necessary. The importance of electrolyte stability cannot be overstated, since this governs the nature of both the ORR and OER processes. This is currently the most challenging hurdle that must be overcome before any other component of the Li-O_2 cell (catalyst, cathode, etc.) can be properly evaluated.

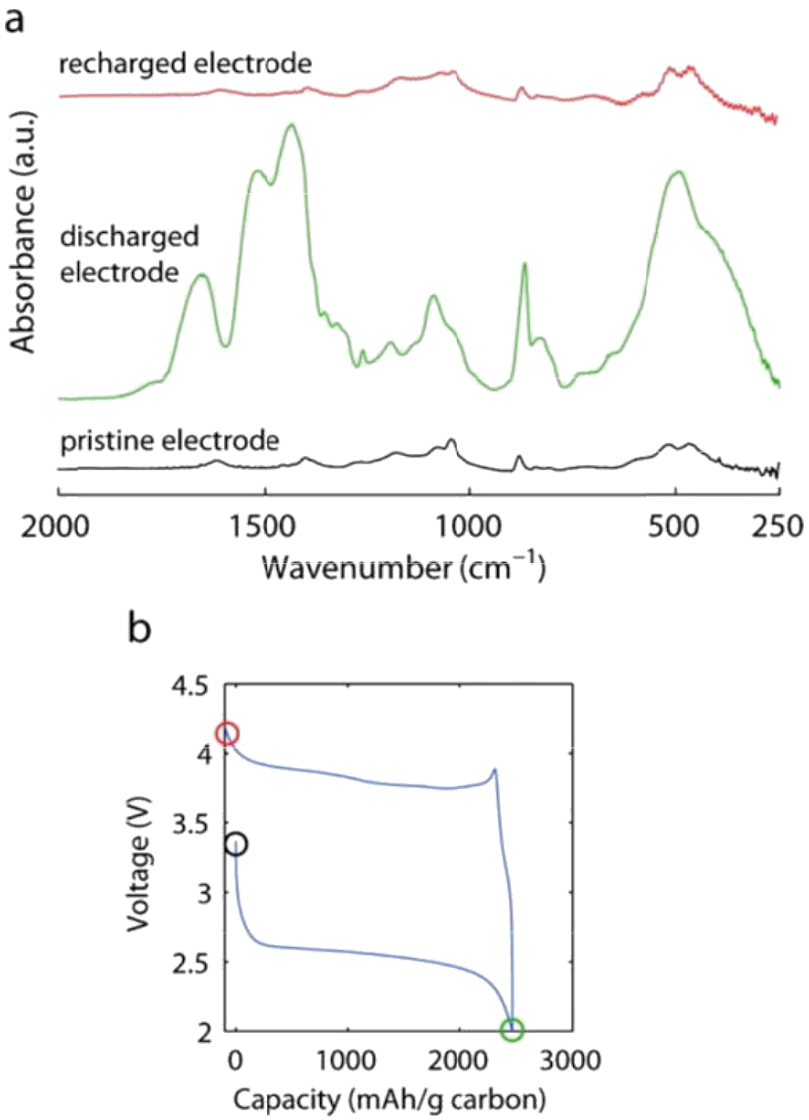

Figure 1.2 (a) FTIR spectra of a pristine electrode (Super P/ α-MnO_2/Kynar) and after the first discharge, then charge in 1 M $LiPF_6$ in PC under O_2. (b) Variation of voltage as cell is discharged then charged. The FTIR data in (a) show the spectra from the pristine electrode and the electrode after one cycle are identical, indicating that the products of electrolyte

decomposition that are formed on discharge (namely $C_3H_6(OCO_2Li)_2$, Li_2CO_3, HCO_2Li and CH_3CO_2Li) are oxidized on charging to 4.2 V as shown in the electrochemical curve in (b).[25]

It has been shown that ether-based electrolytes form Li_2O_2 upon discharge.[29] 1,2-dimethoxyethane (DME) and tetraethylene glycol dimethyl ether (TEGDME) have both been used successfully as solvents to form the desired Li_2O_2 product during discharge.[30,31] While TEGDME is far more stable to $O_2^{\bullet-}$ attack than carbonate-based electrolytes, Freunberger *et al.*[32] have observed some decomposition which resulted in a combination of Li_2CO_3, HCO_2Li, CH_3CO_2Li, polyethers/esters, CO_2, and H_2O in addition to Li_2O_2. The amount of Li_2O_2 formed on the first discharge diminishes after repeated cycling in favour of greater electrolyte decomposition. A recent study that compared PC:DME and DME as solvents suggests that although catalysts aid in lowering the charging overpotential when PC:DME is used as the solvent, the overpotential is identical among the chosen catalysts when DME alone is the solvent.[31]

The major results of this study are shown in **Figure 1.3**. The use of OEMS coupled to galvanostatic cycling of the Li-O_2 cells proved to be a very powerful tool to analyze gas evolution during charging. This work verified that of Lu *et al.*[33]who showed that when PC:DME was used as the electrolyte solvent, Au (and Pt) catalyze ORR and Pt catalyzes OER. However, it also shows that large amounts of CO_2 is produced from the oxidation of lithium alkyl carbonates. In DME, only Pt shows catalytic activity for ORR, yet it decomposes the electrolyte upon charge. This suggests that Li_2CO_3 oxidation can be catalyzed, but Li_2O_2 oxidation cannot. It is possible however, that carbon itself is better at catalyzing the OER from Li_2O_2 than the chosen catalysts of their study.

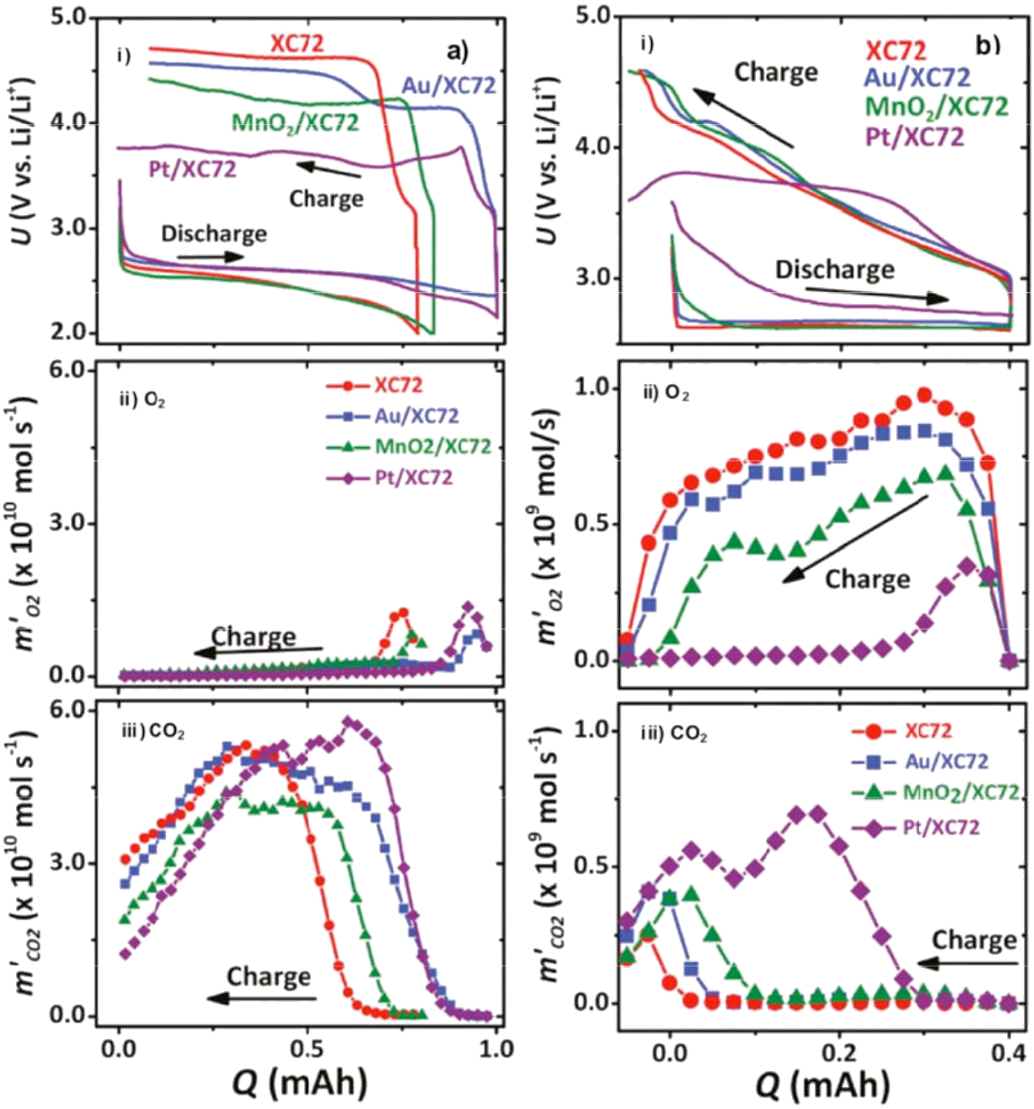

Figure 1.3 Gas evolution from cells employing a) PC:DME and b) DME. i) Discharge-charge voltage curves, and corresponding ii) O_2 and iii) CO_2 evolution during charging of

cells using various cathode catalysts. m'_i is the molar generation of species "i", U is cell output voltage, and Q is cell charge.[31]

Apart from electrolyte decomposition, a few defining electrolyte properties have a very large impact on the ORR process. Solvents that possess characteristics of high oxygen solubility, high ionic conductivity, and low viscosity are optimal. Electrolytes with these characteristics show increased discharge capacity due to a higher concentration of oxygen in solution, as well as improved ORR kinetics due to improved oxygen diffusion.[29] While these studies were performed in carbonate based electrolytes, the knowledge gained from these studies still applies to new electrolytes that are being investigated today. The applicability of ionic liquids, for example, is under investigation. To date, their high viscosity and poor oxygen diffusion has been shown to negatively affect the ORR process.[29] However, other important factors for Li-O_2 cells, such as hydrophobicity (to prevent water from reaching the Li-metal anode) and low volatility to prevent evaporation, are properties of ionic liquids that makes them appealing.[34,35]

Beyond the glyme electrolytes, solvents such as amides have been examined. Giordiani *et al.* [35-37] have studied lithium nitrate in dimethyl acetamide ($LiNO_3$/DMA) electrolyte. DMA is unstable in the presence of metallic lithium, yet the report claims it is stable against attack by superoxide. In this case the lithium nitrate acts to passivate the lithium negative electrode through a synergistic mechanism with oxygen in the electrolyte. However, the work by Chen *et al.*[37] clearly shows that while amides, including DMA and dimethylformamide (DMF), are more stable than the family of glymes and ethers, they are still subject to superoxide attack. The products formed during discharge are Li_2O_2, Li_2CO_3, HCO_2Li, CH_3CO_2Li, NO, H_2O, and CO_2. The carbonate and the carboxylate products accumulate in the electrode with cycling.

Overall, the authors suggest that the stability of amides (mainly DMF) towards reduced oxygen species is insufficient for their use in aprotic Li-O_2 batteries.

Dimethyl sulfoxide (DMSO) has also been used as an electrolyte with non-carbonaceous electrodes to provide high cycling efficiency.[38,39] This being said, using an extensive combination of Fourier-transform infrared spectroscopy (FTIR), nuclear magnetic resonance spectroscopy (NMR), energy dispersive X-ray spectroscopy (EDS), X-ray photoelectron spectroscopy (XPS), mass spectrometry (MS) and X-ray diffraction (XRD) techniques, DMSO was proven to decompose in the Li-O_2 battery by two separate groups of researchers.[40,41] The decomposition products include LiOH, dimethylsulfone, Li_2SO_3, and Li_2SO_4.

1.3. Sodium-oxygen batteries

Achieving a practical Li-O_2 battery has proven difficult due to various reasons that include low rate capability, poor cycle life, and high charge overpotential. Recently, a seminal report on the sodium-oxygen (Na-O_2) batteries has invoked intensive follow up studies. The Na-O_2 battery performance is superior to that of the Li-O_2 battery with respect to charge overpotential (~ 0.1 V vs. 1 V, rate capability, and cycling retention). In aprotic media, the Na-O_2 cell typically forms solid sodium superoxide on discharge and not sodium peroxide, via a one electron process ($Na^+ + O_2 + e^- \leftrightarrows NaO_2$) at a potential of $E° = 2.27$ V vs. Na/Na^+.[42] Although the theoretical energy density of the Na-O_2 battery (~1100 Wh/Kg) is much lower than that of the Li-O_2 battery, its good performance has been suggested to provide the foundation of a more practical cell. Xia *et al,* have shown that its electrochemistry relies on a proton phase transfer catalyst (PPTC) that facilitates the formation and oxidation of NaO_2 in solution via the HO_2 intermediate (**Figure** 1.4). The proton can be derived from many

sources such as impure salt hydrates, trace moisture from the system, or weak acids to produce the highly soluble HO_2 radical. The low charge overpotential allows the battery to operate within an electrochemical window that minimizes oxidation side-products on charge.[43] Thus, the superior reversibility of the Na-O_2 battery is thought to be due to the "cleaner" chemistry associated with the oxygen reduction/evolution (ORR/OER) reactions, at least on the first cycle. Nonetheless, given the high reactivity of NaO_2 and the strongly nucleophilic nature of the $O_2^{\bullet-}$ ion and the HO_2 radical, electrolyte degradation is expected.

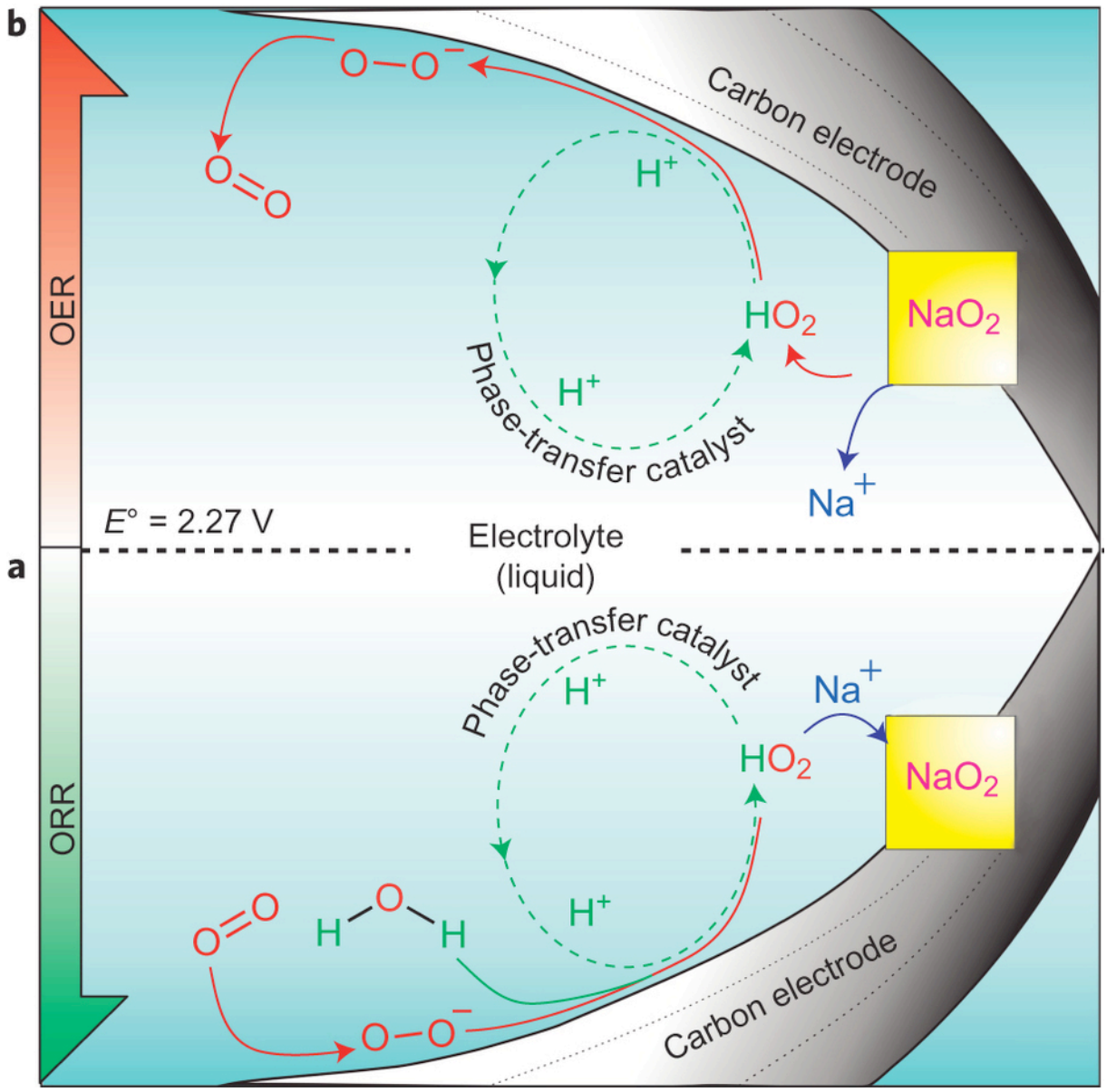

Figure 1.4 Role of water as a proton phase transfer catalyst (PPTC) in a Na-O_2 battery.[43]

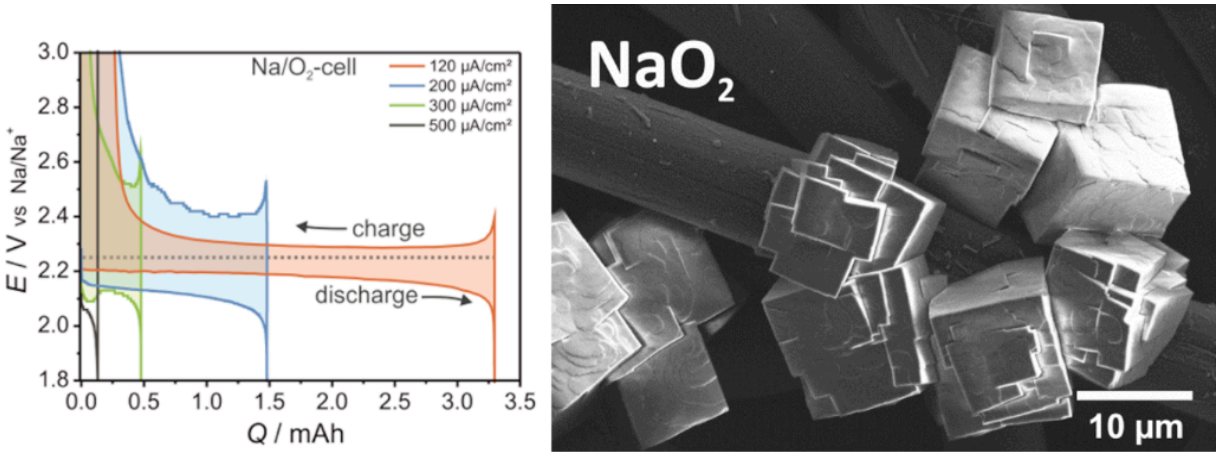

Figure 1.5 Low overpotential during charging of the Na-O_2 battery. SEM image on the right shows the cubic crystals of sodium superoxide formed during discharge.[42]

As in the case of Li-O_2 batteries, glyme based electrolytes are conventionally used for the Na-O_2 batteries owing to their quasi-stability towards superoxide radicals. **Chapter 3** of this thesis is dedicated towards elucidating the nature and type of side reactions taking place in a Na-O_2 battery.

1.4 Lithium sulphur batteries

The lithium-sulphur (Li-S) battery system has been studied for several decades. Over the past 10-15 years there has been a rapid increase in research efforts leading to an exponential rise in publications. The most commonly studied system involves a lithium metal negative electrode and sulphur containing positive electrode. Li_2S is the final discharge and only thermodynamically stable product being formed. The theoretical cell voltage of 2.24 V is comparably low, but due to the high capacity of sulphur (1672 mAh/g), the theoretical

energy density by weight (2615 Wh/kg) exceeds that of lithium-ion batteries by a factor of five.

A typical discharge-charge profile of a Li-S battery is shown in **Figure** 1.6. Both the discharge and charge voltage profiles show two plateaus at 2.3 V, 2.1 V (discharge) and 2.3 V, 2.4 V (charge) respectively. Within the higher discharge plateau, the soluble intermediate polysulphides (S_4^{2-}) are formed accounting for 25% of the overall capacity. Further reduction leads to the formation and precipitation of insoluble species leading to an overall two electron reduction of S_8 with Li_2S as the end product. During the following charge, Li_2S is reconverted to S_8 via intermediate polysulphides. The characteristic minimum between the upper and lower discharge plateau is attributed to the nucleation of the solid products.[44,45] The exact position of the potentials also depends on the electrolyte solvent.[46]

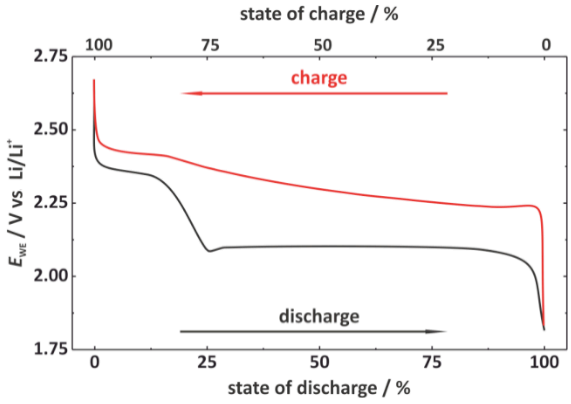

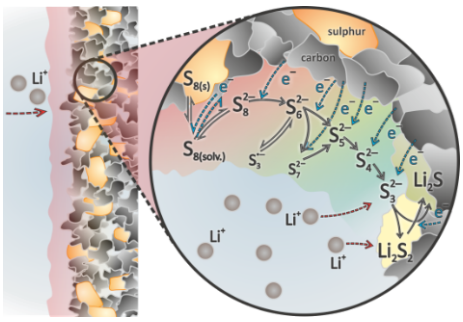

Figure 1.6 Typical voltage profile of a lithium/sulphur cell and schematic illustration of the reduction processes during discharge of a Li-S battery.[47]

1.4.1 Challenges of the lithium-sulphur battery

The main challenges of the lithium-sulphur battery are related to two intrinsic properties:

1. Sulphur and Li_2S are insulators and contact with a conductive support is necessary for a complete cell reaction. At the same time the support should accommodate the volume change (80%) that arises from the difference in molar volumes of sulphur (15.5 mL/mol) and Li_2S (28.0 mL/mol).
2. Polysulphides with the stoichiometry (Li_2S_x; $x>2$) are highly soluble in commonly used electrolytes, meaning that the active material diffuses out of the positive electrode and eventually reacts with the negative electrode or deposits somewhere else in the cell where it remains inactive. Thus cycling sulphur in a Li-S battery is truly based on the dissolution and precipitation processes (**Figure** 1.6). The polysulphide solubility leads to a parasitic phenomenon called "shuttle mechanism"[48](**Figure** 1.7) . This effect leads to continuous self-discharging during the discharge, charge and rest.

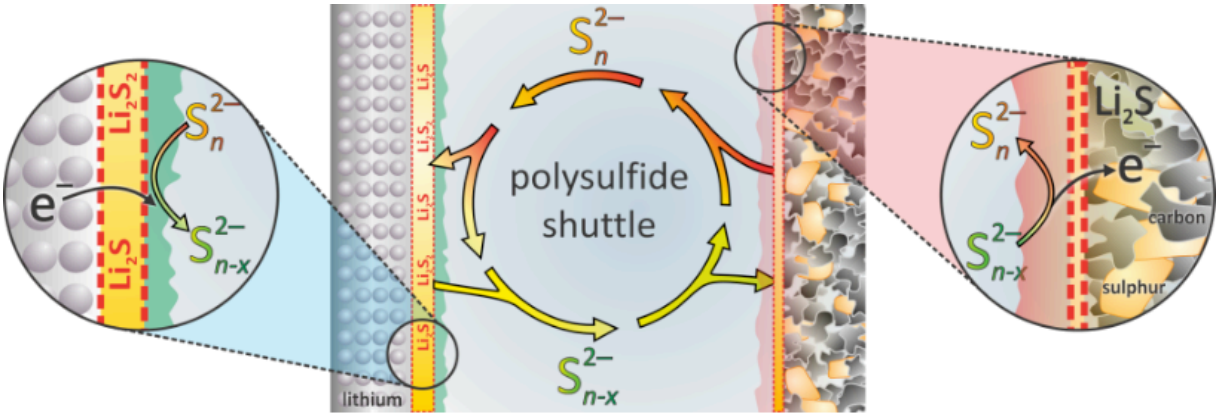

Figure 1.7 Schematic illustration of the polysulphide shuttle.[47]

As a result of these effects, the coulombic efficiency is low, utilization of sulphur in Li-S cells is poor, and the capacity diminishes on cycling. Although overcoming drawbacks through cathode architecture has proved to be highly beneficial for the Li-S system, this thesis focusses on improvements in the electrolyte to overcome these problems.

1.4.2 Electrolytes in a lithium sulphur battery

The electrolyte in a Li-S battery plays the most fundamental role, even greater than cathode architecture, as the solubility of polysulphides, and hence the shuttle effect is influenced mainly by the solvent.[49-52] A typical electrolyte should be suitable for both the highly reactive lithium anode and the sulphur composite electrode. Solvents with good solubility for polysulphides usually demonstrate fast and complete reactions between lithium and sulphur.[50,53] On the other hand, high solubility accelerates shuttling and loss of active material. Most ether based solvent dissolve polysulphides very well, prominent examples being 1,3-dioxolane (DOL), DME and TEGDME. Carbonate based solvents are not used for

Li-S batteries due to their reactivity with polysulphides and their incompatibility with lithium metal.[54-57]

The most common solvent used for a Li-S battery is a mixture of a cyclic ether (DOL) and a linear ether (DME), which provides a good compromise between sulphur utilisation, rate capability and anode compatibility.[58] Aurbach *et al*., pointed out the significance of lithium nitrate as an electrolyte additive[54,59,60] to build up both a relatively stable and flexible solid electrolyte interface (SEI) on the lithium anode that suppresses the polysulphide shuttle. However, $LiNO_3$ is consumed during operation and decomposes at a voltage of 1.6 V during discharge.[59]

Increasing the conductive salt concentration might inhibit the polysulphide shuttle due to increased viscosity and "salting out" effects as stated by Suo *et al.*[61] They used a salt concentration of 7 M and suppressed both polysulphide shuttle as well as dendritic growth. On the other hand, this is an expensive solution, and also results in poorer rate behaviour due to the increased viscosity.

Recently Cuisiner *et al.*[62] reported on a new "binary" electrolyte comprising of a solvent-salt complex and hydrofluoroether that provided minimum solubility of polysulphides. Different electrochemical behaviour was observed. Polysulphides were still formed but with supressed parasitic disproportionation.

Ionic liquids could be potential candidates for this purpose owing to their low Lewis acidity or basicity and thereby potential for low solubility of polysulphides.[63] A major problem with ionic liquids is their high viscosity and low ionic conductivity resulting in low active mass utilization.

Despite intense research, an ideal electrolyte has not been identified yet, that would solve the problem of polysulphide shuttle. **Chapter 5** of this thesis highlights the effort taken towards overcoming this obstacle.

1.5 Scope of the thesis

This thesis will focus primarily on the properties of high energy batteries governed by electrolytes. **Chapter 1** has provided a brief introduction into the various battery systems explored. **Chapter 2** reports on the various characterization methods and techniques used throughout the thesis. **Chapter 3** focusses on the impact of electrolyte decomposition on the Na-O_2 battery. **Chapter 4** describes the design and synthesis of various electrolyte solvents for Li-O_2 and Na-O_2 batteries. Finally **Chapter 5** delves into the approaches taken towards inhibiting polysulphide shuttle in a Li-S battery.

Chapter 2 Basic concepts and characterisation techniques

2.1 Basic concepts

Rechargeable batteries, also known as secondary batteries, can be reversibly charged and discharged for a certain duration (life-time), as opposed to primary batteries which have a one-time use. A rechargeable battery usually consists of a group of electrochemical cells that are connected in series and/or in parallel to satisfy the voltage and current need. Most research is focused on improving the electrochemical performance of an individual electrochemical cell.

This cell consists of a cathode and an anode, which are separated by an electrolyte. The operation of a cell is based on the difference in chemical potential of two active materials in

the electrodes, which gives rise to reduction and oxidation half reactions in the cathode and anode, respectively. The electrodes should be electrically and ionically conductive, as electron transfer and ion transportation occur on the surface and within the electrodes. The electrolyte, being an ionic conductor but also an electric insulator, can be either solid or liquid. An electrolyte-permeable but insulating porous separator is needed for liquid electrolyte cells.

There are some basic characteristics that are often used when evaluating the performance of an electrode, including electrode potential, discharge/charge voltage profile, specific capacity, energy density, rate capability and cycling performance. These are essential for understanding the work in this thesis based on the following:

1) The potential of an electrode is dependent on its chemical potential (*i.e.* redox potential). A large difference of potential between cathode and anode (*i.e.* voltage) is desired, since the output power is the product of voltage and current. The potential difference has to be within the electrochemical potential window of the electrolyte used in order to prevent electrolyte decomposition

2) A discharge/charge voltage profile is a plot of the change in voltage as a function of specific capacity during the galvanostatic cycling of a cell, when a constant discharge/charge current is applied. The profile can reveal information on the redox reactions that are involved. A minimal voltage difference between discharge and charge, an indicator of low degree of polarization, is desired to maximize the energy efficiency.

3) Specific capacity (mAh/g) or volumetric capacity (mAh/cm^3) is defined by the amount of charge (Q, mAh) stored per mass or volume of electrode for one full discharge/charge cycle.

A high theoretical specific capacity is desired for electrode systems, as the energy density is the product of capacity and voltage per mass (W h/kg) or volume (W h/L).

4) The current at which a cell is discharged/charged matters when considering the power density. The "C/n" rate corresponds to the rate (mA/g) at which the theoretical specific capacity is achieved in *n* hours upon discharge. Higher rates give higher power but normally lead to higher polarization, lower energy efficiency and lower specific capacity. High rate capability indicates an ability to maintain its capacity and degree of polarization upon increased rate.

5) Cycling life usually means the capacity retention with prolonged cycle of a cell. For the commercialization of a cell, the cycle life is extremely important. In laboratory research, the examination of cycle life of a cell is usually performed by continuously cycling a cell in a galvanostatic mode until the capacity fades substantially, although in practice the discharge/charge is more complicated (*e.g.*, not always at the same rate and invoking periodic rest periods.)

2.2 Characterisation techniques

2.2.1 Iodometric titration to determine NaO_2 content

The chemical reactions involved in the quantification of sodium superoxide on the cathode are the following:

$$2NaO_2 + 2H_2O \rightarrow 2NaOH + H_2O_2 + O_2 \quad (1)$$

$$H_2O_2 + 3I^- + 2H^+ \leftrightarrows 2H_2O + I_3^- \quad (2)$$

$I_3^- + 2Na_2S_2O_3 \rightarrow Na_2S_4O_6 + 2NaI$ (3)

In a chemical reaction involving H_2O_2 and I^- (2), the former is reduced to water and the latter is oxidized to iodine, which can then be titrated using standard thiosulfate solution to quantify the peroxide concentration. The net reaction between peroxide and iodide is as shown in (2). This reaction is slow without a catalyst but can be quite fast in the presence of catalysts such as Mo(VI), which can force the reaction to occur resulting in the formation of I_3^-

In a standard iodometric estimation of H_2O_2, the peroxide is reacted with excess iodide in acidic media, but acid is known to cause chemical disproportionation of peroxide to water and oxygen. Furthermore, iodide is prone to oxidation in air at acidic pH. Both of these processes are likely to introduce significant error in the peroxide quantification. To circumvent this, a molybdenum catalyst in NH_4OH/NH_4NO_3 solution has been utilized. In our work, we have adopted a modified iodometric method that instead employs a pH neutral iodide-phosphate buffer reaction media to maintain a steady supply of protons for the peroxide-iodide reaction, while maintaining a constant pH. A neutral pH suppresses peroxide disproportionation and decelerates the oxidation of iodide. The inhibition of iodide oxidation was evident from the unchanged color of the post titration solution (colorless) even days after the titration. In a standard iodometric procedure, the post titration solution turns blue very quickly from the oxidation of I^- to I_2, which in turn binds to starch to give the blue color.

The buffer-catalyst solution was prepared by dissolving 65 mg of $(NH_4)_6Mo_7O_{24}\bullet 4H_2O$ (ammonium heptamolybdate) along with 0.11 mol of $H_2PO_4^-$ and 0.03 mol of HPO_4^{2-} in 500 mL of water. Adding 67 g of KI to this buffer solution and diluting it to 1 L resulted in the reagent buffer solution, which was freshly prepared before use. For the NaO_2 quantification,

the discharged/charged cathodes were transferred to a glass vial into which 5 mL of water was added. After vigorous shaking, the content of the vial was transferred to a conical flask with an extra 5 mL of water that was used to rinse the vial. To this mixture, 15 mL of water and 25 mL of buffer catalyst solution was added. The mixed solution immediately turned yellow to indicate the liberation of iodine, which was titrated with standardized thiosulfate solution till a straw yellow color was achieved. The titration was continued after adding starch indicator solution with the end point showing a color change from blue-violet to colorless.

2.3 Electrochemical methods

2.3.1 Two-electrode system

Non aqueous Li and Na-O_2 cells were prepared using a modified Swagelok^{TM} design. Cells were assembled in an argon filled glovebox with a lithium or sodium metal anode, porous separators (millipore glass fiber), and a gas diffusion electrode as the cathode. Electrolyte (50-200μL) was added to the separator during cell assembly. In the case of the cells which were discharged, O_2 (99.999%, Praxair) was introduced through a quick connect gas line system with Swagelok^{TM} fittings and metal tubing. An excess volume of O_2 was stored in the headspace (an aluminium tube above the cathode) at a pressure of 1.5 atm.

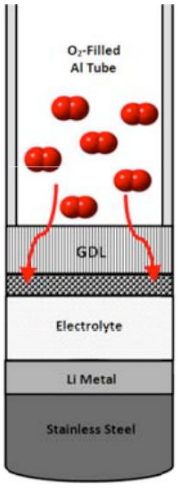

Figure 2.1 Schematic design of the Li-O2 cells used in this study

2.3.2 Coin cell configuration

In **Chapter 5** of this thesis, 2325 type coin cells were used to examine the electrochemical performance of the electrode materials. **Figure 2.2** shows a typical coin cell configuration. The cathode was made by mixing the active material composite, conductive carbon additive and polymer binder in a solvent to form a slurry which was then slurry-cast or drop-cast onto carbon coated aluminium current collectors. The electrode was then dried at 60 ˚C overnight. The cell was assembled in an Ar-filled glovebox.

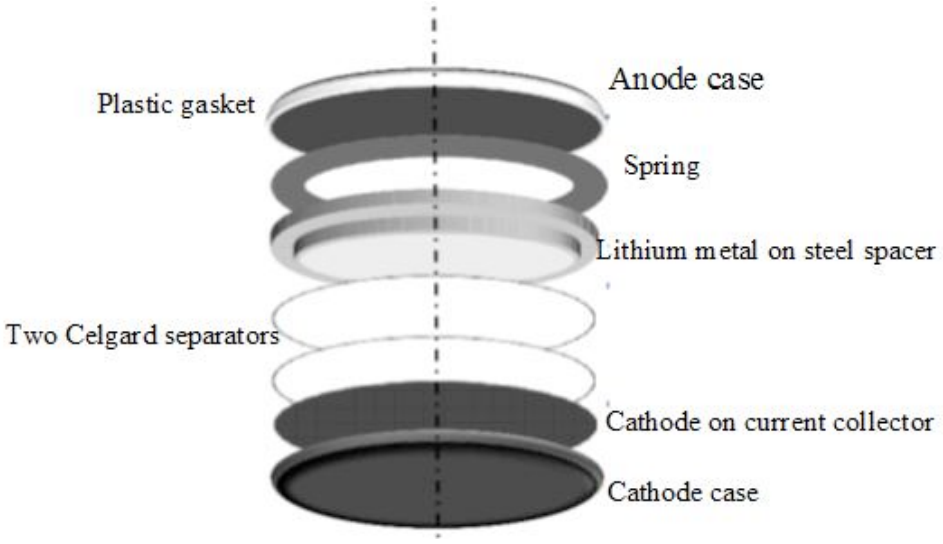

Figure 2.2 Configuration of a coin cell

2.3.3 Galvanostatic cycling

Galvanostatic cycling is an electrochemical technique where a current is applied and the voltage response is measured. With this galvanostatic technique, a constant current is applied to the cell until a predetermined cut-off voltage is reached and the current is reversed. When a negative current is applied (drawing current from the cell), the battery is discharged. When a positive current is applied, charging of the battery occurs. With this technique, a single discharge/charge cycle can be analysed as a plot of cell voltage versus capacity.

2.3.4 Cyclic voltammetry (CV)

CV is a potentiodynamic technique where the potential is swept at a constant scan rate (V/s). A voltammogram is the resultant plot of current vs potential. In CV, the potential is swept in

the forward direction, then in the reverse direction to study the reversibility of an electrochemical reaction.

The CV experiments (chapters 4 and 5) were performed using a coin cell with Li foil as the counter and reference electrodes and stainless steel as the working electrode.

Chapter 3 The Nature and Impact of Side Reactions in Glyme-based Sodium-Oxygen Batteries

3.1 Introduction

As mentioned in **Chapter 1**, the benefits of the Na-O_2 battery compared to the Li-O_2 battery are clear. Although the Na-O_2 battery affords a very low overpotential compared to the Li-O_2 battery, the electrolyte that is currently being utilized in most literature reports falls into the glyme category. These solvents are known to decompose in the presence of superoxide radical or the discharge product Li_2O_2. With similar ORR processes taking place like in the Li-O_2 battery, there would be similar decomposition of the glyme electrolytes during the discharge process. This chapter is dedicated towards identifying the various degradation reactions taking place during the operation of a Na-O_2 battery and to determine whether the source of decomposition processes are from the cathode or the electrolyte.

3.2 Experimental

Cathode Preparation. Stainless steel meshes of area 0.78 cm^2 (100 x 100 mesh) were sonicated in ethanol and dried prior to use. A slurry of ground ^{13}C carbon (Sigma-Aldrich) and PTFE (from a 20 mg/500 μL isopropanol stock solution) was prepared in a 85:15 mass ratio. After it was mixed for 1 minute, the slurry was pressed onto the stainless steel mesh and dried in air at 60 °C for 1 hour. The cathodes were dried at 300 °C under vacuum overnight in a Büchi oven, and then transferred to an Ar-filled glovebox.

Electrochemical Measurements. Cathodes were employed in either 2 or 3-electrode modified-PFA Swagelok cells. Each cathode was placed in a cell with a sodium metal

(Sigma-Aldrich) anode, separated by two glass fibre separators and one Celgard separator (2500). Electrolyte (240 μL) comprised of 0.5 M NaOTf and 15 ppm H_2O (prepared in-house[43]) in distilled diethylene glycol dimethyl ether (DEGDME, or diglyme) was added to the cell. The cell was then sealed and pressurized to 1.5 atm in 5.0 research grade oxygen (Praxair). Prior to measurement, the cell pressure was monitored with a pressure transducer (PX409, Omegadyne) to ensure that each cell was hermetically sealed. The electrochemical measurements were performed with an Arbin galvanostat/potentiostat. The current density for all experiments was 130 $\mu A/cm^2$; capacity and voltage limitations are as indicated.

Determination of NaO_2 content. Iodiometric titration of the dry cathode contents was performed using a slightly modified version[64] of a previously reported method[65] (**Chapter 2)**

^1H NMR. NMR experiments were conducted in D_2O on a 300 MHz Bruker Advance spectrometer at room temperature. ^1H NMR spectra were referenced to the residual HOD peak at 4.78 ppm. The fraction of decomposition products was determined through integration of the peak area with respect to a known amount of benzene standard added to the solution. This stock solution was prepared using 100 g of D_2O and 0.2 mL benzene and was allowed to equilibrate for 24 hrs prior to analysis. Cathodes and separators were removed from the cell and washed with THF. The contents were then left to dry under vacuum for 12 hours before addition of the D_2O/benzene solution. 0.8 mL of the stock solution was added to the cell contents and collected for measurement.

KO_2 Reaction. KO_2 (Sigma Aldrich) and 18-crown ether (Sigma Aldrich) were used as received. Diglyme was distilled prior to use, and NaOTf was prepared as indicated above. For each reaction, 0.02 g KO_2 and 0.13 g dicyclohexyl-18-crown-6 (crown ether)were added to

2.5 mL diglyme. The reaction was left to stir for four days. To produce NaO_2, 0.10 g NaOTf was added immediately following the addition of KO_2 and crown ether. The added NaOTf was twice the molar amount of KO_2 to ensure complete reaction of the O_2^- to NaO_2. After four days, the solid contents were left to settle and were collected via centrifuge. The contents were washed three times with 15 mL THF, and dried under argon overnight. D_2O was added directly to the solid contents for NMR analysis.

Mass Spectrometry: Electrochemistry. To measure gas evolution on cell charge, the cathodes were first discharged using the same Swagelok design described above. Upon completion of discharge, the cell contents (without the metallic sodium electrode) were immediately transferred to an El-Cell electrochemical cell in an argon-filled glove box and an additional 50 μL of electrolyte was added. The cells were attached in-line with a RGA 200 (Stanford Research Systems), and a continuous flow of Argon (Praxair) was used to sweep the evolved gases during cell charge across a 50 μm diameter capillary for analysis. Quantification was performed using a calibration curve comprised of different concentrations of O_2/CO_2 in Ar (0-2000 ppm).

Mass Spectrometry: Chemical. The method for chemical analysis of carboxylates/carbonates was adapted from Thotiyl *et al*.[66] Cells were discharged/charged to specific capacities and removed either immediately upon completion, or removed after a specific rest period as indicated. Both the cathode and separator were removed and placed into a custom-design glass reaction vessel. This vessel was outfitted with Swagelok microconnects for ease of connection in-line with the mass spectrometer. The vessel was sealed air-tight with a fitted septum. The cell was left to rest under flowing argon for 1 hour prior to measurements. The Ar flow rate was then set to 1 mL/min, and approximately 0.5 mL of 2 M H_3PO_4 was added

to the cell contents and stirred. The evolved gases were swept into the mass spectrometer, and the reaction was left to continue until CO_2 levels returned to base level. The concentration of CO_2 (and $^{13}CO_2$) was measured and quantified using the same method for the electrochemical mass spectrometry mentioned above.

Scanning Electron Microscopy. Cathodes were removed from cells immediately after cell completion (no rest unless indicated). The cathodes were washed with THF, dried under vacuum and mounted onto SEM stubs with double sided carbon tape in a hermetically sealed argon-filled box. Transfer from the glovebox to the SEM was performed with minimal exposure (*i.e.*, 1 sec) to the atmosphere upon placement into the SEM load-lock chamber. Analysis was performed with a Zeiss Ultraplus FESEM.

X-Ray Diffraction. XRD measurements were carried out using a Bruker D-8 Advance diffractometer employing Cu-Ka radiation (λ = 1.5406 Å). Samples were mounted on a silicon low-background holder using a moisture-protective barrier.

3.3 Results and Discussion

In our studies, ^{13}C-labelled cathodes were used to identify the source of decomposition reactions in the Na-O_2 cell by tracing their origin to either the reaction of the carbon surface or of the ^{12}C glyme-based electrolyte. To determine the nature of the discharge products, a cell was discharged and charged to a capacity of 1 mAh in 0.5 M NaOTf/diglyme. The electrolyte consisted of distilled diglyme with pure, crystalline NaOTf (synthesized in-house to ensure no contamination from $NaOH•H_2O$ or other species) and 15 ppm H_2O to provide a controlled, albeit very low, fraction of the phase-transfer catalyst necessary to achieve good

discharge/charge properties as previously reported.[43] **Figure 3.1** shows an electrochemical profile for a cell first discharged to 1 mAh, and charged to an upper cut-off voltage of 4.5 V, along with the associated gas evolution quantified by on-line electrochemical mass spectrometry (OEMS). The discharge potential of 2.1 V and initial charge plateau at 2.3 V is representative of a typical Na-O_2 cell and is in agreement with most other reports that utilize carbon-based cathodes and exhibit NaO_2 as the discharge product.[42,67,68] The presence of crystalline NaO_2 as the single discharge product is confirmed by its diffraction pattern (**Figure 3.2**). Few reports have documented the formation of Na_2O or Na_2O_2 hydrate as the discharge product with carbon cathodes and glyme-based electrolytes.[69-71] While the parameters that determine the selectivity of products are not well understood, we observe some Na_2O_2 hydrate on long exposure of the cell to rest periods as discussed in the next section. Such cells exhibit poor rechargeability and much larger overpotentials compared to NaO_2, similar to Li_2O_2.[70,71] The formation energies of bulk NaO_2 and Na_2O_2 are quite close and slightly favour the formation of the latter, but the lower surface energy of nanocrystals that are initially nucleated thermodynamically favours the production of NaO_2.[72] The phase transfer catalyst kinetically drives growth of this phase upon initial nucleation of the superoxide, as previously demonstrated.[43]

The electrochemical charge plateau at 2.3 V in **Figure 3.1a** is accompanied by a flat oxygen evolution profile measured by OEMS that corresponds to the near theoretical 62.0 nmol/min O_2 evolution (based on a 100 μA discharge current). The voltage rises to 3.0 V as oxygen evolution declines to zero, and is suggestive of an overpotential that must be exceeded to complete the process that we ascribe to an impedance layer. Integration of the amount of O_2 evolved (28.6 ± 0.1 μmol) with respect to the total charge passed up to 3.0 V corresponds to 1.10 e^-/O_2, as expected based on the one-step oxidation of NaO_2 to Na^+ and O_2 (**Figure 3.3**). Deviation from the theoretical 1.00 e^-/O_2 ratio agrees closely with other

reports.[43] The loss in charge efficiency is due to electrochemical side reactions that produce degradation products in addition to a very small fraction of NaO_2 entrapment in the separator due to its dissolution in the electrolyte, as illustrated by others.[68] After the initial charging step, CO_2 evolution is observed starting at ~ 3.2 V, followed by a trace of additional O_2 evolution above 3.8 V. CO_2 evolution is attributed to the oxidation of sodium carboxylates present on the cathode surface, similar to the Li-O_2 cells.[73] Evolution of CO_2 and O_2 both cease before electrochemical electrolyte oxidation is evidenced by the onset of a flat voltage profile at 4.45 V. The amount of NaO_2 on cathodes discharged to 1 mAh was determined to be 33.9 ± 0.5 μmols by iodometric titration, 90% of theoretical. This value agrees with previous reports on the NaO_2 formed after a single discharge step, although slightly lower.[42] Thus, about 10% of the electrons passed cannot be accounted for based solely on the NaO_2 present in the cell.

The amount of NaO_2 that remained on the cathode surface after charging the cell to 3.0 V was also measured by iodometric titration. That voltage corresponds to the end of the initial O_2 evolution profile but before CO_2 evolution starts. At 3.0 V, 1.8 μmol of NaO_2 still remained, equivalent to about 5% of the NaO_2 that was deposited on discharge. This explains the lower-than-ideal capacity measured on charge to this point (~0.85 mAh vs 1 mAh). The capacity on charge can be fully accounted for based on the amount of NaO_2 on discharge (90% of theoretical), less the NaO_2 that remains at 3.0 V (5%). The second oxygen evolution process in **Figure 3.1b** between 3.8 and 4.4 V corresponds to oxidation of the remaining NaO_2, as determined by iodometric analysis of the product at 4.4 V. Only a trace (~ 0.4 μmols of NaO_2) remain after this point, indicating that virtually all of the NaO_2 is removed prior to the start of electrolyte oxidation at 4.5 V.

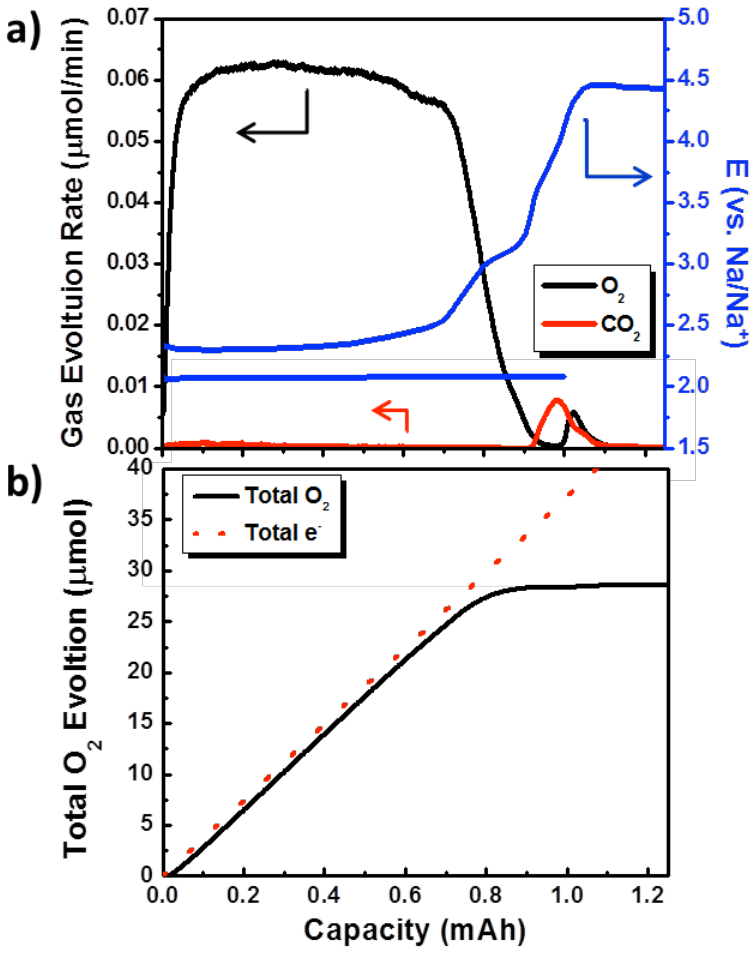

Figure 3.1. a) Representative discharge (D)/ charge (C) curve for the first cycle of a Na-O_2 cell with a ^{13}C cathode, and corresponding O_2 and CO_2 evolution profiles; b) the integrated values of oxygen evolution (black solid line) compared to theoretical O_2 evolution (dashed red line). In the electrochemical profile shown in (a), the onset of the flat profile above 4.4 V indicates the onset of electrolyte oxidation.

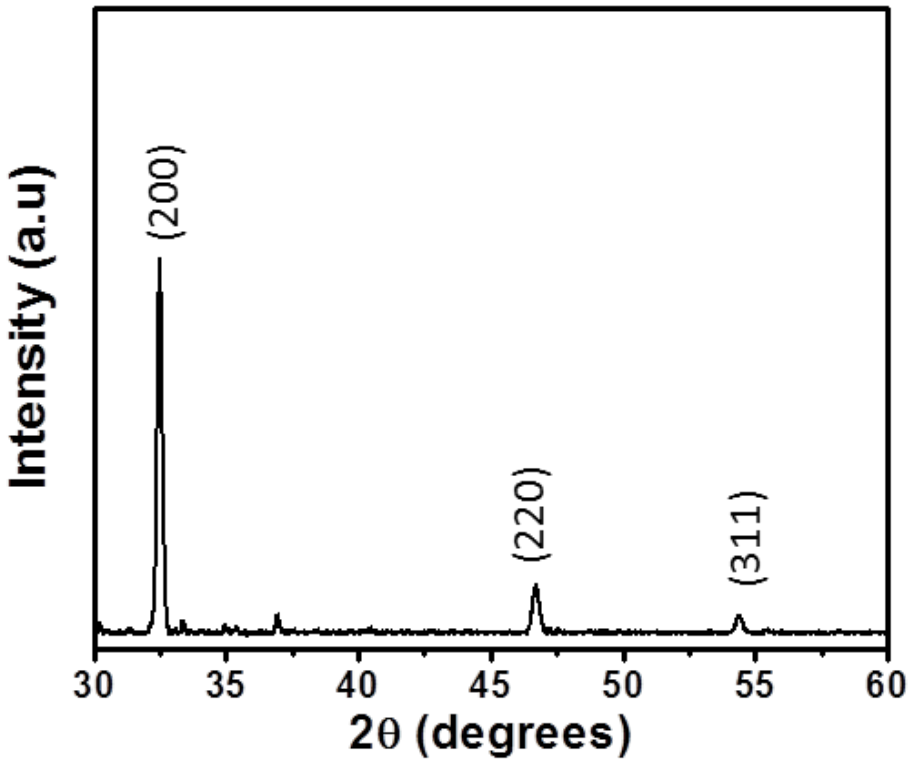

Figure 3.2 Powder X-ray diffraction pattern of a ^{13}C cathode after discharge to 1 mAh in 0.5 M NaOTf/15 ppm H_2O/diglyme. The pattern is indexed to the cubic phase NaO_2.

3.4 Identity of discharge products and their quantification

In order to assess and quantify the carboxylate and carbonate products formed on discharge, the ^{13}C positive electrode and separators were washed in THF and dried under vacuum. These were subjected to acid treatment with 2 M H_3PO_4, utilizing mass spectrometry to quantify the total evolved CO_2 ($^{13}CO_2$) gases.[68] In a parallel study, similarly prepared electrodes were immersed in D_2O to extract the soluble species and providing the ^1H NMR spectrum shown in **Figure 3.3**. The relative contribution of carboxylate side-products was estimated from peak integration. Experiments were carried out in duplicate, and the amount

of side-products was determined from the combined analysis. This reveals that a majority of the degradation product is comprised of sodium acetate (~4% of total discharge product), along with equal contributions of sodium formate, methoxy(oxo)acetic anhydride, and Na_2CO_3 (~1% each of total discharge product). These data are summarized in **Table 1** and **Figure 3.4** which express the products as a percentage of the total theoretical NaO_2 expected. Only a miniscule fraction of the total decomposition products (~0.5%) originate from the carbon cathode as $Na_2{}^{13}CO_3$.

The amount of carboxylate degradation products formed on discharge depends on the cathode composition. Comparison of a very low surface area carbon fiber cathode (Freudenberg GDL, H2315), with a high surface area carbon (Vulcan™) (**Table 2**) shows that the Freudenberg cathode exhibits a significantly higher fraction of NaO_2 formed as a function of current passed (98%). This is reflected in the low fraction of decomposition products, which are also less than those observed from the ^{13}C cathode. In contrast, the NaO_2 and carboxylate fraction exhibited on the Vulcan™ electrode is similar to that of the ^{13}C electrode. These findings agree with a study by Bender *et al.*[74] that reports dramatic differences in the electrochemical performance of different carbon cathodes in the Na-O_2 cell. They reported that the discharge capacity as well as charge efficiency is dependent on the cathode material, with charge efficiencies ranging between 75% to 93%. The wide range is most likely due to variability in the decomposition products, although their nature was not addressed in that study. A comprehensive examination of the role of the carbon is also beyond the scope of the present work.

Because NaO_2 is charged at relatively low potential (owing to phase transfer catalysis) Na-O_2 chemistry is reported to be less affected by side-reactions.[42,68] In the Li-O_2 system, decomposition products are formed on discharge, but a significant fraction is also produced on the oxidation cycle owing to the high overpotential required to oxidize Li_2O_2.[31,65,68,73]

Furthermore, as shown by Thiotyl *et al.*,[66] the stability of the carbon cathode is also an issue: above 3.5 V the carbon undergoes oxidation in the presence of Li_2O_2 to form Li_2CO_3. To confirm that the decomposition products are formed mostly on discharge in the Na-O_2 cell, the products analyzed above were compared to those remaining after a cell was charged to 3.0 V following discharge to 1 mAh (**Table 1**). Analysis was again performed by a combination of ^{1}H NMR, to determine carboxylate contributions, and acid treatment/mass spectrometry (**Figure 3.6)**. In complete agreement with McCloskey *et al.*,[65] the fraction of decomposition products produced on charge is minimal as summarized in **Figure 3.5**. The relative ratio of formate, acetate, carbonate, and anhydride is very similar to that of the discharged cathode, implying that there is no additional decomposition on charge. The only difference is the amount of $Na_2{}^{13}CO_3$, which increases by ~three fold compared to that of the discharged cathodes. Thus, while the charge overpotential for the NaO_2 cell is very low (~0.1 V vs. theoretical), the voltage is sufficient to promote slight oxidation of the cathode and thus form a very small fraction of $Na_2{}^{13}CO_3$, for example by the direct oxidation of carbon with NaO_2, via:

$$5NaO_2 + 2{}^{13}C \rightarrow 2Na_2{}^{13}CO_3 + 2O_2 + Na^+ + e^-.$$

To determine if all or any of these carboxylate decomposition products are removed at elevated voltage and correspond to the CO_2 evolution that is centered at ~3.5 V, the products were analyzed after the cell was charged to 4.4 V. These results are also summarized in **Figure 3.4**. We find that all of the carboxylate products decrease after charge to 4.4 V, but are still present. This suggests that only a fraction can be oxidized, which is consistent with the small amount of CO_2 that is evolved. In a recent study we probed the electrochemical oxidation of Li-based decomposition products and demonstrated that they could not be oxidized on a carbon surface at a potential below that of the stability window of the glyme-based electrolyte.[75] In order to oxidize these decomposition products, a catalyst had to be

employed. The inability to oxidize carboxylate decomposition products on a carbon surface in Li-O_2 cells at a low potential (>4.7 V vs. Li/Li^+) was also reported by Gasteiger *et al.*[76] and Leskes *et al*[77]. Therefore, either the 4.4 V charge voltage in the Na-O_2 cell is below the necessary potential to oxidize the carboxylate side-products, or they are continuously formed in tiny amounts during the charge process.[66] The former is more likely. We further conclude that NaO_2 can be oxidized in the presence of electrolyte decomposition products because solution-based proton phase transfer catalysis (PPTC) governs the charge process. The oxidation of Li_2O_2 does not pass through an LiO_2 intermediate,[78] and hence a proton phase transfer catalyst in the Li-O_2 battery has little positive effect on charge.[79] The large overpotential on oxidation of Li_2O_2 is also partly due to the presence of surface carboxylates which increase the surface impedance.[80] The oxidation of NaO_2 in a solution mediated by a PPTC is not impeded by the presence of these degradation products, however, leads to lower charge overpotential.

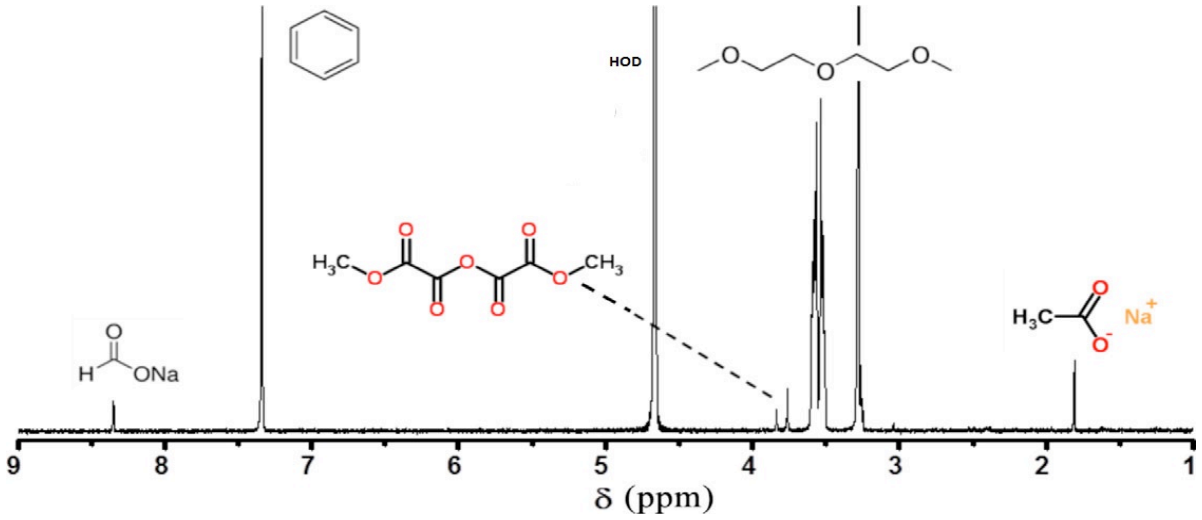

Figure 3.3 ^1H NMR spectrum of a ^{13}C cathode discharged to 1 mAh with major compounds identified: sodium formate δ= 8.4 ppm, sodium acetate δ= 1.8 ppm, methoxy (oxo)acetic

anhydride δ=3.8 ppm. A known amount of benzene (δ=7.3 ppm) was used as the internal standard with D_2O as the solvent.

	Discharge (μmol)	Charge 3.0 V (μmol)	Charge 4.4 V (μmol)
NaO_2	33.9 (± 0.50)	1.80 (± 0.20)	0.37 (± 0.10)
Na_2CO_3	0.5	0.5	0.5
$Na_2{}^{13}CO_3$	0.06 (± 0.02)	0.26 (± 0.06)	0.17 (± 0.06)
Sodium formate	0.6	0.4	0.4
Sodium acetate	1.3	1.5	1.3
Methoxy (oxo)acetic anhydride	0.6	0.4	0.2

Table 1 Absolute amounts of NaO_2 and degradation products formed in the cell at different stages of discharge (to 1 mAh) and charge.

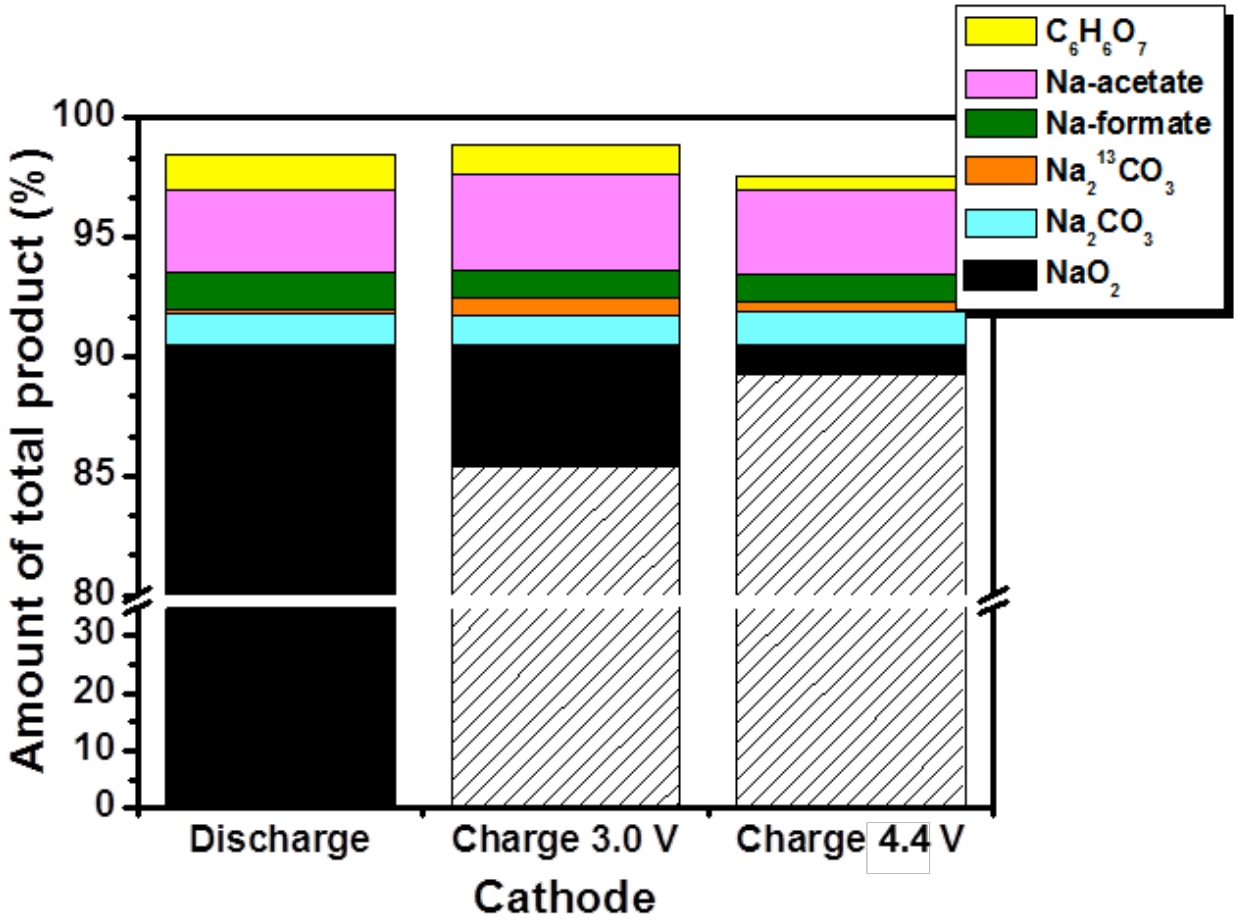

Figure 3.4 Products as a fraction of the total theoretical product (37.7 μmol NaO_2) at different stages of cell operation. The NaO_2 fraction was determined from iodometric titration; and the identity and amount of sodium acetate, sodium formate, methoxy(oxo)acetic anhydride and $Na_2CO_3/Na_2{}^{13}CO_3$ was determined from a combination of ^1H NMR spectroscopy and acid treatment to evolve CO_2 from the carboxylates/carbonate which was measured by mass spectrometry.

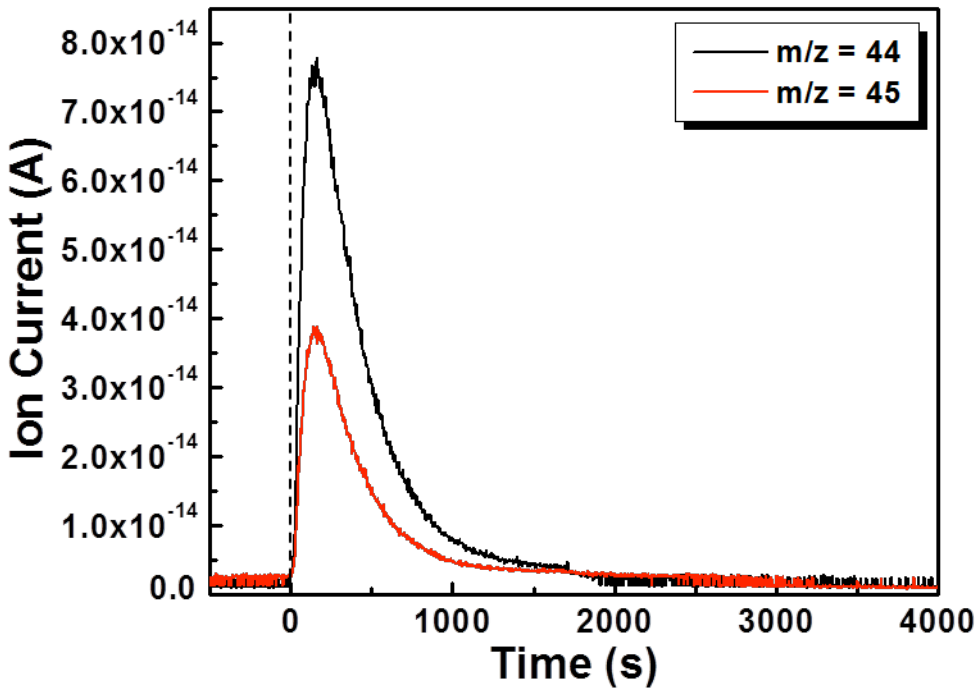

Figure 3.5 The gas evolution profile monitored by on-line mass spectrometry, following 2 M H_3PO_4 injection into an enclosure containing a ^{13}C cathode charged to a voltage of 3.0 V after previous discharge to 1.0 mAh (see **Table** 1). The gases correspond to CO_2 (m/z = 44) and $^{13}CO_2$ (m/z = 45).

	NaO_2	Na_2CO_3	Na-formate	Na-acetate	Methoxy(oxo)acetic anhydride
^{13}C-carbon	33.9	0.5	0.6	1.3	0.6
Freudenberg	36.2	0.2	Trace	0.3	Trace
Vulcan	32.8	0.9	Trace	3.9	1.1

Table 2 Absolute amounts in μmols of NaO_2 and degradation products after discharge of different carbon electrodes to 1 mAh capacity. The theoretical amount of NaO_2 is 37.7 μmols.

3.5 Decomposition mechanism

Hydrogen abstraction from glyme by the highly nucleophilic $O_2^{\bullet-}$ species is a known cause of DME decomposition in Li-O_2 cells, which leads to the formation of lithium formate and lithium carbonate on the cathode surface.[32,81,82] Recent work also suggests that reactivity of Li_2O_2 with water used to determine speciation in NMR experiments may exacerbate carboxylate formation.[83] Much research has been dedicated to the mitigation of electrolyte degradation by exploring alternative solvents, such as sulfones,[84] amides,[85] ionic liquids,[86] and backbone-protected ethers,[81] but no truly stable electrolyte has yet been discovered. In Li-O_2 cells another source of reactivity is the surface of the discharge Li_2O_2 product. Kumar *et al.* showed that the rate of glyme decomposition is faster on the superoxide-terminated ($O_2^{\bullet-}$) surface of Li_2O_2 than on that of its peroxide-terminated (O_2^{2-}) surface using a combination of computational techniques.[87] It was proposed that the highly reactive superoxide surface of Li_2O_2 accelerates the degradation of glyme by a very similar mechanism to that of hydrogen abstraction by $O_2^{\bullet-}$. This has implications for the Na-O_2 cell, as it implies that the superoxide NaO_2 surface will play a major role in the production of these decomposition products as we confirm below.

The sodium formate, sodium acetate, and methoxy(oxo)acetic anhydride products identified in the cell through NMR analysis enable us to propose a mechanism for the decomposition of diglyme, and higher order glymes (see **Figure 3.6**). In this figure, sodium formate is generated via path 1, where a methyl hydrogen abstraction by $O_2^{\bullet-}$ is followed by β-scission of an ether bond to give formaldehyde, which is then oxidized by highly nucleophilic NaO_2 to formate. The mechanism by which sodium acetate is generated requires translocation of a hydrogen atom to generate the required methyl-containing two carbon unit

of acetate. The most plausible mechanism by which this could occur is an *intramolecular* 1,5-hydrogen abstraction, which conforms to the reactivity profile expected for radical species'. A dialkyl ether radical (such as that generated during the initial β-scission of path 1) would be expected to undergo a 1,5-hydrogen abstraction to give a thermodynamically favoured oxygen-stabilized secondary radical. β-scission of this secondary radical would give methyl vinyl ether and an ethoxy radical, from which a hydrogen abstraction would lead to acetaldehyde and, upon further oxidation with NaO_2, sodium acetate. Whereas only sodium formate is observed for monoglyme,[65] we note that 1,5-intermolecular hydrogen abstraction reaction can only occur with higher order glyme electrolytes - explaining why we observe a majority of sodium acetate as a side-product. The formation of methoxy(oxo)acetic anhydride and related compounds are proposed to occur via path 2 as a result of sequential oxidation events where backbone methylene hydrogens are abstracted by superoxide $O_2^{\bullet-}$ radicals. The predominance of sodium acetate (also see below) suggests that hydrogen abstraction from the terminal hydrogen in diglyme, path 1, is favored for sodium superoxide. On the other hand, computations[87] – and experiments[81] - suggest that methylene hydrogen abstraction is slightly more thermodynamically favourable for glyme in the presence of Li_2O_2, regardless of whether the surface is $O_2^{\bullet-}$ or O_2^{2-} terminated. Nonetheless, the fact that we observe both path 1 and path 2 products in detectable amounts demonstrates the dynamic processes at play.

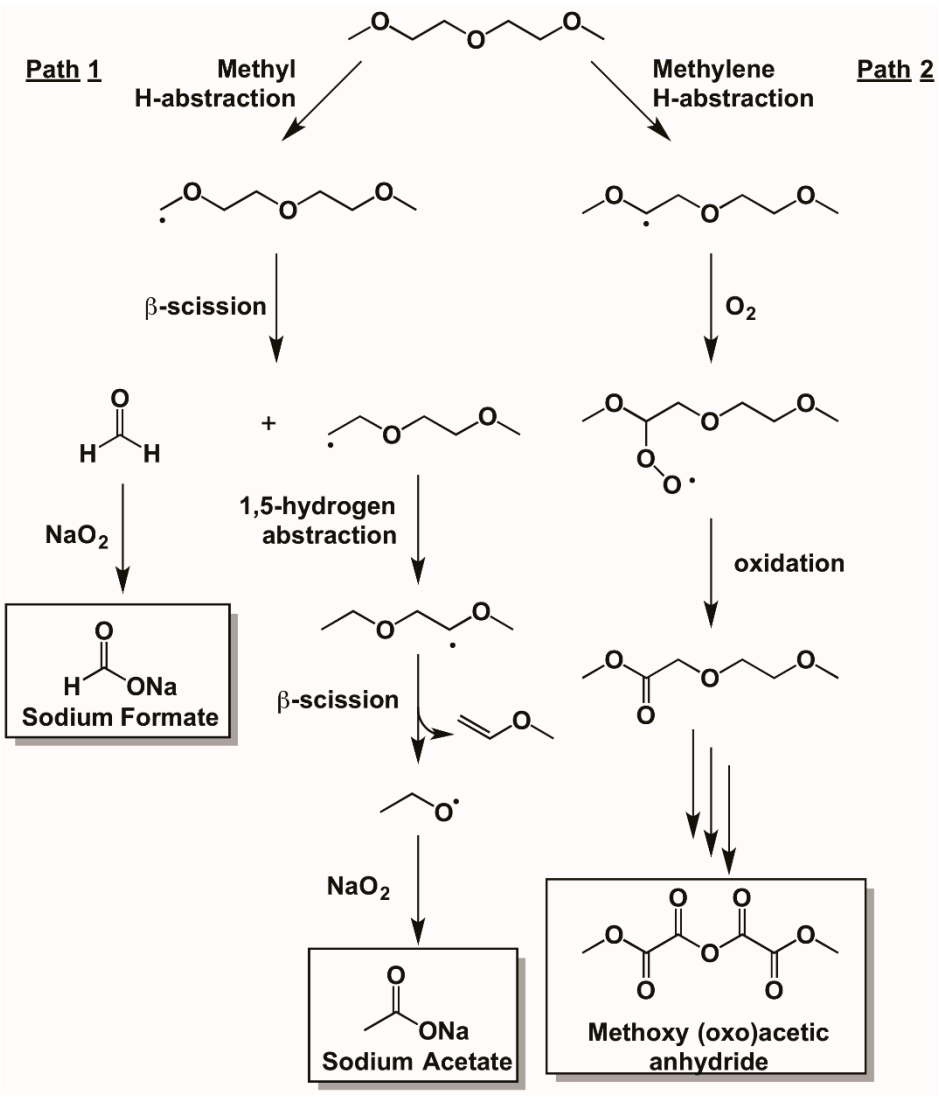

Figure 3.6 Proposed reaction pathway. The formation of sodium formate and sodium acetate occurs via Path 1, and is initiated by a methyl hydrogen abstraction. If hydrogen abstraction initially occurs from a methylene hydrogen, as shown in Path 2, the production of methoxy (oxo)acetic anhydride results.

3.6 Effect of Side-Products on Cycling and Stability at Open Circuit Potential

The fact that NaO_2 and carboxylate products are not completely removed on charge to a typical 3.0 V has implications for cell cycling. **Figure 3.7a** shows a typical electrochemical curve of a cell cycled four times with a charge voltage limitation of 3.0 V, followed by a 4.4 V cut-off at the end of 5th charge. **Figure 3.7b** shows SEM images of the cathode surface at the end of the 5th discharge. The surface is covered with 8 μm NaO_2 cubes that possess a relatively clean, smooth surface. **Figure 3.7c** shows the cathode surface at the end of the 5th charge, at a potential limit of 3.0 V (chosen to correspond to the initial O_2 evolution peak in **Figure 3.1a**. Here, the surface is not covered with pristine NaO_2 cubes, but is populated with smaller structures. These resemble collapsed cubes that appear to have been oxidized from the center outwards to leave behind a roughened shell. This suggests that the inner NaO_2 product is oxidized from within the interior of the cubes (via PPT catalysis in solution), leaving the surface of the cubes covered with sodium carboxylate products which require a high overpotential for stripping. On cycling, these products accumulate along with the NaO_2. This was confirmed by iodometric titration: 4.48 μmols of NaO_2 remain after 5 cycles at a charge cutoff of 3.0 V, which is greater than the amount of NaO_2 remaining after a single discharge/charge cycle (1.80 μmol).

To fully remove the remaining decomposition species, the cathode was charged on the 5th cycle to 4.4 V; beyond the point of CO_2 and O_2 gas evolution, but below that of electrolyte decomposition. The SEM image in **Figure 3.7d** shows a relatively clean surface. Unsurprisingly, the amount of CO_2 and O_2 that is evolved on the 5th charge process beyond 3.0 V is greater than that of charging beyond 3.0 V for a single cycle (**Figure 3.8**). In summary, while the generation and decomposition of NaO_2 could occur on cycling in a

narrow window if it were the only product, extended charge to higher voltage is necessary in order to completely remove the remaining NaO_2 that is trapped due to the accumulation of decomposition products. However, cycling a cell with this upper limitation is not an ideal method to improve Na-O_2 cell cycling.

The effect of cycling a cell to an upper potential limit of 4.4 V is illustrated by the working electrode profile (**Figure 3.9a**). On subsequent discharge, an overpotential that preceeds the normal ORR discharge plateau is ascribed to the reduction of a species generated at high charge potential, although its nature has not yet been identified. In contrast to Hartmann *et al.*,[42] the cell can still discharge after it is charged to a high potential. Another difficulty with a high voltage charge cutoff is illustrated in **Figure 3.9b**, a plot of the potential of the working potential of the anode with respect to a sodium metal reference electrode. Charging a Na-O_2 cell to the voltage necessary to remove decomposition products is clearly detrimental to the anode. The overpotential required to strip sodium increases with each subsequent cycle, implying the growth of insulating layers that form on the metallic sodium anode. We speculate that this is due to the accumulation of decomposition products and impedance layers that form on the metallic sodium anode. This is in contrast to a cell operated within the potential window between 1.8 V vs. 3.0 V, (**Figure 3.11**) shows that the stripping/plating profile of the anode does not change upon cycling, and the stripping voltage is lower. Such a profile is similar to electrochemical stripping/plating of lithium in glyme-based electrolytes.[88] However, the cell is only able to achieve < 20 cycles with an upper voltage cut-off of 3.0 V (**Figure 3.12**) before capacity fading begins, followed by eventual cell termination. Visual inspection of the cathode (inset, **Figure 3.12**) suggests that accumulation of the discharge product on the cathode surface is the cause of cell termination. In short, other methods are necessary in order to completely charge the NaO_2 and remove the decomposition products since their removal via electrochemical charge not only requires a high overpotential, but also

acclerates decomposition on the anode.

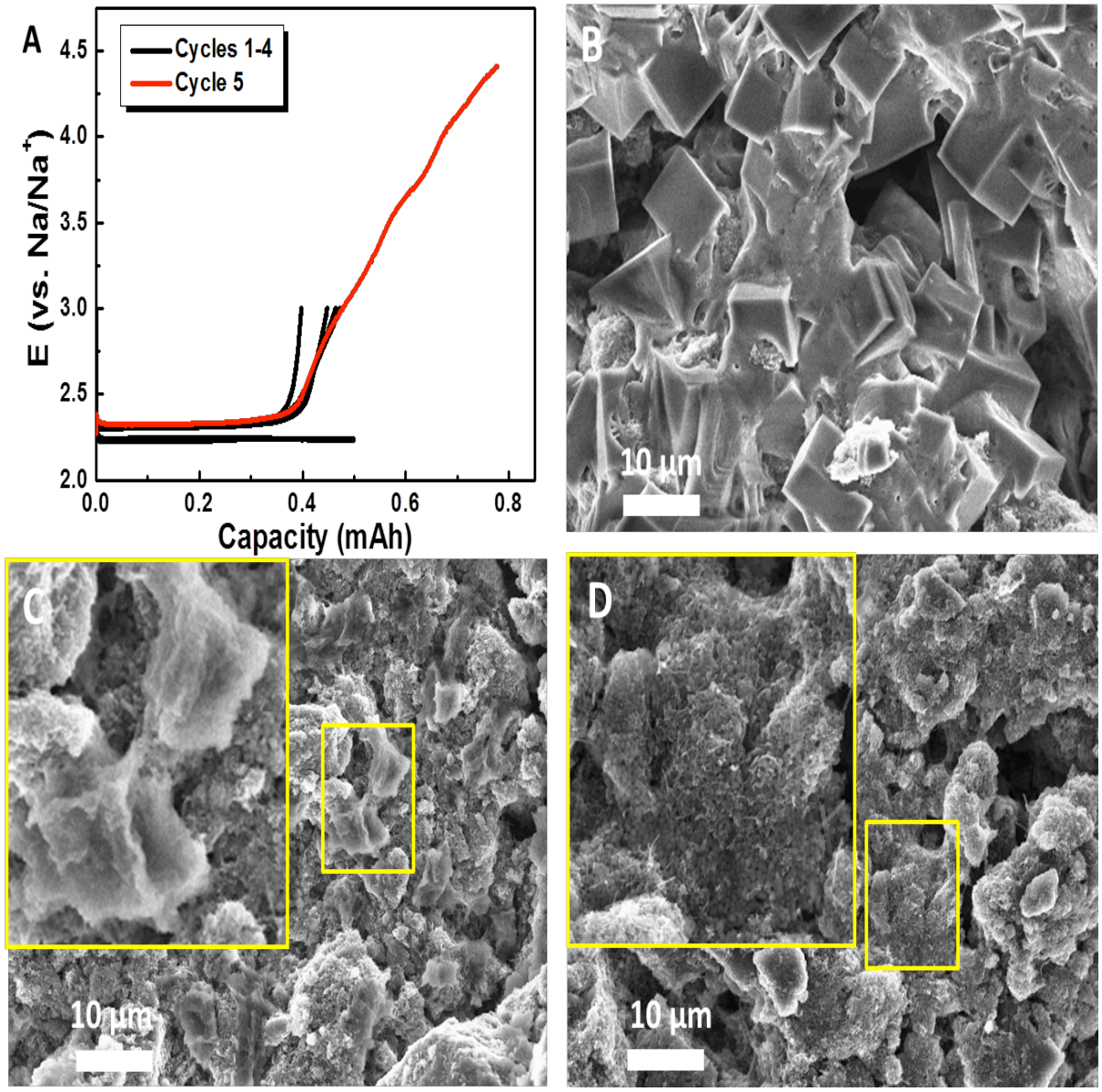

Figure 3.7 a) Electrochemical discharge/charge profiles of a ^{13}C cathode cycled 5 times, with the 5th charge ending at a voltage of 4.4 V. SEM micrographs of the cathode surface at b) the end of 5th discharge; c) the end of 5th charge to 3.0 V; d) the end of 5th charge to 4.4 V.

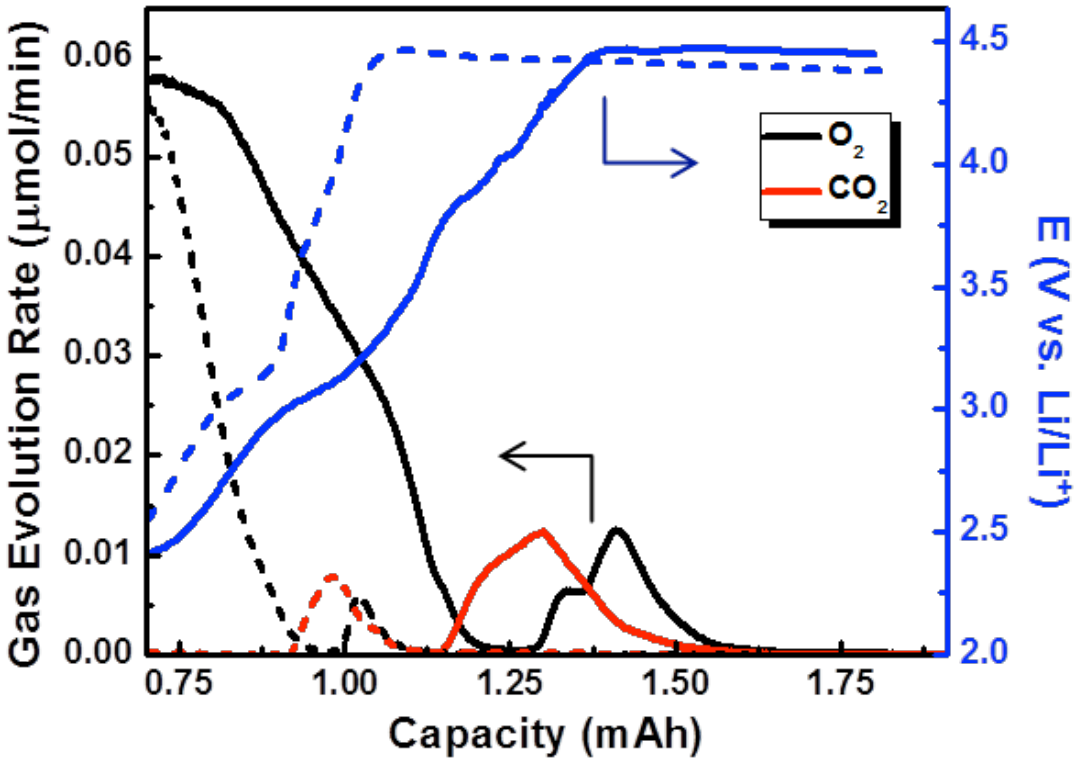

Figure 3.8 Electrochemical profile (blue curve) together with O_2 (black curve) and CO_2 (red curve) evolution profiles for a cell charged on the 1st cycle (dotted line) and the 5th cycle (solid line). The 5th charge was obtained after 4 cycles with a charge voltage limitation of 3.0 V and a capacity limitation of 1.0 mAh. The fraction of CO_2 and O_2 generated beyond 3.0 V is greater for the 5th cycle compared to the 1st cycle due to the respective oxidation of accumulated sodium carboxylates, and NaO_2 that could not be oxidized at V < 3.0.

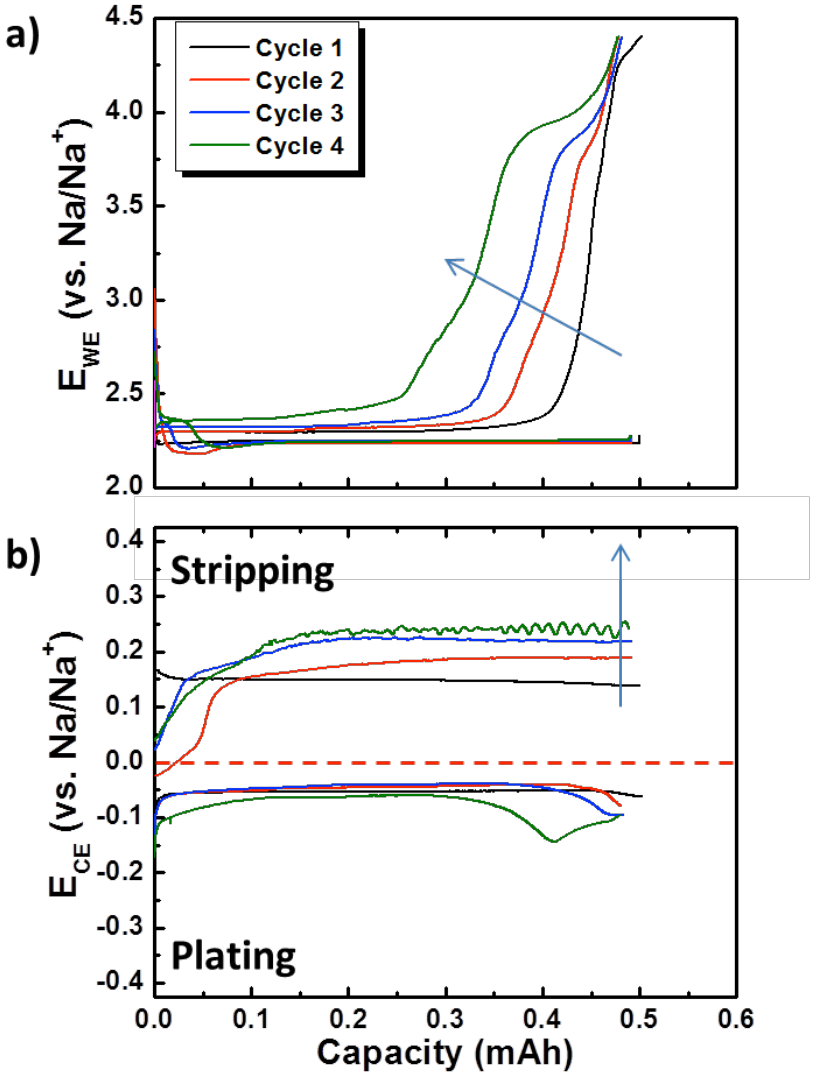

Figure 3.9 a) Working electrode and b) counter electrode potential of a Na-O_2 cell using a ^{13}C cathode cycled 5 times with an upper potential limit of 4.4 V. Plating of sodium onto the anode occurs when the cathode is charged, and stripping of the anode occurs when the cathode is discharged.

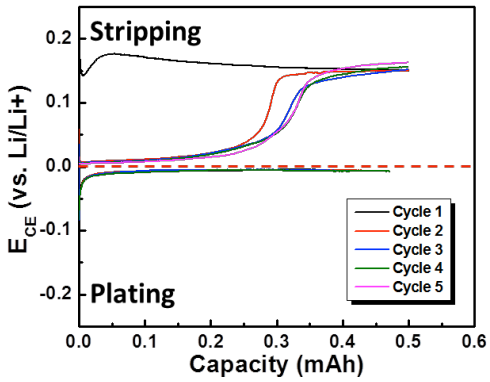

Figure 3.11 The voltage profile of the metallic metal negative electrode (*i.e.,* counter electrode) in a Na-O_2 cell cycled with a working electrode (^{13}C- carbon) cut-off potential of 3.0 V on charge. The stripping/plating profile shows very little variance from cycle to cycle.

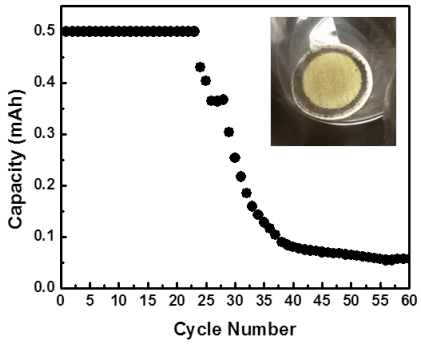

Figure 3.12 Discharge capacity as a function of cycle number of a ^{13}C cathode in 0.5 M NaOTf/15 ppm H_2O/diglyme electrolyte. The cell was operated with a capacity limitation of 0.5 mAh, in a voltage window of 1.8 – 3.0 V. Approximately 20 cycles are reached before capacity fade begins, where a rapid decrease in capacity is observed, that eventually leads to cell death. A post-mortem image of the cathode is shown in the inset.

.

3.7 Reactivity of superoxide/sodium superoxide at open circuit potential

Reactivity of NaO_2 with diglyme can be of concern for the lifetime of Na-O_2 cells that utilize this electrolyte, as any period of rest in a cell at open circuit voltage (OCV) could induce electrolyte decomposition and consumption of the superoxide. To "mimic" OCV conditions on discharge, diglyme was reacted with KO_2 in the presence of crown ether. Superoxide, *i.e.,* "solvated $O_2^{\bullet-}$" is liberated through chelation of K^+ ions with dicyclohexyl-18-crown-6 (crown ether).[89] This method was previously utilized to determine electrolyte stability.[26,81,90] For comparison, a second solution was prepared with the same concentration of KO_2/crown-ether, except sodium triflate was added to the reaction after 1 hour of reaction to immediately trigger precipitation of NaO_2. Reactivity of solvated $O_2^{\bullet-}$ can thus be partly distinguished from that of solid NaO_2, although we recognize that sodium superoxide itself has some - albeit limited - solubility in diglyme. After the solutions were allowed to stir to mimic cell conditions, the solids were recovered and analyzed with ^{1}H-NMR. Regardless of whether solvated $O_2^{\bullet-}$ or NaO_2 is present, formate and acetate are both observed; however, *3-5 fold more* of these products are generated in the presence of NaO_2 (**Figure 3.13**). Furthermore, the ratio of formate/acetate varies. In the presence of $O_2^{\bullet-}$, sodium formate is the most abundant decomposition product, and only minimal sodium acetate is observed (Na-acetate/Na-formate = 0.18). In the presence of NaO_2, the proportion of sodium acetate is three times greater (Na-acetate/Na-formate = 0.60). While we do not yet fully understand the reason for the observed difference, it may result from solution vs surface reactivity.

The reactivity of NaO_2 within the cell was further confirmed by discharging cathodes to a capacity of 1 mAh while holding the cell at open circuit for a period of 100 hours. SEM images that compare a freshly discharged cathode surface (**Figure 3.14a)** to a discharged cathode held for 100 hours (**Figure 3.14b)** show that the NaO_2 cubic morphology is greatly altered after extended diglyme exposure. A similar phenomena was observed by Hartmann *et al*.[42] In accord, the amount of NaO_2 determined by iodiometric titration is drastically reduced. Only 16 μmols of NaO_2 remain, which amounts to 43% of the theoretical value, and nearly 50% less than that of the NaO_2 content of a freshly discharged cathode (**Figure 3.14c**). X-ray diffraction analysis of the cathode, shown in **Figure 3.14d**, reveals that some of the NaO_2 converts to $Na_2O_2•8H_2O$, which would be expected to require a high voltage to oxidize. Compared to the freshly discharged cathode, the reduction in fraction of superoxide is also associated with a very large increase in the amount of carboxylate-based decomposition products (**Figure 3.14e**). While the fraction of sodium carbonate doubles during the rest period, the fraction of sodium acetate increases by as much as 50-fold, with a lesser increase in formate. This agrees with the quantification of the reaction products described above, which shows an increased fraction of sodium acetate resulting from contact of diglyme with NaO_2. The SEM images (**Figure 3.14a,b)** indicate that the interior of the NaO_2 cubes have been etched away in this process, leaving hollow outer shells. It suggests that the outer surface of the NaO_2 crystallites react with diglyme to form an incomplete passivating layer of side-product, and as the cubes crack, dissolution/reaction of the interior superoxide follows.

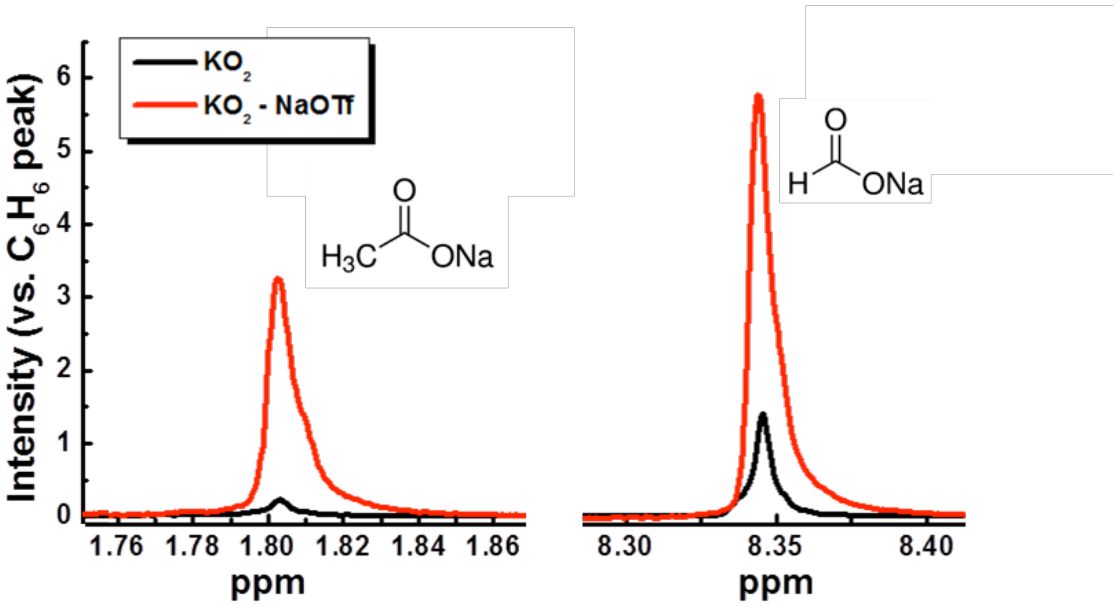

Figure 3.13 ^{1}H NMR solution spectra of D_2O-extracted solid products after exposure of diglyme to chemically generated $O_2^{\bullet-}$ for four days. Each reaction was conducted with 2.5 mL diglyme, 0.02 g KO_2, and 0.13 g crown ether (black line). To generate NaO_2, 0.1g of NaOTf was introduced into the solution at the same time as KO_2/crown ether addition (red line). The spectral peaks are assigned to sodium acetate (left) and sodium formate (right). Both spectra were normalized to an internal benzene standard.

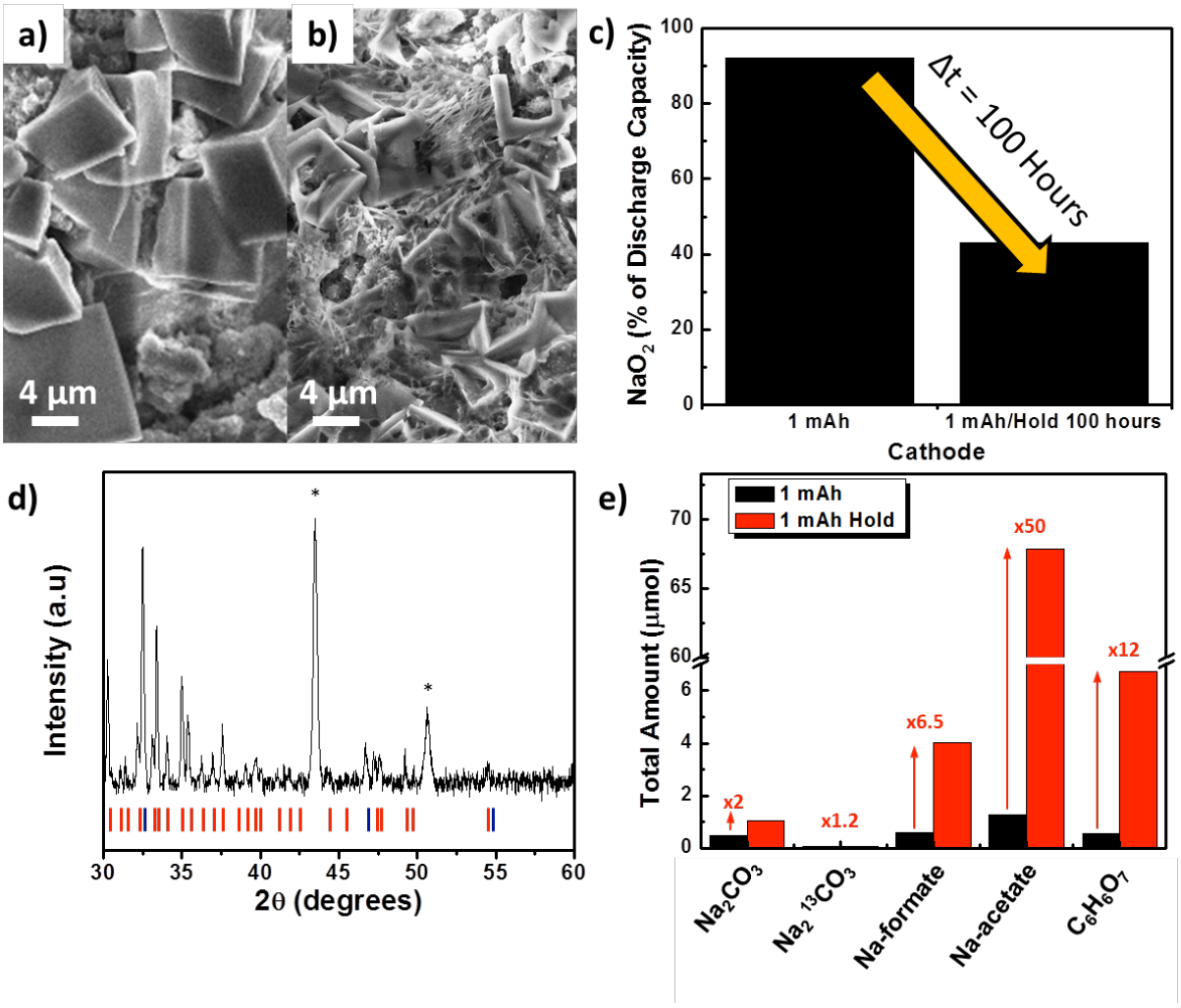

Figure 3.14 SEM images of a) a discharged cathode removed immediately upon completion of discharge; b) a discharged cathode rested at open circuit potential in the cell for 100 hours; c) comparison of the fraction of NaO_2 in the product at the end of discharge, and after 100 hours of rest based on the theoretical capacity of 1 mAh (37.7 µmols); d) X-ray diffraction pattern of the product of cell discharge after rest at open circuit for 100 hours. A mixture of Na_2O_2 (blue ticks) and $Na_2O_2•8H_2O$ (red ticks) is formed, as shown by comparison of the reflections to those in the JCPDS data base; asterisks represent the stainless steel mesh

current collector; e) Decomposition products of the freshly discharged cathode compared to the discharged cathode held at open circuit potential for 100 hours.

3.8 Conclusions

Our study regarding the decomposition products formed during operation of a Na-O_2 battery shows that on cell discharge, solvated O_2^- and NaO_2 react with both the carbon cathode and the diglyme electrolyte on discharge to form a variety of Na-carboxylate decomposition products. On charge, minimal additional decomposition occurs. The consumption of NaO_2 through chemical reactivity with diglyme (to form sodium carboxylates) gives rise to the majority of the capacity loss. Even in the presence of these decomposition products, a large overpotential is not observed for the oxidation of NaO_2 (in contrast to the case of the Li-O_2 battery) due to the dominance of a solution-based process mediated by a phase transfer catalyst. However, since the decomposition products cannot be oxidized within the narrow electrochemical window that ideally characterizes the Na-O_2 cell; they accumulate over many cycles, leading to cell death. This is different from the Li-O_2 cell, where electrolyte degradation is acclerated on charge owing to inherently high overpotentials unless redox mediators are invoked. In the Li-O_2 cell, the rapid conversion of lithium superoxide to lithium peroxide means that superoxide does not aggravate glyme degradation on discharge. Thus, while the low charge overpotential of the Na-O_2 cell does limit the amount of decomposition products that form on charge, the highly reactive $O_2^{\bullet-}$ (or HO_2), as well as the nucleophilic character of the NaO_2 itself, make glyme-based electrolyte degradation in the NaO_2 cell a very real concern. This is especially true on storage unless the cell is fully charged, because the formation of $Na_2O_2 \bullet 8H_2O$ occurs upon extended exposure, which would require a high voltage to oxidize. The performance of the Na-O_2 cell is nonetheless very

promising because of its low overpotential, and once significant improvements in electrolyte stability are discovered, very good cycling properties and charge efficiency can be expected.

Chapter 4: Design and synthesis of electrolyte solvents for Li, Na-O_2 batteries

4.1 Introduction

The most prominent challenge to overcome in order to achieve a working Li or Na-O_2 battery is to find a suitable electrolyte that would be stable towards superoxide radical species produced during discharge. Although the search for more stable systems has resulted in many investigations of different solvent/salt combinations, it is generally agreed that there is presently no electrolyte that fits these requirements. A few classes of solvents that have been studied are listed below.

4.1.2 Alkyl carbonates

Alkyl carbonates have been extensively studied for Li-O_2 batteries as they are used for Li-ion batteries.[31] A study on the decomposition mechanism of the carbonates in the presence of superoxide radical showed that the nucleophilic attack takes place at the less hindered ethereal carbon rather than the carbonyl carbon (**Scheme 4.1**).[27,30,91] This results in the ring opening of the carbonates, leading to the formation of the peroxide ion which is shown to be more reactive than the superoxide ion. The compounds formed as a result of these reactions were confirmed by IR, NMR and XRD studies. Mccloskey *et al*.,[30,31] studied using atom labelling with ^{13}C and DEMS analysis that during charging of carbonate based cells, there

was a little evolution of oxygen initially. This was then followed by a predominant evolution of CO_2 that evolved primarily due to electrolyte decomposition.

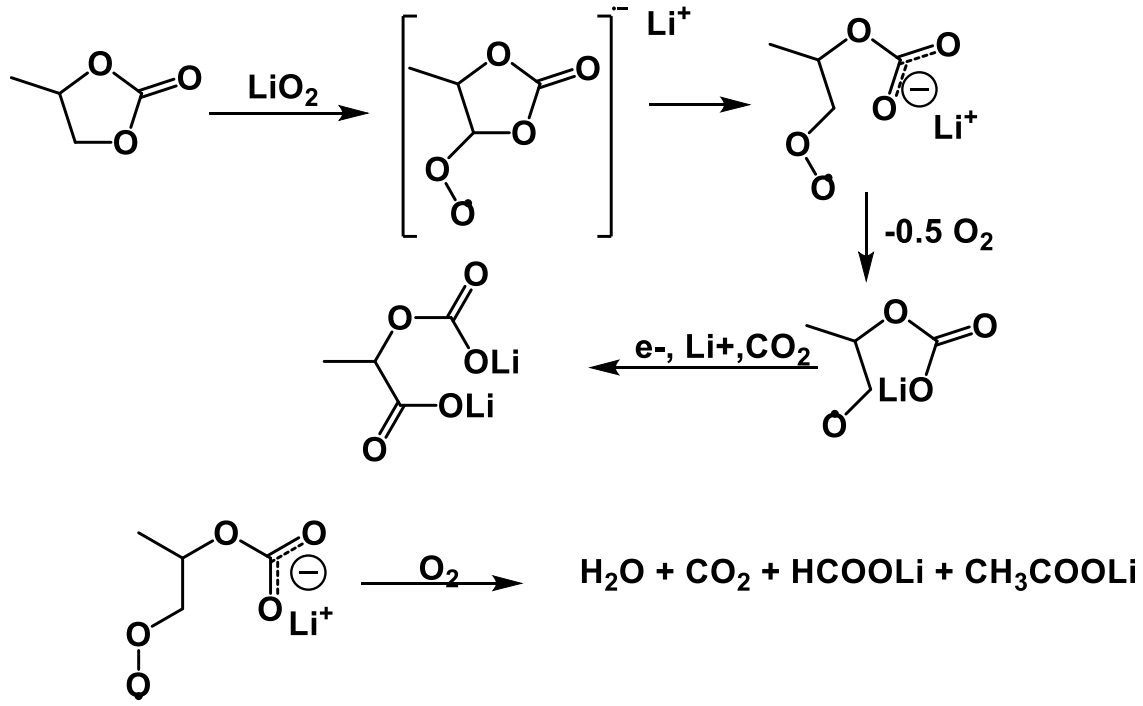

Scheme 4.1

4.1.3 Esters

Cyclic esters usually exhibit high polarity along with high viscosity, while linear esters exhibit low polarity and low viscosity. A mixture of these two esters was an ideal choice as an electrolyte.[92] As with the case of carbonates, esters also undergo nucleophilic attack by the superoxide species. Along with this drawback, it was also found out that esters are not stable with metallic lithium, *i.e.*, a stable solid electrolyte interface (SEI) could not be formed on the surface of the lithium metal.[93]

4.1.4: Nitriles

Nitriles are a category of solvents which could be potentially used as an electrolyte for both the Li and Na-O_2 batteries owing to their high electrochemical oxidative stability as well as stability towards superoxide species.[31,94] The major drawback with nitrile solvents is their instability with lithium or sodium. These react exothermically with nitrile based solvents and thus, once a proper protective membrane for the negative electrode is formulated, these class of solvents could potentially end up being the solvents of choice for the metal-O_2 battery systems.

4.1.5 Sulphones

Quantum chemical calculations have shown that sulphones are fairly stable against the superoxide radical species.[95,96] This calculation has been confirmed by the use of sulpholane such as tetramethylene sulphone. The major problem with sulphones is that most are solids at room temperature, which becomes an inconvenience when applying them as electrolyte solvents. A particular example of a sulphone that does not fall into the category of solids is methylmethoxyethylsulfone (M.P 2˚C).[97] This compound, although a liquid at room temperature, has a very high viscosity.

4.1.6 Amides

Theoretical calculations have predicted that amides are stable against the attack of the superoxide species.[98] The most commonly employed amides are the *N,N*-dialkyl compounds.[85] One of the major disadvantages involved with these compounds are their reactivity towards the anode to form an unstable SEI which inhibits the function of the

battery.[99] Along with this, a number of side reactions are observed as shown in **Scheme 4.2**. The decomposition products formed are the result of the nucleophilic attack at the carbonyl carbon.

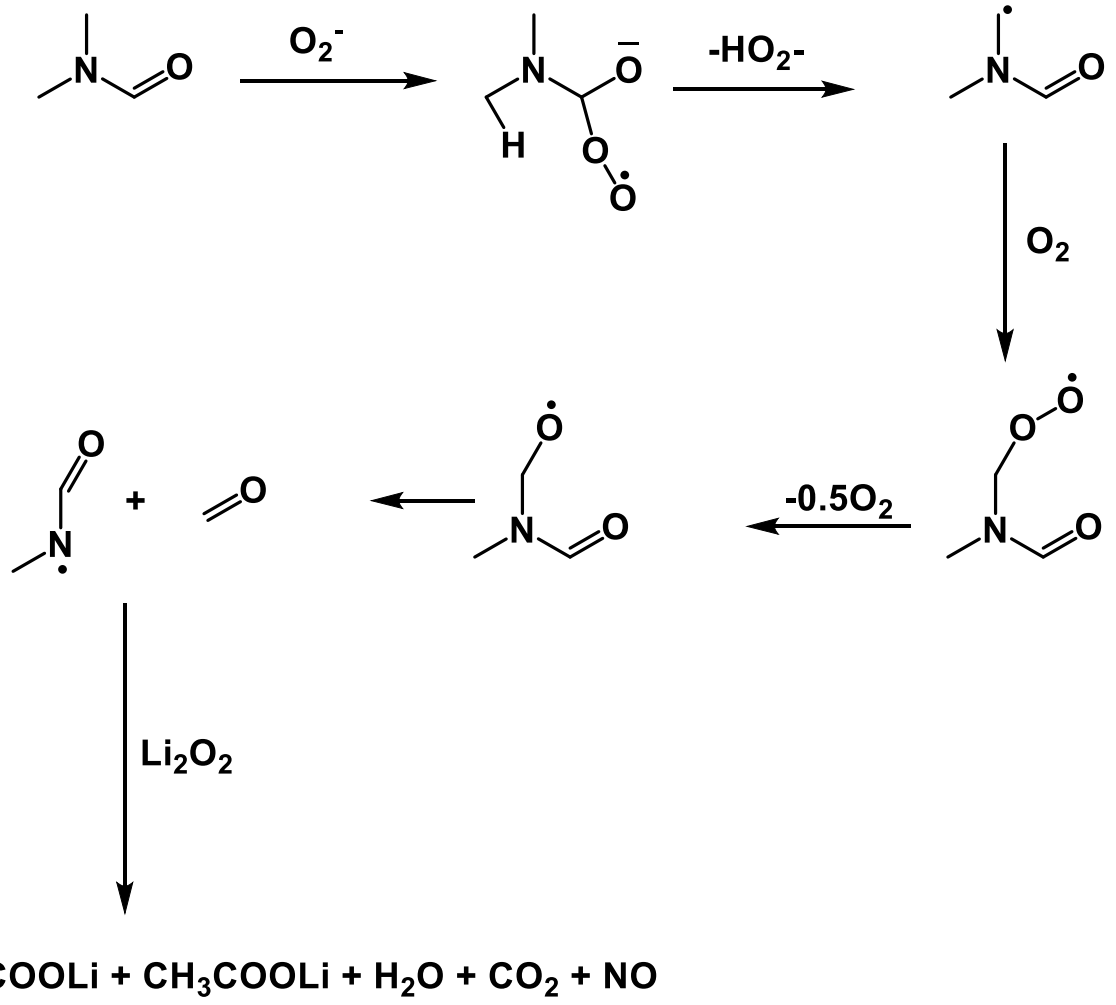

Scheme 4.2

4.1.7 Ethers

At present, ethers are the class of solvents that satisfy most of the required properties needed as an electrolyte solvent for a Li or Na-O_2 battery. DME, diglyme, TEGDME are widely employed as solvents owing to their low viscosity, high ionic conductivity, high boiling point

(diglyme and TEGDME), good SEI forming ability on the metallic anode and *quasi*-stability towards superoxide species. As observed in **Chapter 3**, glymes themselves undergo decomposition through a hydrogen abstraction mechanism (**Figure 3.6**).

Over the last two years, no work has been published on a new electrolyte solvent for the Li-Na-O_2 batteries except for the work of Adams *et al*.[81] carried out in the Nazar lab. In that work, dimethyl pinacol or 2,3-dimethoxy-dimethyl butane (DMDMB) was successfully synthesized and its performance in a Li-O_2 battery was evaluated. By substituting the methylene hydrogens with methyl groups, decomposition path 2 in **Figure 3.6** was avoided. Although not an ideal solvent, this provided a motivation to pursue further studies into the synthesis of other solvents based on a similar process of inhibiting decomposition reactions.

4.2 Derivatizing DMDMB

One of the major problems with DMDMB was that it could only dissolve lithium bis(trifluorosulphonimide), [LiTFSI], in one particular molar ratio (2:1 of solvent to salt). This resulted in the system having high viscosity and low ionic conductivity requiring tests to be carried out using low current rates and at higher temperatures in order to achieve better kinetics.[81]

To overcome the problem of high visocosity, we decided to introduce a methylene linkage between the tertiary carbons in the DMDMB molecule leading to compound **2,** otherwise known as 2,4-dimethoxy-dimethyl pentane (DMDMP). This molecule was successfully synthesized according to **Scheme 4.3**

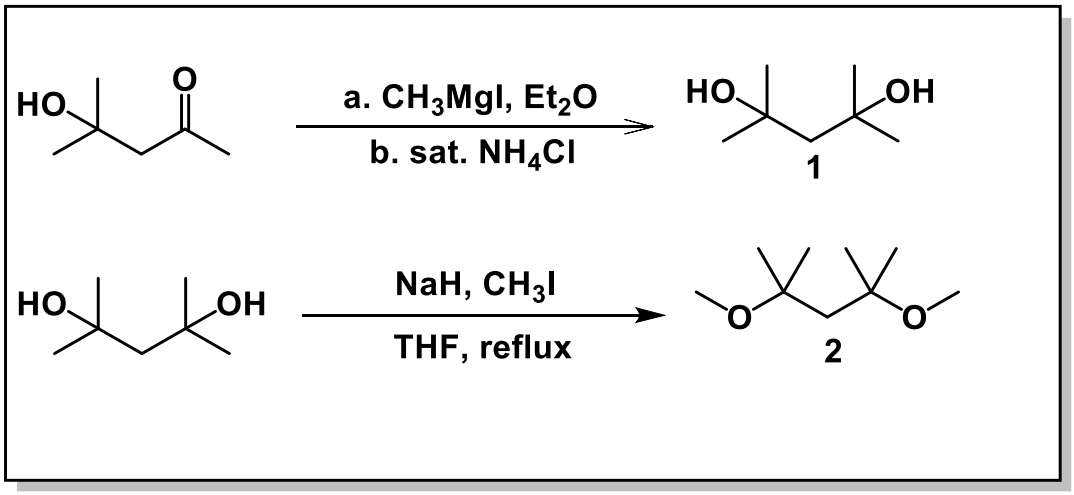

Scheme 4.3

In order to understand the effect of the introduced methylene linkage, a new compound with the methylene linkage substituted with methyl groups was also synthesised (compound **5**) according to **Scheme 4.4**.

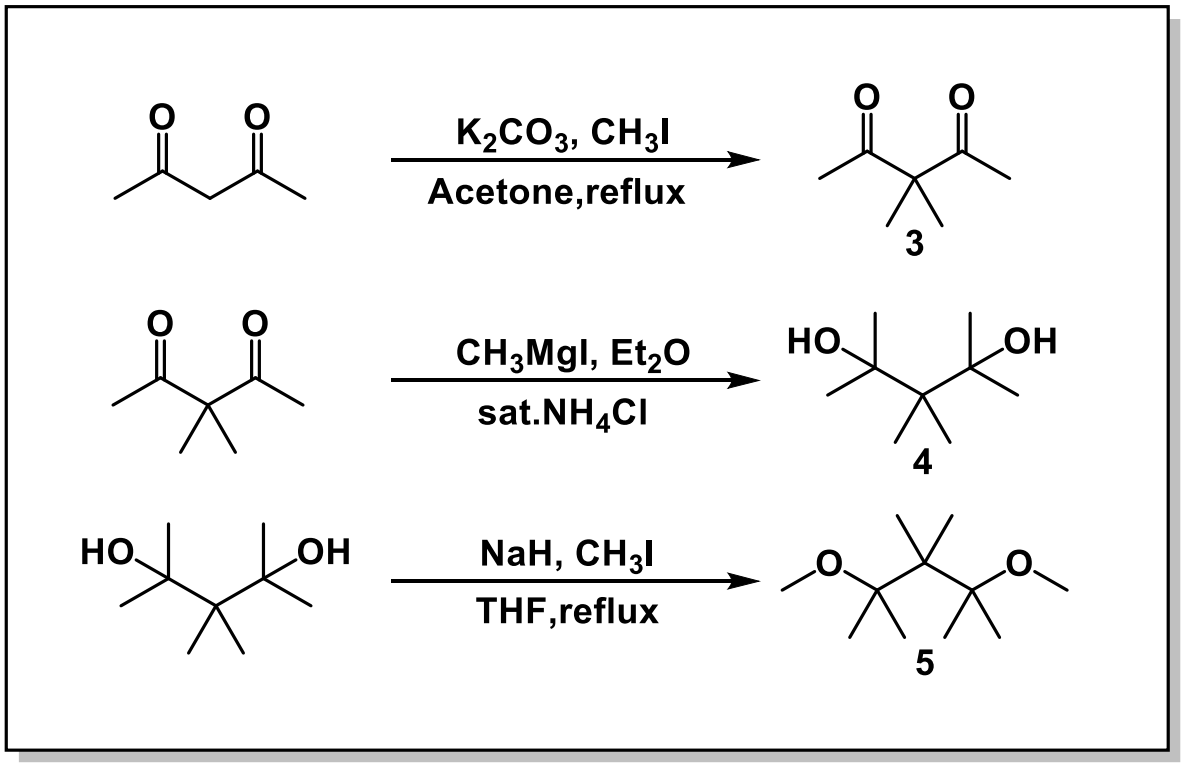

Scheme 4.4

Once compounds **2** and **5** were made, the solubility of the salt was the next test to conduct. Unfortunately both compounds **2** and **5** were unable to dissolve any of the salts (**Table 4.1**) commonly used for both Li and Na-O_2 batteries. Although a clear reason for this phenomenon is not established, it is assumed that the Lewis basic sites in both **2** and **5** are sterically hindered by the methyl groups, thus preventing any sort of interaction between the cation of the salt and the solvent molecule.

Lithium bis(trifluoromethylsulphonimide)
Lithium trifluoromethylsulphonate
Lithium hexafluorophosphate
Lithium bis(oxalatoborate)
Sodium triflate
Sodium bis(trifluoromethylsulphonimide)

Table 4.1 List of salts used to dissolve in solvent

As the opportunity to use these compounds as a single solvent was ruled out, the next step was to identify if it would be possible to use it as a co-solvent along with DMDMB. No convincing results were obtained when such a system was formulated.

4.4 *N,N*-Dimethyl triflamide

Over the past 100 years, the use of sulphonamides in electrolyte chemistry has been reported just once, where methyl sulphonamide was used as an electrolyte additive for a lithium ion

battery.[100] Most of the sulphonamides are solids at room temperature, and hence to achieve liquids as working solvents is quite difficult. One of the few ways to make liquid sulphonamides is to introduce fluorine into the molecule. *N,N*-dimethyl triflamide (compound **6**) was successfully synthesized according to **Scheme 4.5.**

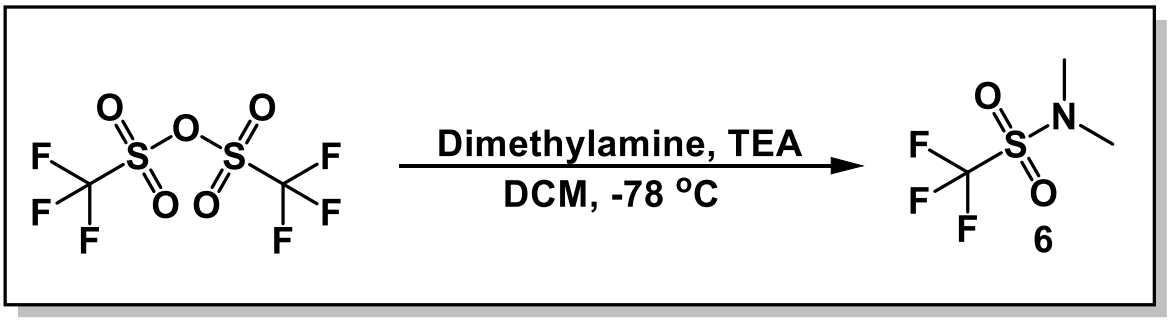

Scheme 4.5

Compound **6** was obtained in high yield and readily dissolved the LiTFSI salt. It did not dissolve any of the sodium salts, and thus its use was restricted to Li-O_2 batteries. **Table 4.2** lists certain properties of the DMT solvent.

Boiling point	172-173 ˚C
Density	1.64 g/mL
Ionic conductivity (1M LiTFSI)	1.63 mS/cm
Viscosity (1M LiTFSI)	4.33 mPa.s

Table 4.2 Properties of the DMT solvent

As can be seen from **Table 4.2**, almost all the properties suggest that this solvent could actually prove to be a good electrolyte solvent for Li-O_2 batteries.

4.4.1 Electrochemical window

Prior to testing any materials performance in Li-O_2 batteries, the stability towards lithium and its ability to withstand oxidation within the operating voltage of a Li-O_2 battery needs to be analysed. Cyclic voltammograms were carried out with 1 M LiTFSI in DMT with lithium as the working and the reference electrode and stainless steel as the counter electrode and is shown in **Fig 4.1**.

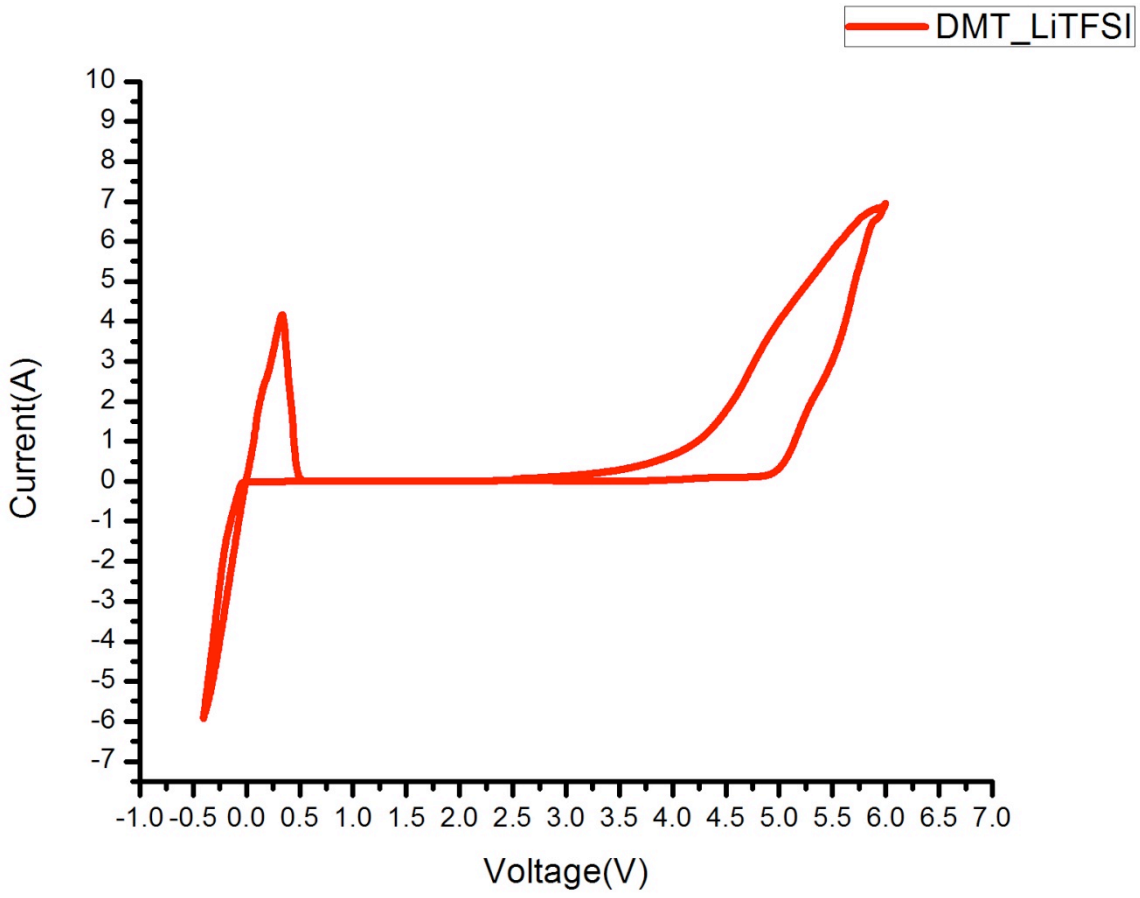

Figure 4.1 CV of 1M LiTFSI in DMT solvent

Fig 4.1 is a clear indication that the solvent is stable with lithium, as can be seen with the stripping of lithium starting beyond 0 V. It also shows the high oxidative stability of the system because oxidation starts at about 5.2 V. Not only does this prove the concept of the stability of sulphonamides, but it provides us with a solvent that can operate within the voltage window of the Li-O_2 battery.

4.4.2 Performance in a Li-O_2 battery

With the stability issue in terms of the voltage window satisfied, the DMT electrolyte was put in practise for a Li-O_2 battery. Based on our knowledge about mechanistic pathways of superoxide attack, this molecule could decompose along path 1 (**Figure 3.6**) leading to the formation of formate type products. The 1st cycle of a cell cycled at 50 μA is shown in **Figure 4.2**.

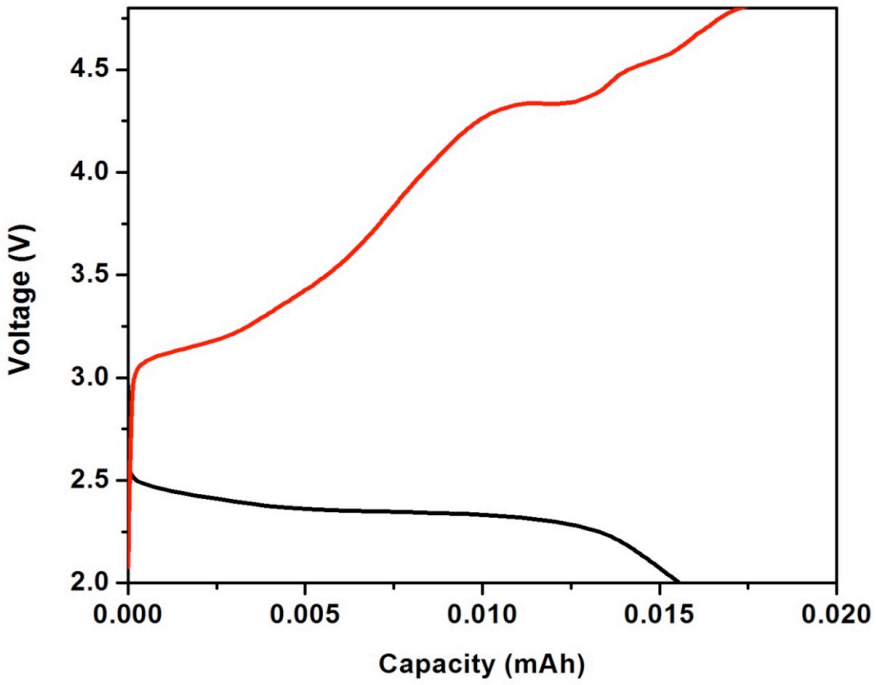

Figure 4.2 1st cycle of DMT electrolyte in a Li-O_2 battery

Figure 4.2 shows us that the cell could be discharged to only about a 0.015 mAh capacity when the voltage cut off was at 2 V and that there is an overpotential during charge which resembles Li-O_2 batteries tested with electrolytes prone to decomposition. This cell was tested with a carbon based cathode, and therefore there is a possibility of side products formed from the reaction of Li_2O_2 with carbon to produce lithium carbonate. The cell could not even discharge properly, and so the stability of the electrolyte with the superoxide species needed to be first evaluated.

4.4.3 Superoxide stability

The DMT electrolyte was subjected to the superoxide stability test by treating it with potassium superoxide. The ^{1}H NMR spectra before and after the reaction with KO_2 is shown in **Figures 4.3** and **4.4** respectively.

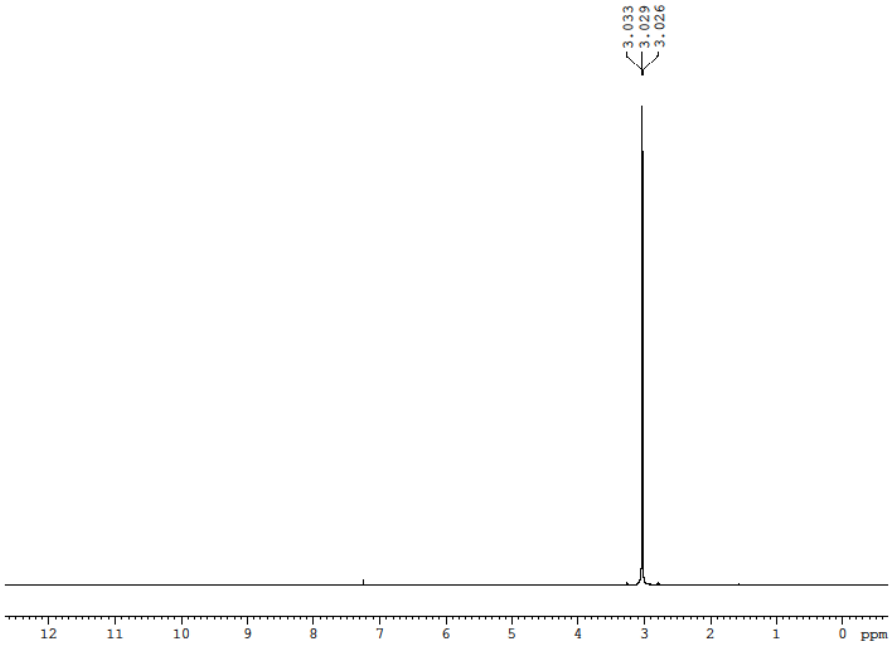

Figure 4.3 ^{1}H NMR spectra of pure DMT in $CDCl_3$.

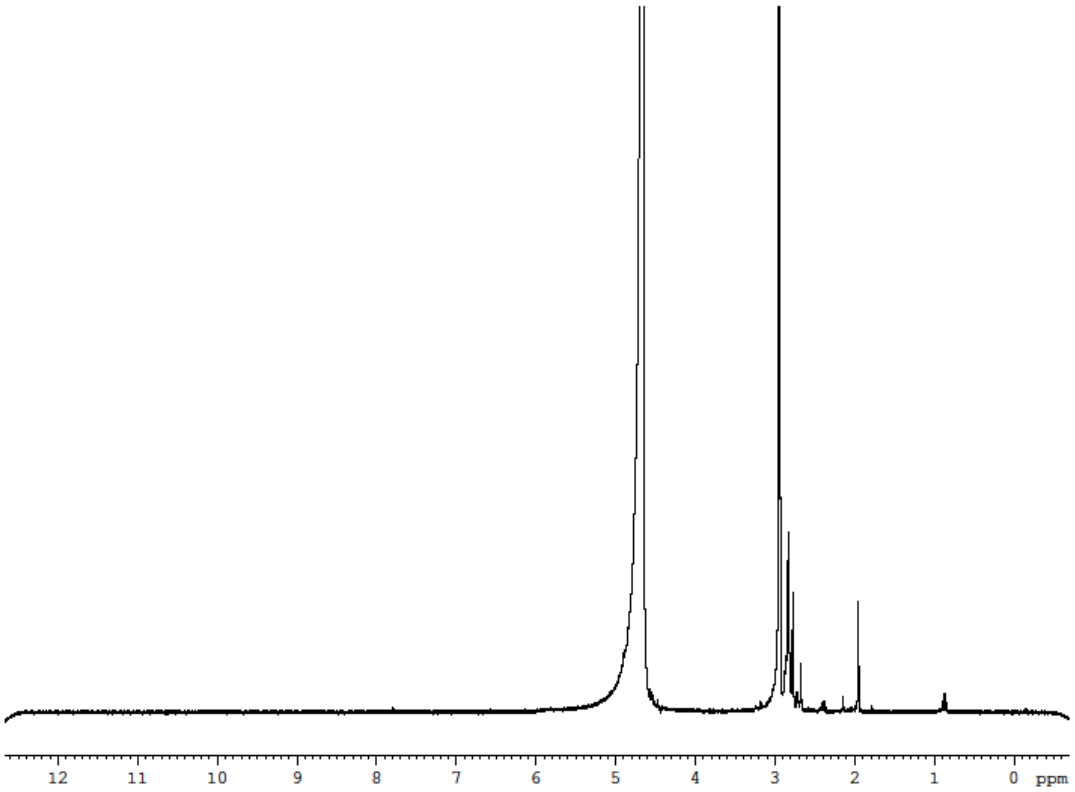

Figure 4.4 ^{1}H NMR spectra of DMT after reaction with KO_2 in D_2O.

Surprisingly no formate was observed when the electrolyte was treated with KO_2, but quite a significant amount of acetate was observed as can be seen from **Figure 4.4**. The reason for the formation of only acetates in reaction with KO_2 is difficult to explain due to the presence of only three carbon atoms in the molecule, and one of them is a CF_3 group. Further work is being carried out to arrive at a reasonable mechanism to show the formation of acetates from the DMT solvent.

Further studies on this solvent will involve utilizing different cathode materials at lower current rates to get a clear idea of the behaviour of DMT as an electrolyte solvent.

4.5 Molecules with tertiary carbons next to heteroatoms

We had observed that the presence of any protons on a carbon atom adjacent to a heteroatom, results in electrolyte decomposition due to the superoxide radical. One way to avoid this is to have molecules that have tertiary carbon atoms next to heteroatoms. **Compound 7** (dimethyl methylene ditrilfone) was one such molecule and it was synthesized according to **Scheme 4.6**.

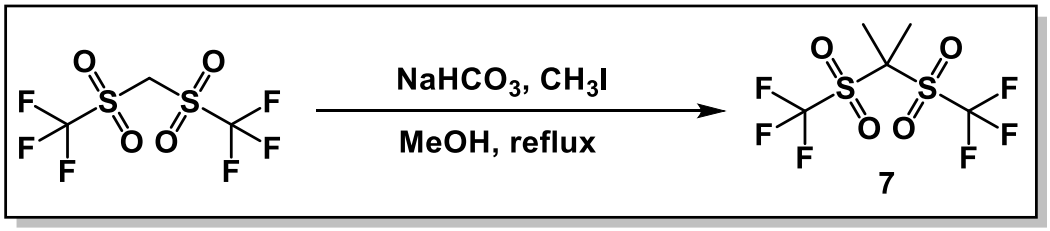

Scheme 4.6

This molecule was chosen based on the fact that the starting material was a low melting solid (M.P 30 ˚C). By introducing branching, it was believed that the molecule will lose the ability to pack well within its framework and thus be a liquid at room temperature.

Unfortunately compound **7** was a solid at room temperature, and had a melting point of 170 ˚C. Further work is being carried out in attempts to increase the chain length on the alkyl fragments introduced, which may result in the molecule to exist as a liquid at room temperature. But as we have observed before, increasing the side chain could potentially introduce a steric problem thus leading to an inability to dissolve salts.

4.6 Experimental

4-hydroxy-4-methyl-2-pentanone,acetyl acetone, trifluromethanesulphonic anhydride, sodium hydride (60% in mineral oil), potassium carbonate, methylmagnesium iodide solution in diethylether (3M), triethyl amine were purchased from Sigma Aldrich and were used as received. Anhydrous dimethyl amine was purchased from the Linde gas group.

All reactions were carried out in flame dried or oven dried glassware. ^{1}H, ^{13}C, ^{19}F were recorded on a 300 MHz Bruker Advance spectrometer at room temperature. Melting points were obtained with a Mel-Temp II instrument.

4.6.1 Synthesis

Compound 1:[101]

To 2.2 equivalents of methyl magnesium iodide in diethylether in a flame dried flask fitted with a reflux condenser was added slowly 1 equivalent of 4-hydroxy-4-methyl-2-pentanone dissolved in diethylether with continuous stirring. Once the bubbling had stopped, the mixture was allowed to stir for a further 30 mins, after which sat. NH_4Cl was added. The organic phase was separated, and the aqueous phase was washed with diethyl ether two more times. The combined organic phases were dried, and concentrated at reduced pressure to give a yellow oily liquid which was used without further purification. (Yield: 68%. Analytical data consistent with previously reported.)

Compound 2:[81]

To a three neck flask fitted with an addition funnel and a reflux condenser was added 2.2 equivalents of sodium hydride in THF under nitrogen. Compound **1** was dissolved in THF and transferred to the addition funnel and was added slowly to the NaH solution with rapid stirring. Once the addition was complete, the mixture was refluxed for 12 hours and cooled to 0 ˚C using an ice bath. 2.2 equivalents of methyl iodide was slowly added using a syringe pump over a period of 15 mins at 0 ˚C. After the addition, the mixture was allowed to warm to room temperature and was further refluxed for another 12 hours. The mixture was filtered and concentrated under reduced pressure to give an orange liquid which on distilling at reduced pressure afforded **2**.(Yield 75%;B.P 210 ˚C at 760mm of Hg;) ^{1}H NMR(300 MHz in $CDCl_3$): δ 3.15 (s, 6H), 1.68 (s,2H), 1.22 (s, 12H). ^{13}C NMR (75.5MHz. in $CDCl_3$) δ 74.46, 48.22,46.85,25.85.

Compound 3:[102]

To a two neck flask fitted with a reflux condenser was added 2.5 equivalents of potassium carbonate in acetone under nitrogen. To this mixture was added 1 equivalent of acetyl acetone and the mixture was allowed to reflux with stirring for 12 hours and cooled to 0 ˚C using an ice bath. 2.5 Equivalents of methyl iodide was added slowly to the mixture using a syringe pump over a period of 15 mins at 0 ˚C. After the addition, the mixture was allowed to warm to room temperature and was further refluxed for another 12 hours. The mixture was filtered and concentrated under reduced pressure to give a light yellow liquid which on distilling under reduced pressure afforded **3**.(Yield 81% . Analytical data consistent with previously reported.)

Compound 4:

The same procedure for **1** was used with substitution of 4-hydroxy-4-methyl-2-pentanone with compound **3** to produce **4**. (Yield 65%. Analytical data consistent with previously reported)

Compound 5:

The same procedure for **2** was used with substitution of **1** with **4** to produce **5**. (Yield 45%; B.P 220 ˚C at 760mm of Hg; ^{1}H NMR(300MHz in $CDCl_3$) : δ 3.23(s. 6H), 1.26 (s, 12H), 0.91(s, 6H). ^{13}C NMR(75.5 MHz in $CDCl_3$) δ 73.2, 48.3, 46.2, 25. 6, 18.1.

Compound 6:[103]

To a two necked flask fitted with a dry ice condenser, connected to a bubbler was added triethyl amine (1 eq) in dichloromethane at -78 ˚C under nitrogen. Dimethyl amine was passed through the mixture for a period of 15 mins at -78 ˚C. Trifluoromethanesulfonic anhydride (1 eq) was added dropwise to the mixture using a syringe pump over a period of 15 mins. The reaction mixture was further stirred for 2 hours at -78 ˚C. The reaction mixture was warmed to room temperature and once all the excess dimethyl amine had evaporated, water was added. The aqueous phase was extracted with dichloromethane twice and the combined organic phases was washed with brine, dried, filtered, and evaporated to dryness under vacuum to afford a light yellow liquid, which upon distillation under reduced pressure afforded **6**. **(**Yield 84%; Analytical data consistent with previously reported).

Compound 7:

2 equivalents of sodium bicarbonate was added to methanol under nitrogen. To this mixture was added 1 equivalent of methylene ditriflone (Synquest labs) with rapid stirring. The

mixture was refluxed for 3 hours, and cooled to 0℃, when 2 equivalents of methyl iodide were added. The mixture was further refluxed for 12 hours. The mixture was filtered, and concentrated under reduced pressure to afford brown crystals, which were recrystallized with hot chloroform to afford white crystals of **7**. **(**Yield 56%; M.P 173 ˚C; ^{1}H NMR(300 MHz in D_6 [DMSO] : δ1.79 (s, 6H). ^{19}F NMR (282 MHz in D_6 [DMSO]: δ -80.1 . ^{13}C NMR (75.5 MHz in D_6[DMSO]: δ 120 (q), 54.3, 13.2.

4.6.2 Electrochemistry

Cyclic voltammograms were carried out on a VMP-3 instrument (Biologic) using a coin cell setup, with lithium as the working and the reference electrode and stainless steel current collector as the counter electrode.

Li-O_2 batteries were made with a modified Swagelok^{TM} design. Cells were assembled in an argon filled glovebox with a lithium metal anode, Millipore glass fiber separators and a gas diffusion electrode as a cathode. 90 μL of electrolyte was added to the separators during assembly.

4.6.3 Viscosity and ionic conductivity

The viscosity was measured using a μVISC viscometer (Rheosense) and the appropriate chip (0-100 mPa.s or 100-20000 mPa.s) and the ionic conductivity with a 3-star conductimeter (Orion) equipped with a 2-electrode epoxy conductivity probe (cell constant of 1.0 cm^{-1}).

4.7 Conclusions and future work

The search for a working electrolyte solvent for the Li-O_2 battery is regarded with the highest priority within battery chemists as it could very well bring the technology a step closer towards actual application. With such a taxing environment for the solvent to operate in *i.e.*, contact with a strong reducing agent (lithium), superoxide radical, which is considered highly nucleophilic and a broad voltage window to operate in, finding a suitable electrolyte is considered extremely difficult. Up to now, many molecules have been investigated, and yet an ideal solvent has not been discovered.

With all the work that has been carried out, the next step going forward is to diverge from molecules that contain protons. Compound **8** can be made and could potentially overcome the problem of stability towards superoxide species.

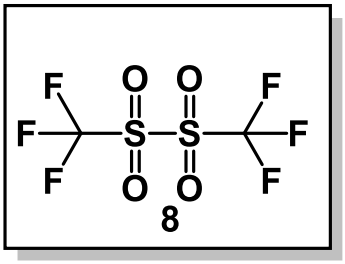

8

Another aspect of research that can help find a suitable electrolyte solvent is to focus on finding newer salts which could dissolve easily in hydrophobic solvents. The most important field of research that could potentially help with the electrolyte research is to find a suitable protective membrane for the lithium anode. Further research is being focussed on this field at the moment, primarily because of the inability to find a suitable solvent. Perfluorinated ethers can prevent superoxide attack, but they have very low solubility for lithium salts.

Chapter 5: Inhibiting the polysulphide shuttle in Li-S batteries through low-ion pairing salts coupled with a novel electrolyte solvent

5.1 Introduction

Lithium batteries based on elemental sulphur are one of the most promising candidates as successors to the insertion based Li-ion technology.[104] Sulphur is exceedingly abundant, inexpensive, and exhibits a high theoretical specific capacity of 1672 mAh/g based on the reaction (Eq 5.1)[60,105]

$$S_8 + 16Li \rightleftharpoons 8Li_2S \qquad \text{[Eq 5.1]}$$

However, there are numerous problems with practical Li-S cells that arise from the complex discharge process during which multiple redox equilibria occur. Lithium polysulphide intermediate species Li_2S_n ($2< n <8$) readily dissolve into the organic solvents commonly used in electrolytes.[47,104,106] Their migration to and from the negative electrode creates a redox "shuttle" phenomenon that can lead to poor coulombic efficiency, loss of active material from the positive electrode on repeated cycling, and impedance build up on the electrode surfaces.[48,53] On the other hand, electrochemical reactions that occur in solution offer the advantage of faster kinetics compared to the solid state, especially when the solid products exhibit ultra-low electronic conductivities, which is the case for both sulphur and Li_2S.[53]

Therefore design of an optimized electrolyte solvent or solvent blend for the Li-S system is of utmost importance.[47,50,58] Along with the properties mentioned above, the electrolyte also needs to meet certain critical properties, such as a wide voltage window, sufficient Li^+

conductivity to ensure rate capability, and stability with respect to chemical attack from Li_2S_n species formed during discharge.[51,53]

5.1.1 Previous work

Many approaches have been made to tackle the parasitic polysulphide shuttle in Li-S_8 batteries through modifying cathode architecture,[107] but only a handful of approaches have been made through altering electrolyte systems. Cuisiner *et al.*[62] reported an electrolyte system based on a solvent-salt complex using acetonitrile and LiTFSI as the solvent and salt, respectively. They reported an acetonitrile-LiTFSI 2:1 complex which completely supressed polysulphide solubility [**Figure 5.1**]. Since all of the acetonitrile molecules were effectively bound by the formation of the 2:1 complex, reaction with metallic lithium is prevented.

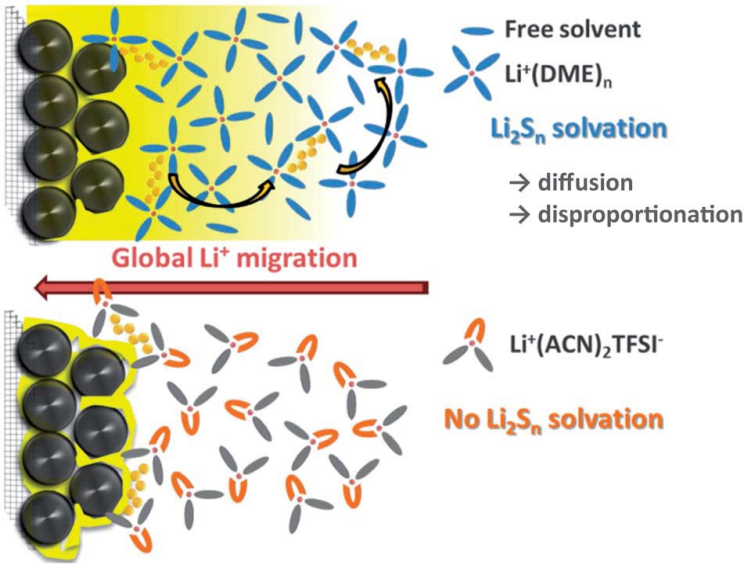

Figure 5.1 Schematic illustration of the (acetonitrile)$_2$: LiTFSI complex

Due to the high concentration of the salt, the viscosity of the electrolyte was extremely high (138 cP). Thus they used a hydrofluoroether (HFE), which did not affect the ability to solvate polysulphides due to the high extent of fluorination present in the molecule. By incorporating

HFE into the electrolyte system the viscosity was drastically lowered (8.6 cP) and better kinetics with regard to sulphur utilization was achieved. They reported a capacity of 750 mAh/g (44% of the theoretical value) over 100 cycles at rates of C/5 and almost 98% coulombic efficiency.

Although the approach of having a super concentrated electrolyte (9.7 M) provided positive results in terminating polysulphide shuttle in Li-S batteries,[52,61] a more straightforward approach would be to use a solvent which will inherently avoid polysulphide solubility without any modification. These solvents (usually of low polarity) do not dissolve the usual Li-battery salts used and thus, a new class of salts need to be utilized to implement this approach.

5.1.2 Low ion-pairing salts

Conventional electrolyte salts that are used for a Li-S battery are shown in **Figure 5.2**. Among these the most commonly used salt is LiTFSI, owing to its stability towards nucleophilic attack by the polysulphide species.[108]

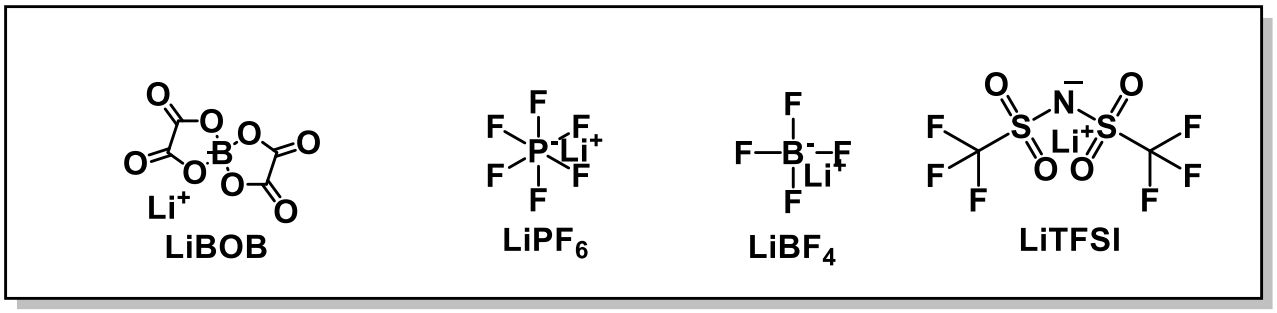

Figure 5.2 Electrolyte salts used for a Li-S_8 battery

Any solvent that dissolves LiTFSI, is believed to dissolve lithium polysulphides, and thus it is essential to utilize or develop a salt that exhibits low ion pairing between the ionic

species'.[109] With this category of salt, we would be able to dissolve a lithium salt in a solvent that does not dissolve polysulphides.

Low ion pairing salts are salts that contain weakly coordinating anions. These anions have electron withdrawing groups attached to the central atom, and thus the negative charge is delocalised, thereby reducing the interaction between the cationic species. **Figure 5.3** shows a list of weakly coordinating anions.[110,111]

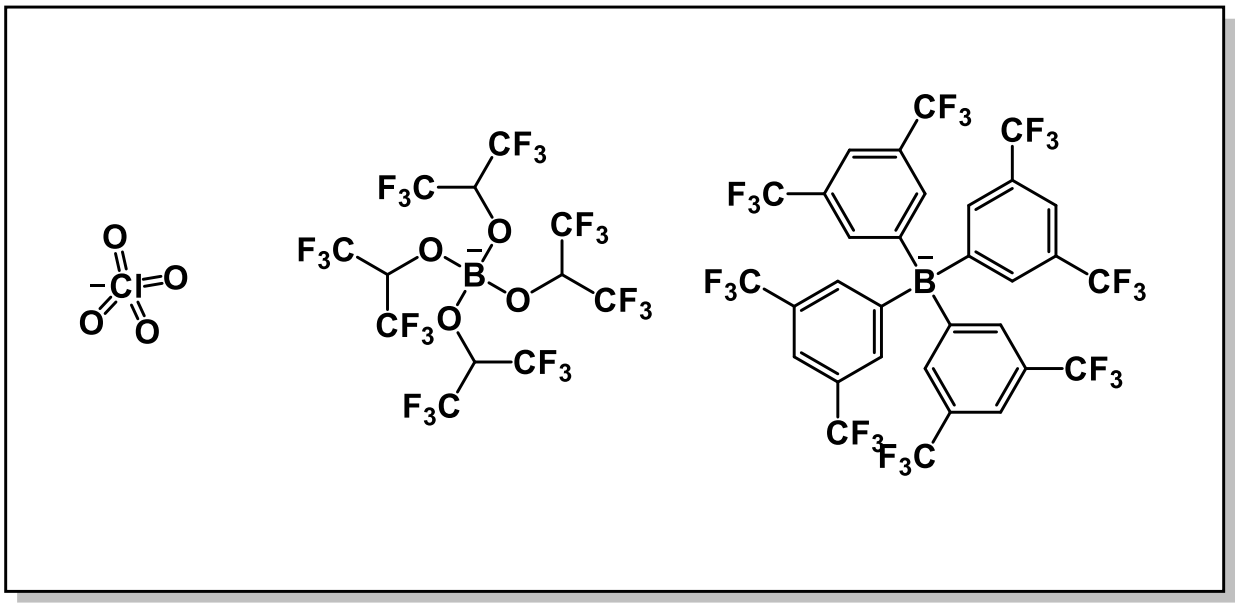

Figure 5.3 Some weakly coordinating anions

For use in this study, a low ion pairing salt was provided through the BASF network by Proffessor Ingo Krossing from the University of Freiburg. The salt is termed as the HIP salt, due to the use of hexafluoroisopropanol (HIP),[112] in its synthesis. **Figure 5.4** shows the structure of the HIP salt used to carry out experiments pertaining to this study.

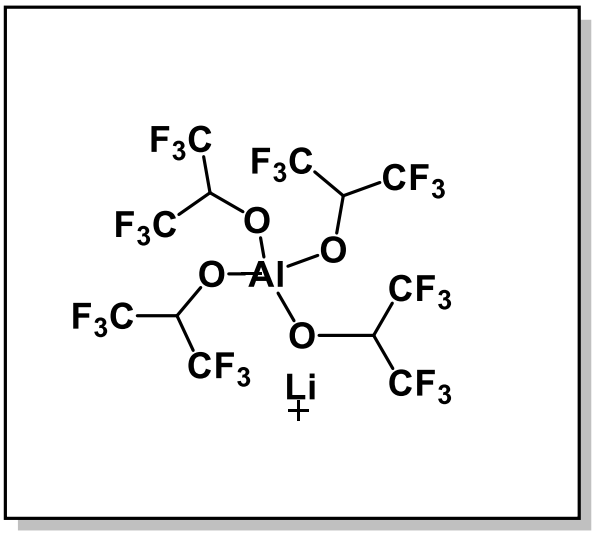

Figure 5.4 HIP salt provided through the BASF network

5.1.3 Solvents

Three different categories of solvents were examined during the study,

1. Solvents that have a low dielectric constant;
2. Solvents that are sterically hindered;
3. Sulphonamides

Choosing a solvent with low dielectric constant will account for the insolubility of the polysulphides, but also provide with an electrolyte system that will have very limited ionic conductivity. Based on values obtained from the literature,[113] three different solvents were examined. 2-Methyl-THF, dibutyl ether and anisole. All three solvents were ether based and had dielectric constants of 4.76, 3.1 and 4.33 respectively. Although low in dielectric constant, they exhibited partial solubility of polysulphide species, which would provide better kinetics towards sulphur utilization and not completely initiate polysulphide shuttle. Cells were tested with a 0.2 M solution of HIP salt in these solvents, and a discharge curve was

obtained only for dibutyl ether, which was identical to that of solvents that have little to no solubility of polysulphide species (**Fig 5.5**). No significant charge curve was obtained for this system, the reason for which is still under investigation. A more detailed study into the use of dibutyl ether as a solvent is under investigation, which is beyond the scope of the thesis.

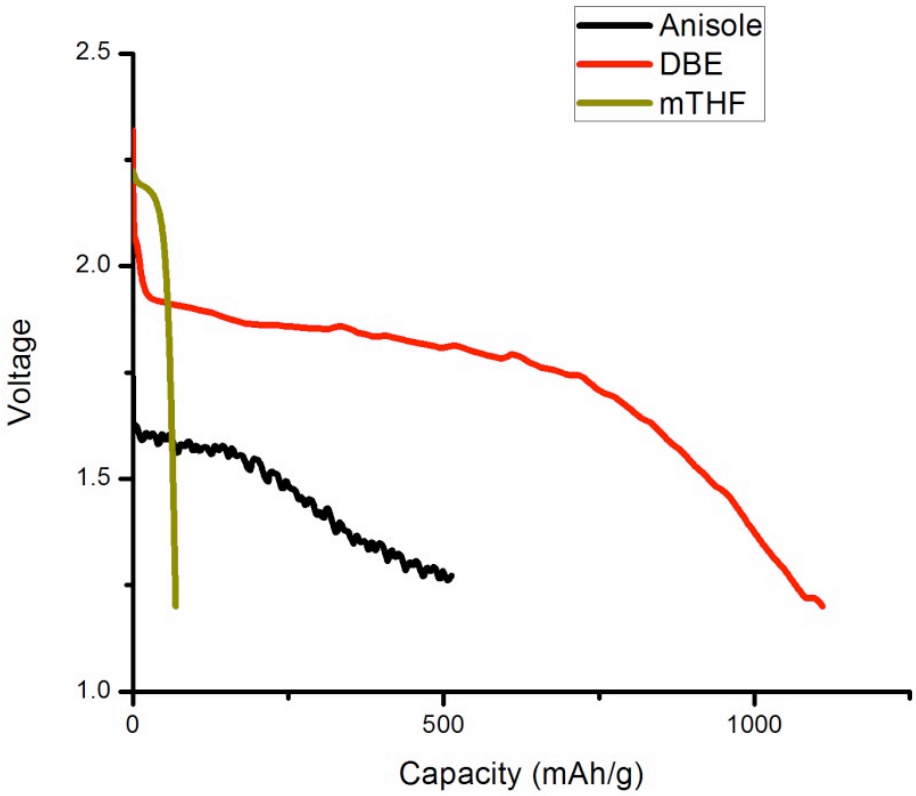

Figure 5.5 Discharge curves of 0.2M solutions of anis**o**le(black), dibutyl ether(red) and 2-methyl THF(olive), at C/20.

Some solvents described in **Chapter 4**, which were synthesized (compounds **2** and **5**) for Li-O_2 or Na-O_2 batteries, were not able to dissolve any salt. These solvents as described before

were considered sterically hindered wherein the Lewis basic sites in the molecule were blocked by methyl groups (See **Figure 5.6**).

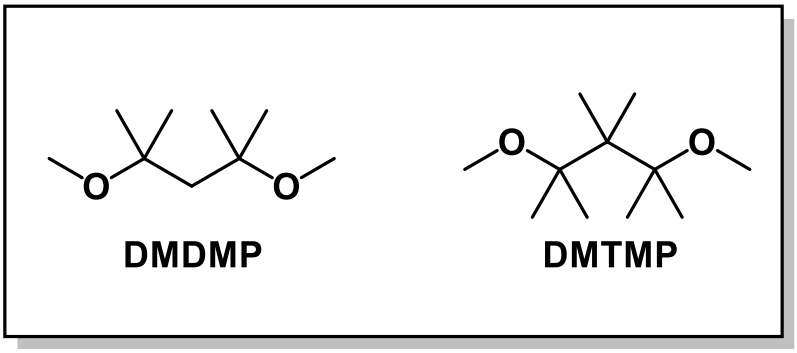

Figure 5.6 Sterically hindered solvents that were not able to dissolve salts

On attempting to dissolve the HIP salt, these solvents readily dissolved along with absolutely no polysulphide solubility (See **Figure 5.7**). Cells were tested with 0.2 M solution of HIP salt in these solvents, and as in the case of dibutyl ether, a discharge profile corresponding to those solvent which show limited to no solubility of polysulphides was observed, along with an absence of a charge curve (**Figure 5.8**). No proper reason has been identified for the absence of a charge curve, but since all of the solvent systems are ether based, it might be an issue with the compatibility of solvent to salt. Further investigation is being carried out to establish an absolute reason for the cell failure, by experimenting with other ether based solvents like diglyme and TEGDME to identify whether the problem is solvent or salt related.

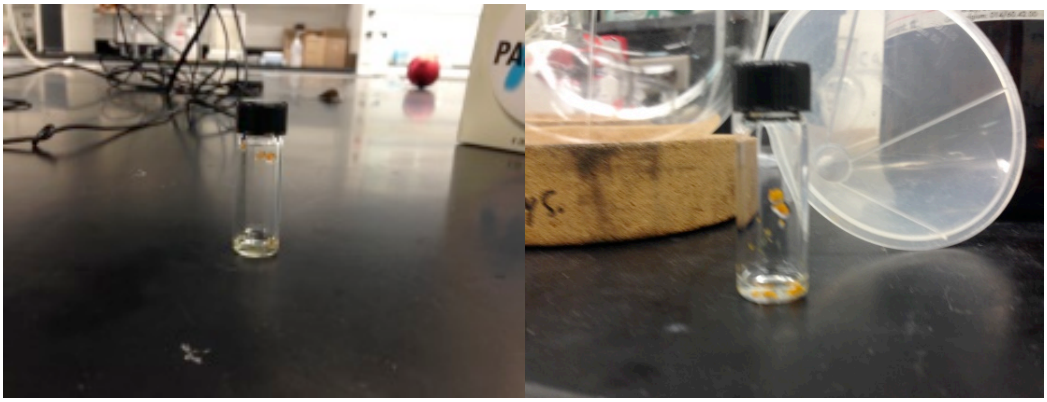

Figure 5.7 Polysulphides in DMDMP(left) and DMTMP(right)

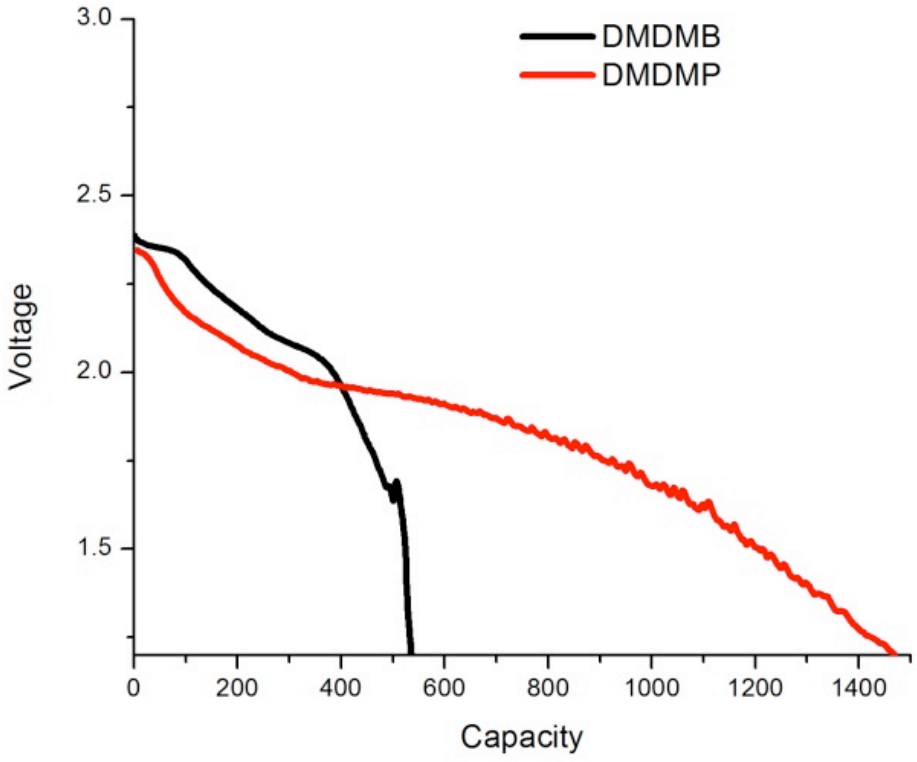

Figure 5.8 Discharge curves of DMDMP(red) and DMTMP(black) with 0.2M solutions of HIP salt at C/20

Another set of solvents as described in **Chapter 4** that were synthesized to provide a wide electrochemical voltage window in terms of stability were the sulphonamides. These sulphonamides were not sterically hindered, but like the previously mentioned solvents also did not dissolve typical battery salts (except *N,N*-dimethyltriflamide(DMT)). As mentioned in **Chapter 4** they are stable towards lithium and provide high oxidative stability thereby an ideal solvent to operate within the voltage limitations of a Li-S battery. Several triflamides were synthesized with increasing chain length on the aliphatic group (Scheme **5.1**) and these solvents provided the best results for this particular study.

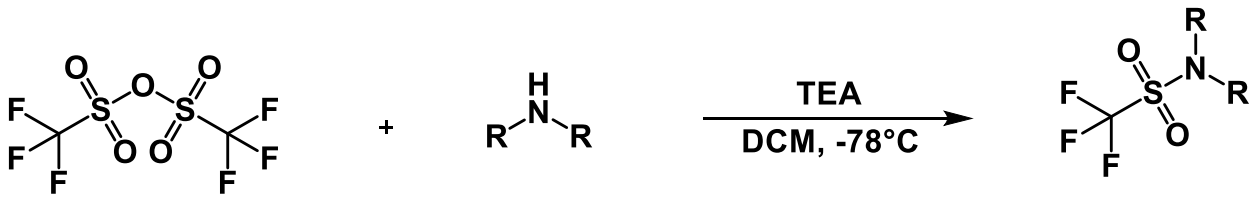

R	Yield
Methyl	86%
Ethyl	85%
Propyl	84%
Butyl	84%

Scheme 5.1

5.2 Electrochemical evaluation of triflamide-HIP salt systems

The *N,N*-dimethyl triflamide (DMT) was the only solvent that could dissolve LiTFSI , but on the other hand, complete solubility with HIP salt was possible with all the synthesized triflamides. In order to understand the influence of increasing chain length on the ability to solvate polysulphides, commercially available orthoesters (**Figure 5.9**) were used and by increasing the chain length from trimethyl orthoformate (TMOF) to trimethyl orthovalerate (TMOV), a trend was clearly observed as depicted in **Figure 5.11**. With increasing chain length, the ability to solvate polysulphide species decreased, and voltage profiles also suggest the same.

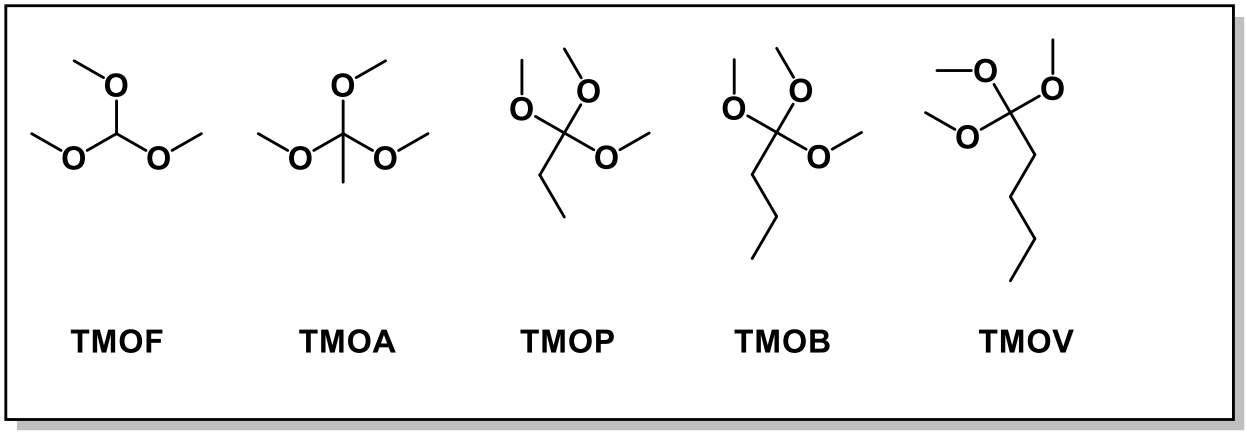

Figure 5.9 Orthoesters used to probe the influence of increasing chain length

Moving from TMOF to TMOV, we observe that the clearly defined plateaus corresponding to the reduction of polysulphides slowly diminish,[46] and are almost completely absent in TMOV. This suggests that the polysulphide solubility reduces as we increase chain length in the solvent molecule.

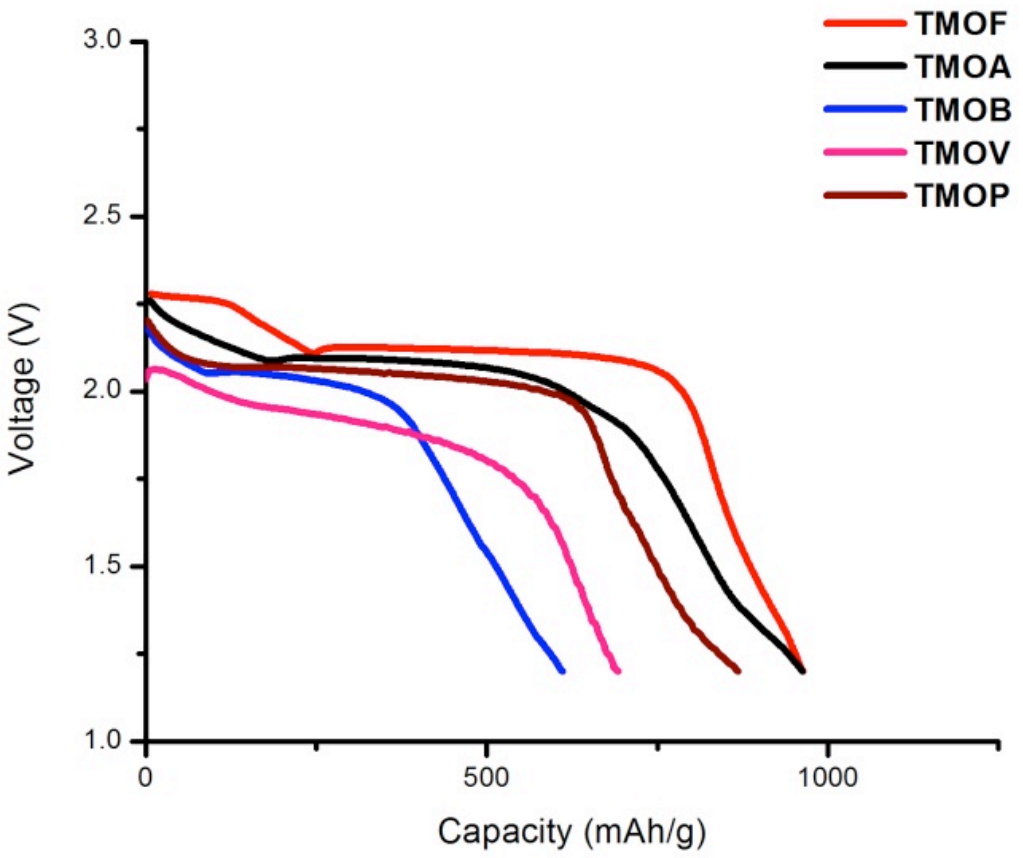

Figure 5.11 Discharge curves of various orthoesters using 0.2 M solution of HIP salt at C/20.

Based on this result, two triflamides were chosen owing to their ability to dissolve polysulphides. *N,N*-dimethyl triflamide (DMT), which demonstrates partial solubility of polysulphides, and *N,N*-dipropyl triflamide (DPT), which demonstrates no solubility of polysulphides.

5.2.1 Redox stability

Prior to understanding the behaviour of these two solvents, the stability of the solvent-salt mixture with regards to oxidation and reduction needs to be evaluated. Cyclic voltammograms of 0.2 M solutions of HIP salt in DMT and DPT were carried out with lithium as the working electrode and a stainless steel current collector as the counter electrode (based on a coin cell setup). As shown in **Figures 5.12** and **5.13,** the onset of stripping of lithium occurs only after 0 V, suggesting that the electrolyte is stable with lithium, and no peaks are observed below 4 V, implying the oxidative stability of the electrolyte within the working potential of the Li-S battery.

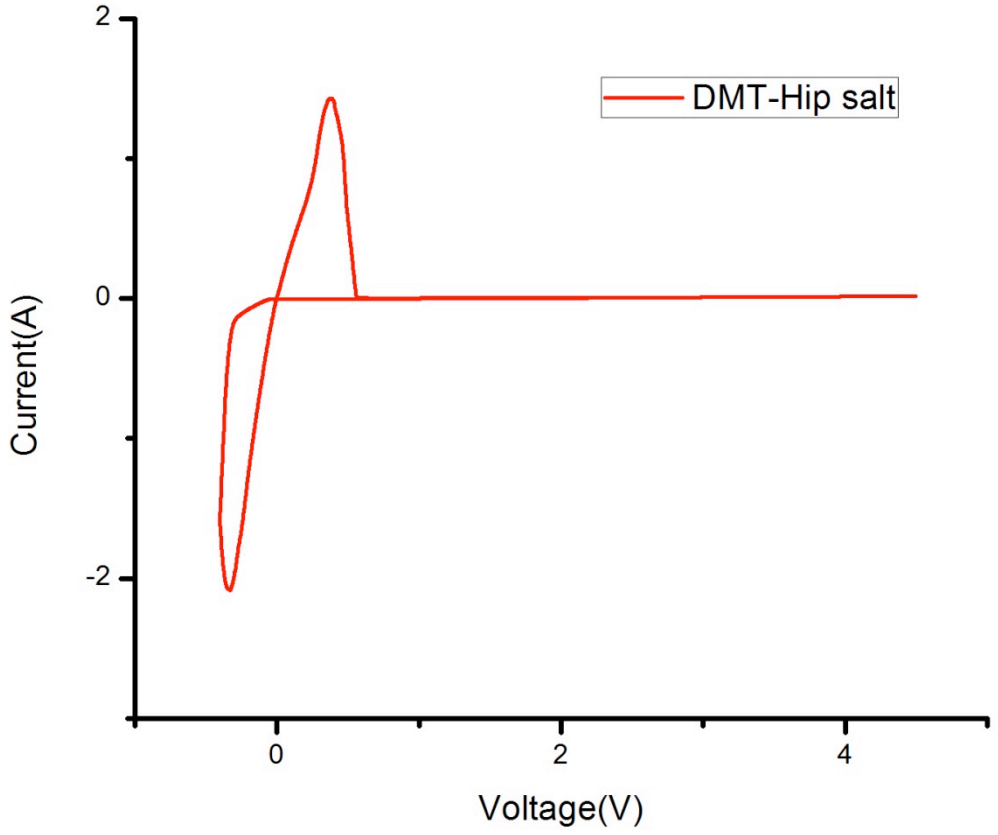

Figure 5.12 CV of 0.2 M HIP salt in DMT

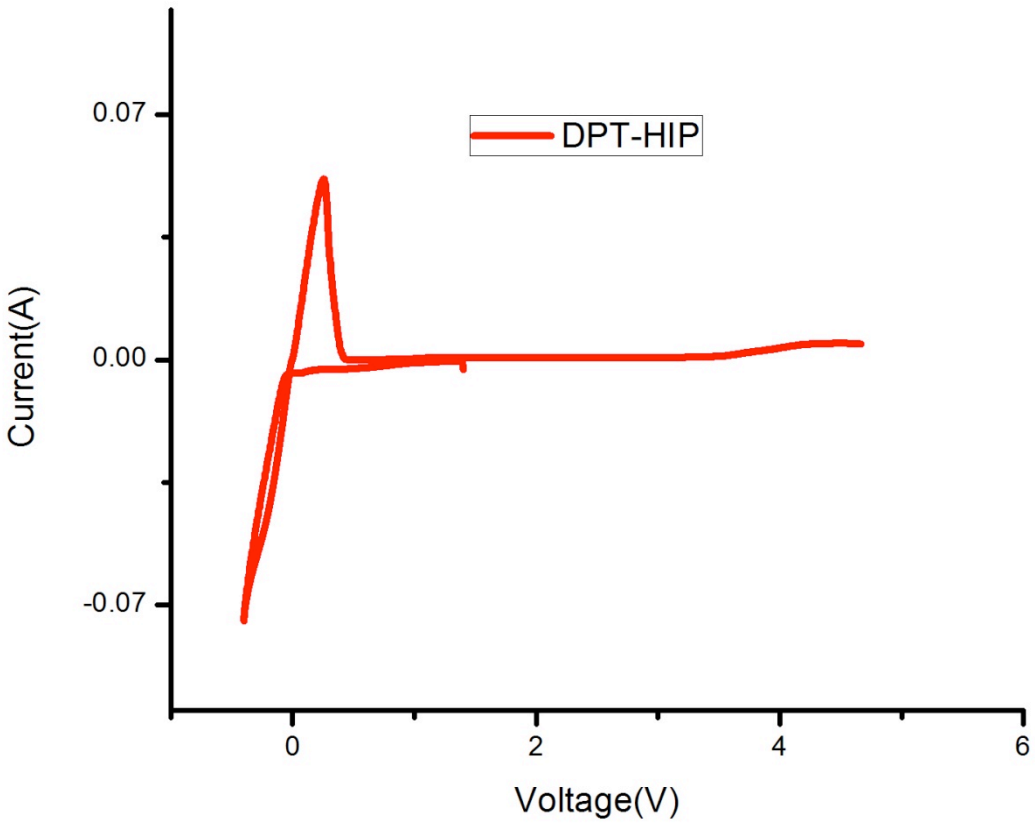

Figure 5.13 CV of 0.2 M HIP salt in DPT

5.2.2 Performance in a Li-S battery

Two electrolyte solutions made up of 0.2 M HIP salt in DMT and DPT were tested in a Li-S battery. Cells were discharged and charged at rates of C/20. The discharge and charge plateau at the end of the first cycle of both DMT and DPT clearly indicate that some capacity during discharge is not accounted for during charge (**Figure 5.14**). This pattern, although observed during the first cycle, is not seen in the following cycles. A reason for this could very well be the electrochemical formation of an interphase layer on the anodic surface,[55,114] which is not oxidized during charge. Proof of the formation of this interphase layer can be confirmed by

carrying out XPS analysis on both pristine lithium soaked in the electrolyte, as well as a lithium anode after the first discharge. This work is currently being carried out and those results are not included in this thesis.

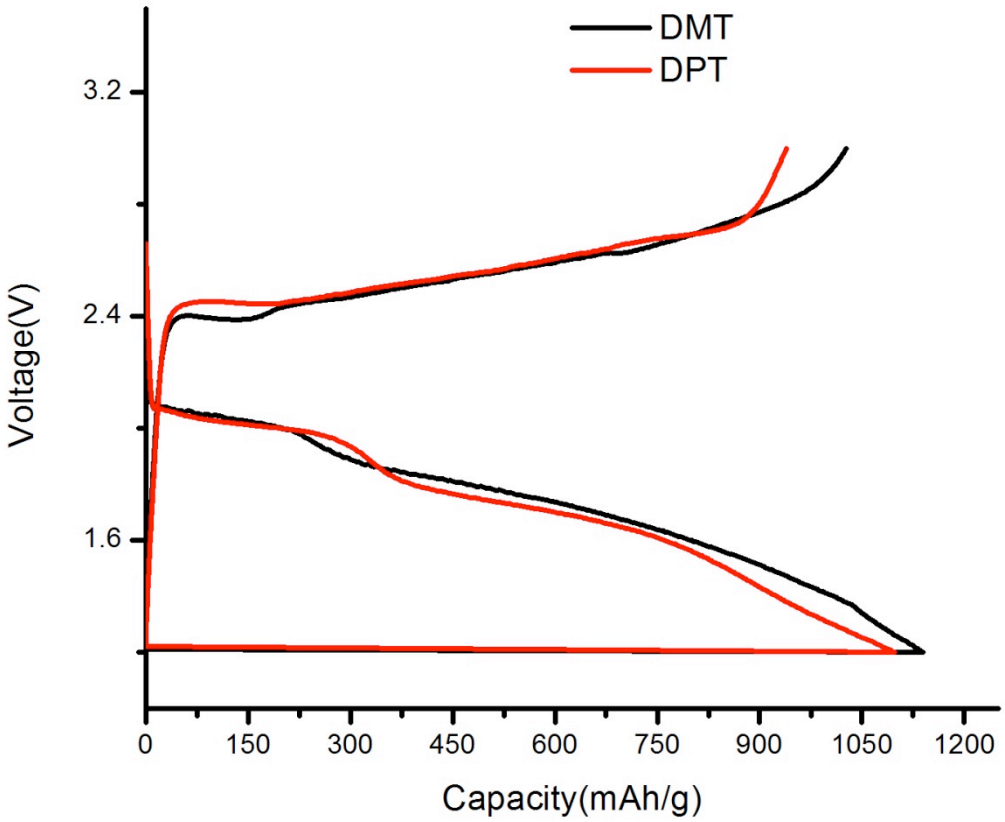

Figure 5.14 1st discharge and charge of 0.2 M HIP salt in DMT (black) and DPT(red) at C/20

It is clearly observable from **Figure 5.14** that the discharge pattern resembles that of solvents that have limited to no solubility of polysulphides. It is also noticeable that the cells exhibit slow kinetics evidenced by the observed capacity (60-65% of the theoretical value). In order to prove that the reason for this lack in capacity, is due to the lower ionic conductivity, cells

were cycled at rates of C/5 and the observed discharge and charge profiles are shown in **Figures 5.15** and **Fig 5.16.**

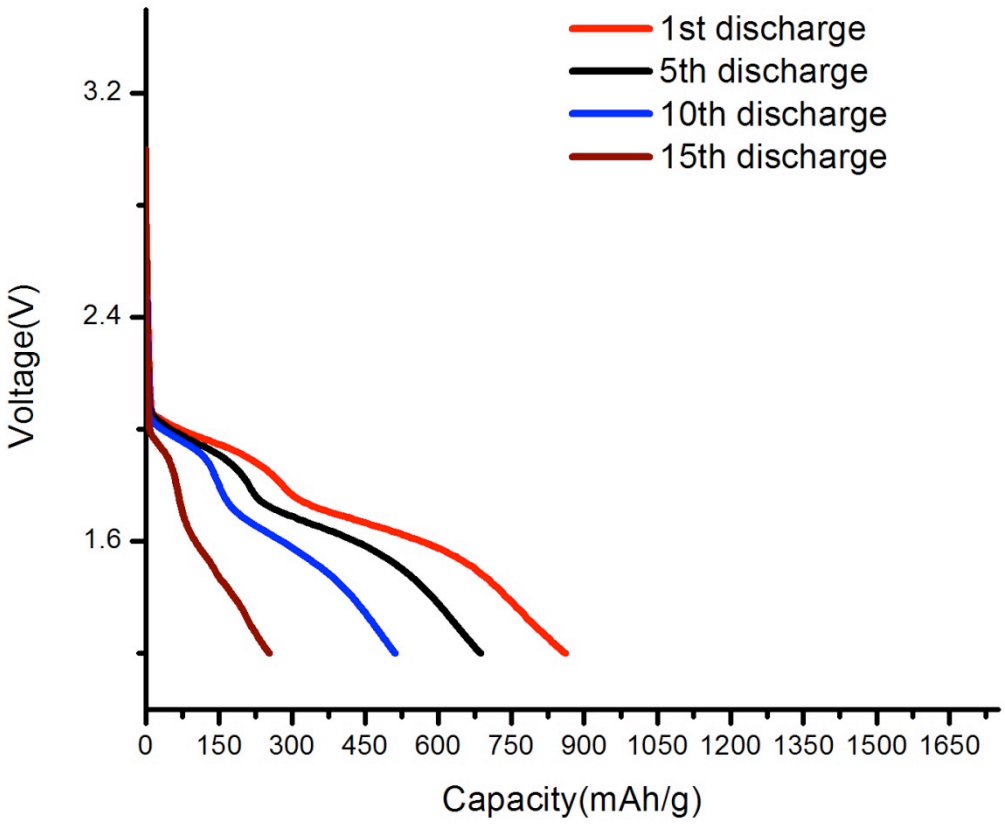

Figure 5.15 0.2 M HIP salt in DPT discharge profiles at C/5

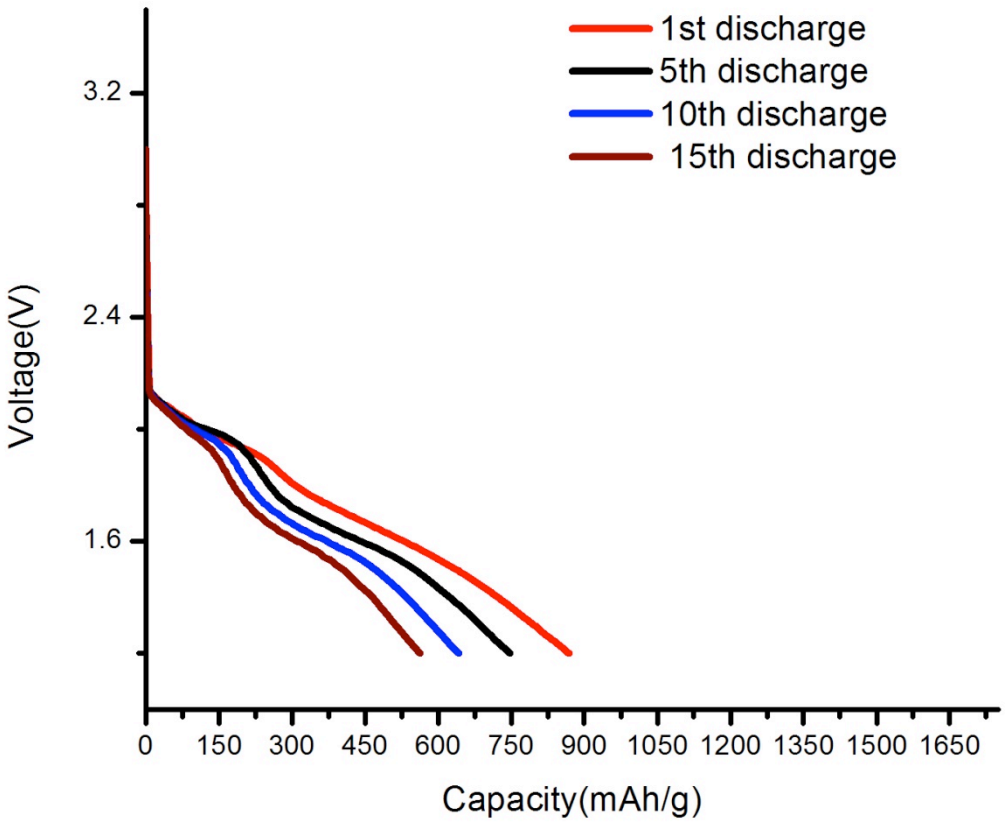

Figure 5.16 0.2 M HIP salt in DMT discharge profile at C/5

Figures 5.15 and **5.16** clearly illustrate the loss in capacity over cycling for both DMT and DPT. At a high discharge rate, this is observed with electrolyte solutions having low ionic conductivities. It is also a clear indication that almost all of the reduction reactions of polysulphides taking place are in the solid state (no solubility in electrolyte) which is indicated by the absence of any identifiable plateaus. There is also an indication of low sulphur utilization, which is partly due to sulphur being electronically inactive (the conductivity of sulphur is 1 x 10^{-15} S/m) and the ability of the electrolyte to partially dissolve sulphur.

Although the capacity fade is still a problem, the main focus on using these solvents is to identify an absence of a polysulphide shuttle for which we need to look at the coulombic efficiency of the cells that were tested. **Figure 5.17** shows the coulombic efficiency and the discharge capacities observed for both electrolytes over cycling (shown are the first 50 cycles).

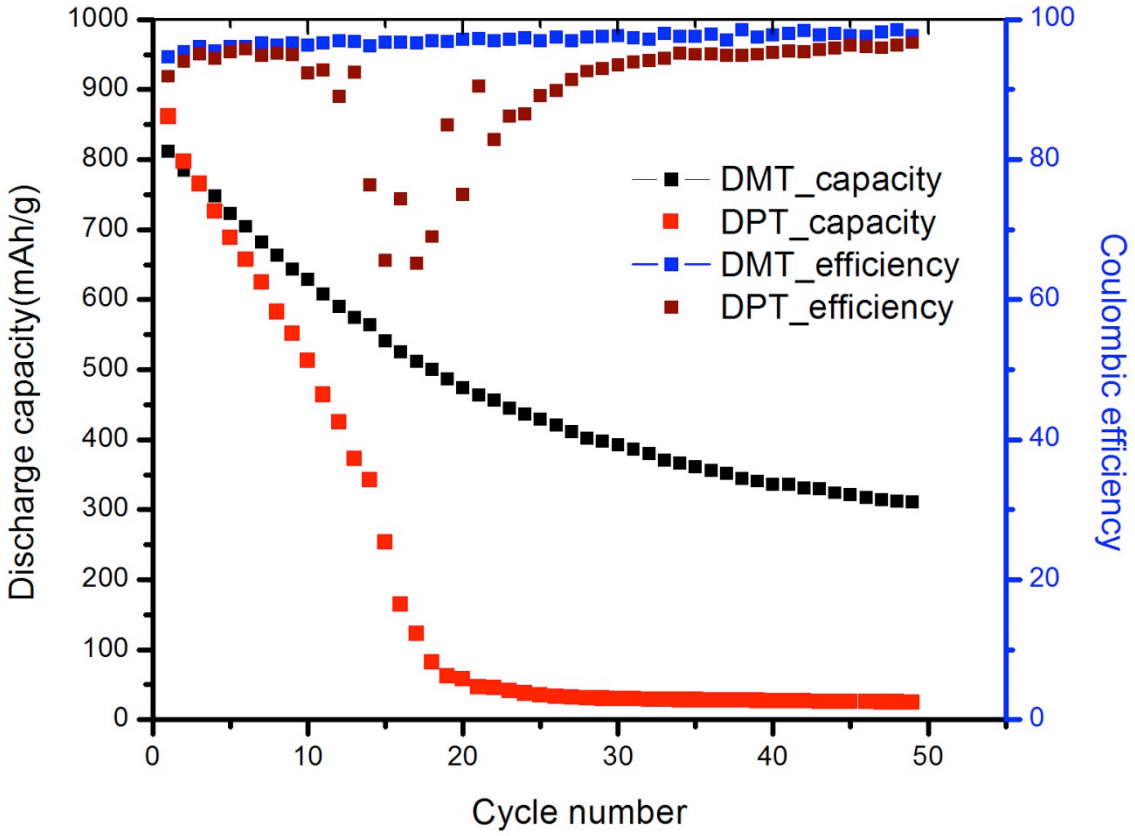

Figure 5.17 Discharge capacities and coulombic efficiency observed for DPT and DMT

Figure 5.17 shows that the performance of DMT is much superior to that of DPT. This can be partly attributed to the ability of DMT to partially dissolve polysulphides and provide a better kinetic pathway for the redox to occur. Also, it is known that during the reduction of polysulphides, an anionic radical $S_3^{-\bullet}$ is formed, which potentially decomposes the electrolyte

similar to the action of the superoxide radical in the Li-O_2 battery. With the presence of a methylene hydrogen to abstract, the DPT solvent might undergo decomposition processes during cycling.[115] Conclusive evidence for the decomposition of the DPT electrolyte is still under investigation.

5.2.4 High temperature study

In order to overcome the drawbacks of rapid capacity fade and lower ionic conductivity, both the DMT and DPT systems were tested in Li-S batteries at 50 ˚C. With an increase in temperature, there would certainly be an increase in the solubility of polysulphides, which could lead to better reaction kinetics. **Figures 5.18** and **5.19** show the first galvanostatic cycle of both the DMT and DPT electrolytes at both 50 ˚C and room temperature.

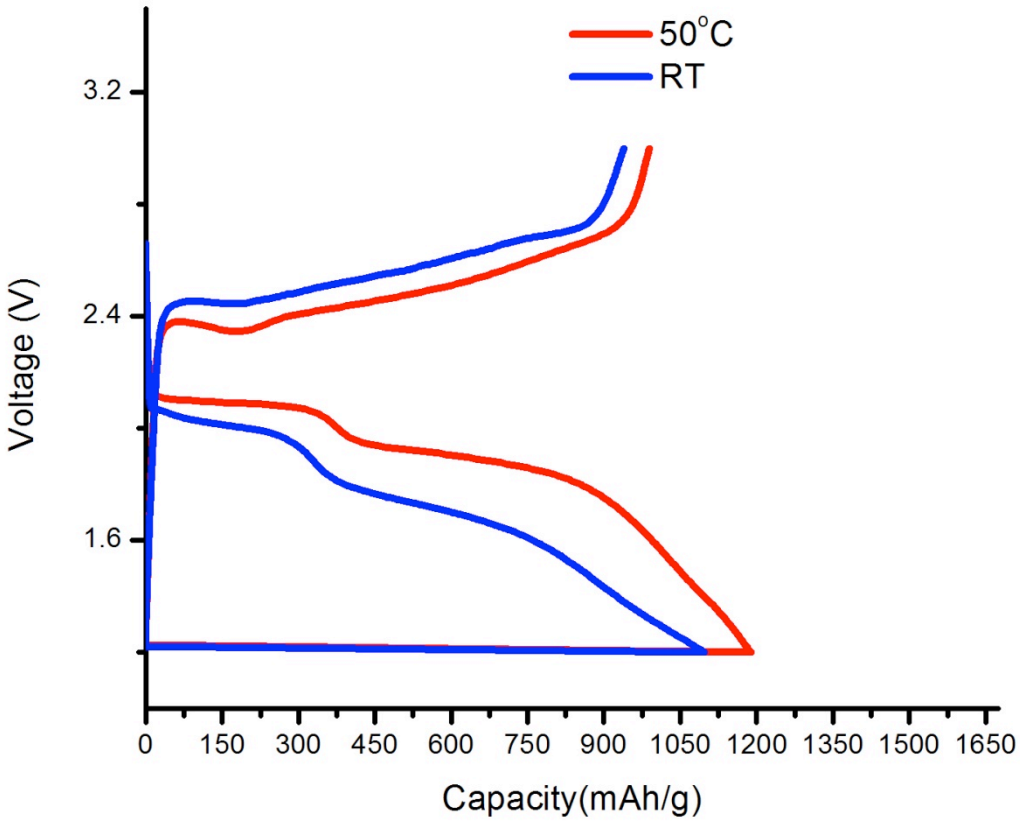

Figure 5.18 First cycle of DPT electrolyte at room temperature and 50 ˚C

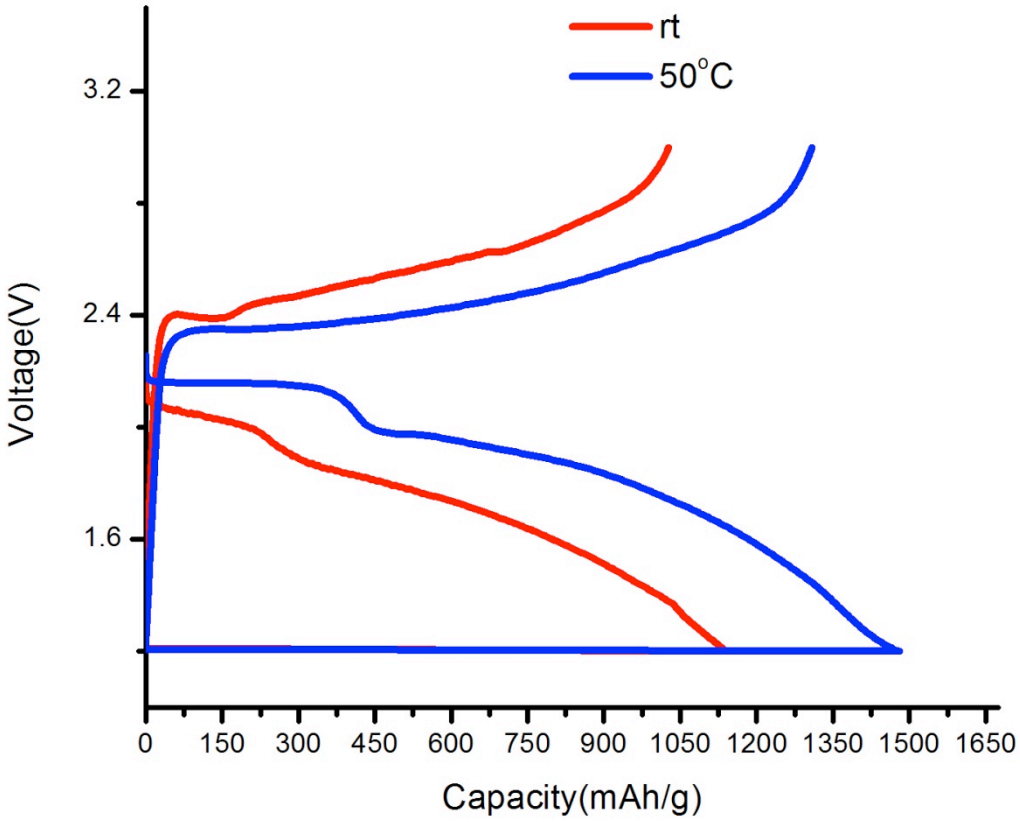

Figure 5.19 First cycle of DMT electrolyte at room temperature and 50 ˚C

It is quite clear from **Figures 5.18** and **5.19** that with increase in temperature the performance of the battery is enhanced, evidenced by the high discharge capacity and low overpotential during charge. The appearance of a more distinct plateau at around 2.1 V during discharge in both systems at 50 ˚C is a clear indication that there is a slight increase in polysulphide solubility compared to room temperature.[52] As in the case of the room temperature study, there exists a part of the discharge capacity that is not accounted for during charge, which again suggests formation of an interphase layer on the lithium anode.

Figures 5.21 and **5.22** show the discharge profiles observed over cycling for the DPT and DMT systems.

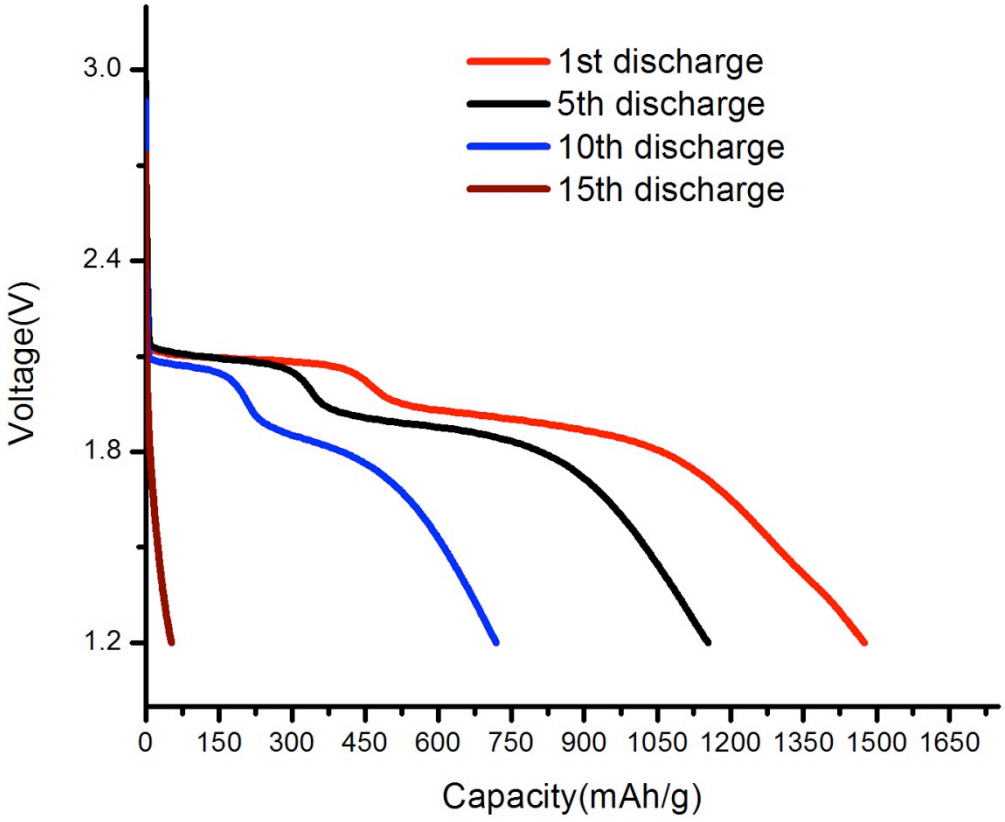

Figure 5.21 Discharge profiles of DPT at 50 ˚C

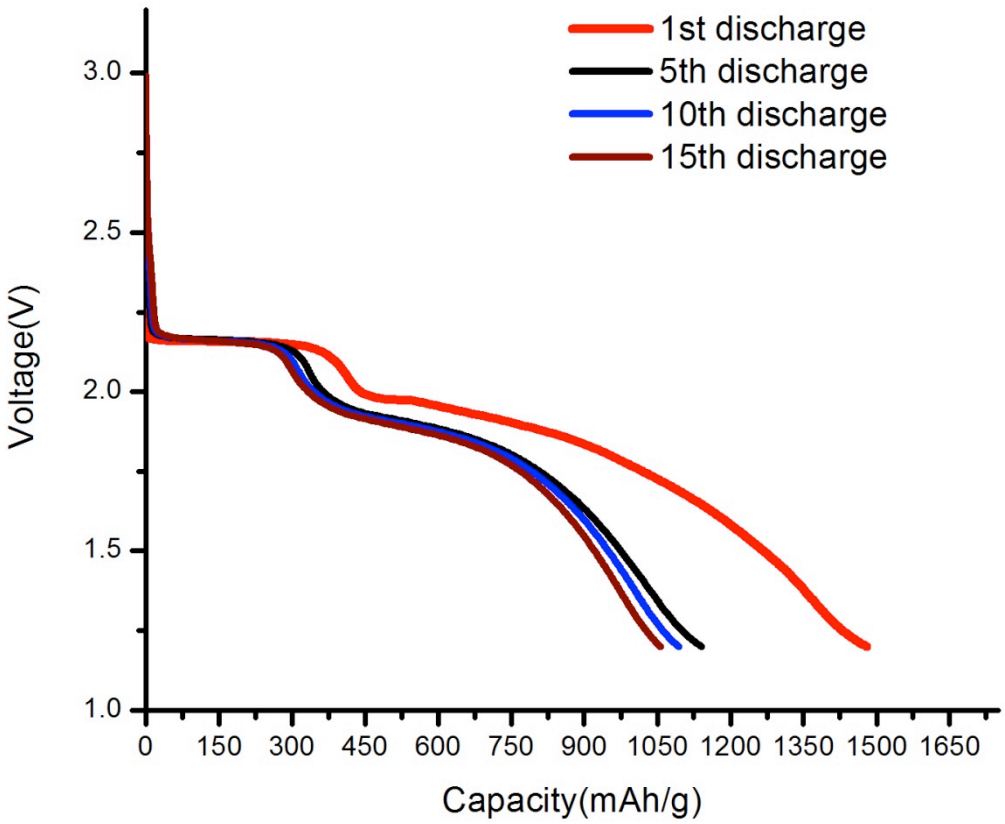

Figure 5.22 Discharge profiles of DMT at 50 ˚C

Similar to the case at room temperature, there is rapid capacity fading with the DPT electrolyte , which may be due to the decomposition reactions taking place.[115] After the first discharge, DMT, on the other hand shows very slow and gradual decrease in capacity over cycling. The capacity value of 1100 mAh/g (65% of the theoretical value) in the 10th cycle is quite significant for a new electrolyte (salt and solvent) system.

In order to investigate if the compatibility of salt with DPT is an issue, we decided to switch to LiTFSI as a salt. Unfortunately DPT did not dissolve LiTFSI and further studies could not be performed.

DMT on the other hand did dissolve LiTFSI, and to see what role the salts play in the observed performance, cells were tested with a 0.2 M LiTFSI/DMT system. **Figure 5.23** shows the 1st cycle of DMT electrolyte with HIP salt and LiTFSI at rt and 50 ˚C,

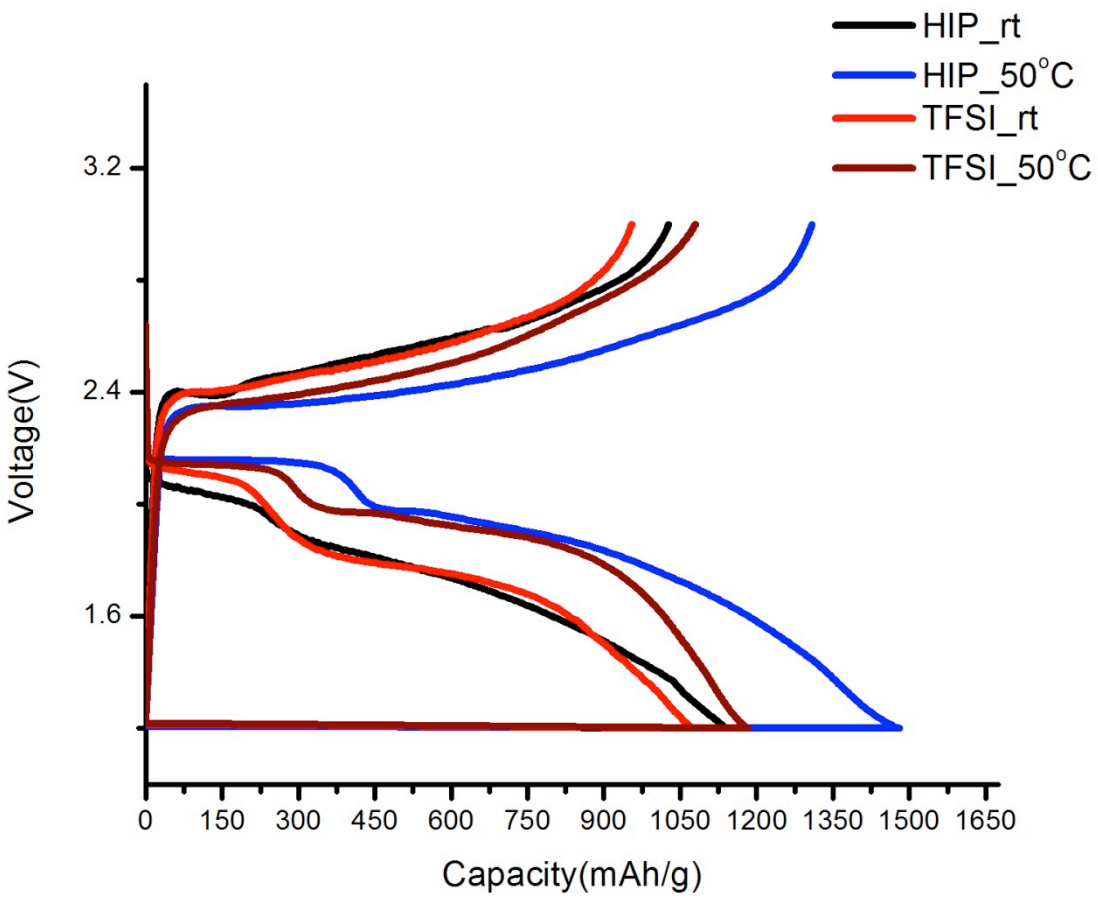

Figure 5.23 Cycle 1 of DMT solvent with LiTFSI and HIP salt at C/5

By substituting the HIP salt with LiTFSI, there are no significant changes observed as shown in **Figure 5.22**. There is a slight increase in discharge capacity for LiTFSI salt system at 25 ˚C, which is mainly due to better ionic conductivity. In the high temperature study, the profile resembles the second cycle of DMT-HIP salt where there is no unresolved discharge capacity. This could be because the LiTFSI salt helps in forming an interphase on the lithium

metal (which may be lithium fluoride).[116] Thus even with substituting the salt, we are able to reproduce results that were presented with our novel HIP salt.

With increased solubility of polysulphides at higher temperature, a possibility of polysulphide shuttle exists. In order to verify this, the coulombic efficiency over cycling of all the systems with DMT solvent is shown in **Figure 5.24**.

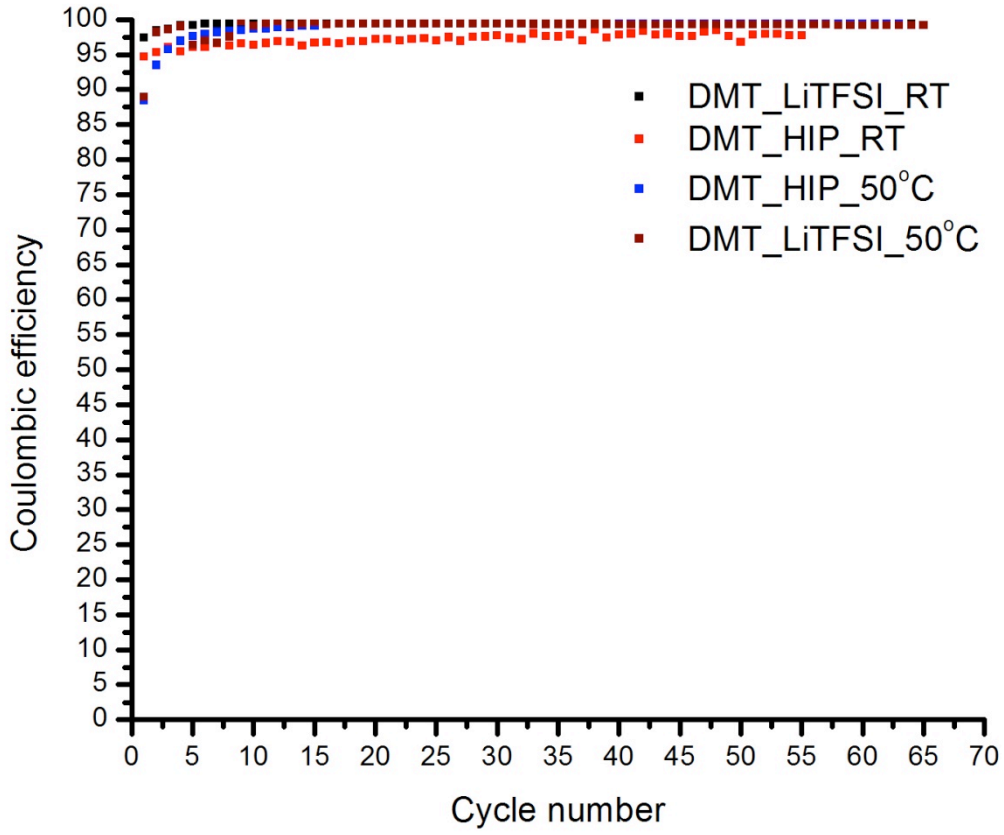

Figure 5.24 Coulombic efficiency of DMT solvent with different salts at different temperature

With an increase in temperature, we have successfully altered the kinetics of the reaction and did not cause any parasitic shuttle processes as can be seen from **Figure 5.24**. Coulombic

efficiency is almost 100% over 50 cycles, and is a clear indication that this particular solvent inhibits the polysulphide shuttle. By increasing the temperature sulphur utilization was increased by approximately 23% as shown in **Fig 5.25**.

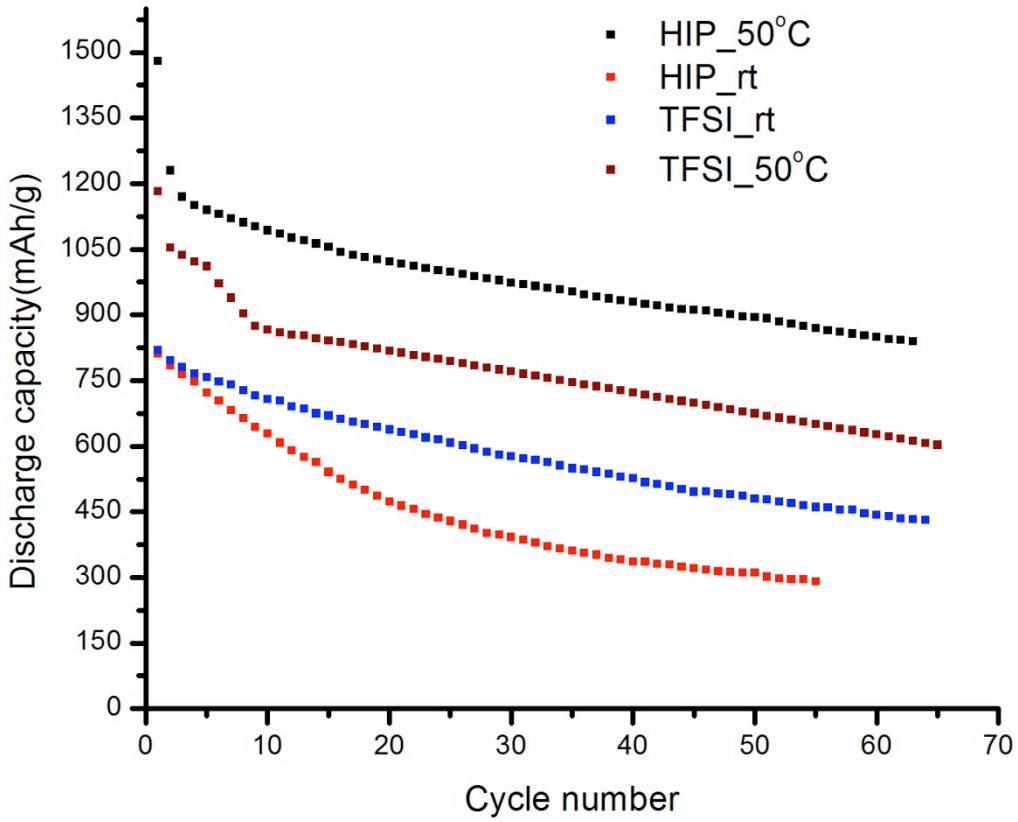

Figure 5.25 Discharge capacities over cycling of DMT based electrolytes at rt and 50 ˚C

5.3 Experimental

All orthoesters used in this study were purchased from Sigma Aldrich and were distilled before use. TEGDME (Sigma Aldrich) was distilled and stored over 4 Å sieves in an amber glass bottle. All solvents had a water content of less than 5 ppm as measured with a KF titration inside a glovebox with water and oxygen content less than 0.1 ppm.

5.3.1 Synthesis of sulphonamides[103]

The sulphonamides were synthesised according to the following procedure. Amine (2.56 mmol) and triethyl amine (2.73 mmol) were dissolved in anhydrous dichloromethane at -78 ˚C. Trifluoromethanesulfonic anhydride was dissolved in dichloromethane, added dropwise over a period of 15 mins and stirred at -78 ˚C for 2 hours. After which water was added and the reaction mixture was allowed to reach room temperature. The aqueous phase was extracted with dichloromethane twice and the combined organic phases was washed with brine and dried over anhydrous magnesium sulphate, filtered, and evaporated to dryness. The resulting residue was distilled under vacuum to afford the corresponding sulfonamides.

***N,N*-dimethyl triflamide**: Yield 85%. Analytical data are in agreement with those previously reported

***N,N*-diethyl triflamide**: Yield 84%. Analytical data are in agreement with those previously reported

***N,N*-dipropyl triflamide**: Yield 88%. Analytical data are in agreement with those previously reported.

***N,N*-dibutyl triflamide**: Yield 86%. Analytical data are in agreement with those previouslt reported.

5.3.2 Preparation of positive electrodes:

In order to rule out limitations due to poor electronic conduction and volume expansion, “standard” electrodes were based on a 50 wt% sulphur/Ketjenblack (S/KB) composite prepared by melt diffusion. Positive electrode were prepared by drop casing a slurry containing 80 wt% S/KB composite, 10 wt% Super-P carbon and 10 wt%

poly(vinylidenedifluoride) binder in N,N-dimethylformamide onto a carbon coated aluminium current collector(Intelicoat). Sulphur loading was fixed to 1mg.

5.3.3 Electrochemistry

Coin cells(2325, NRC) were fabricated in an argon-filled glovebox using a sulphur electrode, two sheets of Celgard^{TM} separators, a Li foil negative electrode and 40 μL of electrolyte. For galvanostatic cycling at room temperature, an Arbin instrument was used. For high temperature study, a VMP-3 instrument (Biologic) was used with a Thermoscientific oven. The same instrument was used to perform the cyclic voltammogram studies as well.

5.4 Conclusion and future work

A new electrolyte system composed of a sulphonamide electrolyte and a HIP salt have proved to be efficient in overcoming the parasitic polysulphide shuttle processes in a Li-S battery. With a low concentration of salt and stable solvent (with respect to reactivity with lithium), this thesis work has opened a new avenue into tackling problems of the polysulphide shuttle through altering the electrolyte component of the Li-S battery. This system provides capacities of 900 mAh/g over 50 cycles (53% of the theoretical value) at 50 ˚C and a coulombic efficiency of almost 100 %.

Future work would involve the use of *operando* X-ray absorption near edge spectroscopy (XANES) to examine sulphur speciation during the redox processes in the cell. *In-situ* XRD can also be employed for the systems at room temperature, and in the case of poor solubility of polysulphides, we might be able to visually inspect the various products formed on the cathode provided they are crystalline. Use of a higher loading of sulphur along with varying

the cathode architecture could also be a valid approach to examine the role that cathodes play in the performance of the DMT systems.

References

(1) Goodenough, J. B.; Kim, Y. *Chemistry of Materials* **2009**, *22*, 587.

(2) Goodenough, J. B.; Park, K.-S. *Journal of the American Chemical Society* **2013**, *135*, 1167.

(3) Hofmann, M.; Raab, S.; Schaefer, M.; Ponomarov, P.; Ackva, A. In *Power Electronics for Distributed Generation Systems (PEDG), 2015 IEEE 6th International Symposium on*; IEEE: 2015, p 1.

(4) Black, R.; Adams, B.; Nazar, L. *Advanced Energy Materials* **2012**, *2*, 801.

(5) Lu, J.; Li, L.; Park, J.-B.; Sun, Y.-K.; Wu, F.; Amine, K. *Chemical Reviews* **2014**, *114*, 5611.

(6) Lu, Y.-C.; Gallant, B. M.; Kwabi, D. G.; Harding, J. R.; Mitchell, R. R.; Whittingham, M. S.; Shao-Horn, Y. *Energy & Environmental Science* **2013**, *6*, 750.

(7) Jung, H.-G.; Jeong, Y. S.; Park, J.-B.; Sun, Y.-K.; Scrosati, B.; Lee, Y. J. *ACS Nano* **2013**, *7*, 3532.

(8) Abraham, K.; Jiang, Z. *Journal of The Electrochemical Society* **1996**, *143*, 1.

(9) Read, J.; Mutolo, K.; Ervin, M.; Behl, W.; Wolfenstine, J.; Driedger, A.; Foster, D. *Journal of The Electrochemical Society* **2003**, *150*, A1351.

(10) Débart, A.; Paterson, A. J.; Bao, J.; Bruce, P. G. *Angewandte Chemie International Edition* **2008**, *47*, 4521.

(11) Laoire, C. O.; Mukerjee, S.; Abraham, K.; Plichta, E. J.; Hendrickson, M. A. *The Journal of Physical Chemistry C* **2009**, *113*, 20127.

(12) Lu, Y.-C.; Gasteiger, H. A.; Parent, M. C.; Chiloyan, V.; Shao-Horn, Y. *Electrochemical and Solid-State Letters* **2010**, *13*, A69.

(13) Zhang, J.; Xu, W.; Li, X.; Liu, W. *Journal of The Electrochemical Society* **2010**, *157*, A940.

(14) Trahey, L.; Johnson, C.; Vaughey, J.; Kang, S.-H.; Hardwick, L.; Freunberger, S.; Bruce, P.; Thackeray, M. *Electrochemical and Solid-State Letters* **2011**, *14*, A64.

(15) Lee, J. S.; Tai Kim, S.; Cao, R.; Choi, N. S.; Liu, M.; Lee, K. T.; Cho, J. *Advanced Energy Materials* **2011**, *1*, 34.

(16) Ogasawara, T.; Débart, A.; Holzapfel, M.; Novák, P.; Bruce, P. G. *Journal of the American Chemical Society* **2006**, *128*, 1390.

(17) Laoire, C. O.; Mukerjee, S.; Abraham, K.; Plichta, E. J.; Hendrickson, M. A. *The Journal of Physical Chemistry C* **2010**, *114*, 9178.

(18) Laoire, C.; Mukerjee, S.; Plichta, E. J.; Hendrickson, M. A.; Abraham, K. *Journal of The Electrochemical Society* **2011**, *158*, A302.

(19) Mitchell, R. R.; Gallant, B. M.; Thompson, C. V.; Shao-Horn, Y. *Energy & Environmental Science* **2011**, *4*, 2952.

(20) Xiao, J.; Mei, D.; Li, X.; Xu, W.; Wang, D.; Graff, G. L.; Bennett, W. D.; Nie, Z.; Saraf, L. V.; Aksay, I. A. *Nano Letters* **2011**, *11*, 5071.

(21) Sawyer, D. T.; Valentine, J. S. *Accounts of Chemical Research* **1981**, *14*, 393.

(22) Peng, Z.; Freunberger, S. A.; Hardwick, L. J.; Chen, Y.; Giordani, V.; Bardé, F.; Novák, P.; Graham, D.; Tarascon, J. M.; Bruce, P. G. *Angewandte Chemie* **2011**, *123*, 6475.

(23) Mo, Y.; Ong, S. P.; Ceder, G. *Physical Review B* **2011**, *84*, 205446.

(24) Mizuno, F.; Nakanishi, S.; Kotani, Y.; Yokoishi, S.; Iba, H. *Electrochemistry* **2010**, *78*, 403.

(25) Freunberger, S. A.; Chen, Y.; Peng, Z.; Griffin, J. M.; Hardwick, L. J.; Bardé, F.; Novák, P.; Bruce, P. G. *Journal of the American Chemical Society* **2011**, *133*, 8040.

(26) Black, R.; Oh, S. H.; Lee, J.-H.; Yim, T.; Adams, B.; Nazar, L. F. *Journal of the American Chemical Society* **2012**, *134*, 2902.

(27) Bryantsev, V. S.; Blanco, M. *The Journal of Physical Chemistry Letters* **2011**, *2*, 379.

(28) Assary, R. S.; Curtiss, L. A.; Redfern, P. C.; Zhang, Z.; Amine, K. *The Journal of Physical Chemistry C* **2011**, *115*, 12216.

(29) Read, J. *Journal of The Electrochemical Society* **2002**, *149*, A1190.

(30) McCloskey, B. D.; Scheffler, R.; Speidel, A.; Bethune, D. S.; Shelby, R. M.; Luntz, A. *Journal of the American Chemical Society* **2011**, *133*, 18038.

(31) McCloskey, B.; Bethune, D.; Shelby, R.; Girishkumar, G.; Luntz, A. *The Journal of Physical Chemistry Letters* **2011**, *2*, 1161.

(32) Freunberger, S. A.; Chen, Y.; Drewett, N. E.; Hardwick, L. J.; Bardé, F.; Bruce, P. G. *Angewandte Chemie International Edition* **2011**, *50*, 8609.

(33) Lu, Y.-C.; Xu, Z.; Gasteiger, H. A.; Chen, S.; Hamad-Schifferli, K.; Shao-Horn, Y. *Journal of the American Chemical Society* **2010**, *132*, 12170.

(34) Kraytsberg, A.; Ein-Eli, Y. *Journal of Power Sources* **2011**, *196*, 886.

(35) Giordani, V.; Walker, W.; Bryantsev, V. S.; Uddin, J.; Chase, G. V.; Addison, D. *Journal of The Electrochemical Society* **2013**, *160*, A1544.

(36) Uddin, J.; Bryantsev, V. S.; Giordani, V.; Walker, W.; Chase, G. V.; Addison, D. *The Journal of Physical Chemistry Letters* **2013**, *4*, 3760.

(37) Chen, Y.; Freunberger, S. A.; Peng, Z.; Fontaine, O.; Bruce, P. G. *Nature chemistry* **2013**, *5*, 489.

(38) Xu, D.; Wang, Z.-l.; Xu, J.-j.; Zhang, L.-l.; Zhang, X.-b. *Chemical Communications* **2012**, *48*, 6948.

(39) Trahan, M. J.; Mukerjee, S.; Plichta, E. J.; Hendrickson, M. A.; Abraham, K. *Journal of The Electrochemical Society* **2013**, *160*, A259.

(40) Sharon, D.; Afri, M.; Noked, M.; Garsuch, A.; Frimer, A. A.; Aurbach, D. *The Journal of Physical Chemistry Letters* **2013**, *4*, 3115.

(41) Kim, Y. J.; Lee, H.; Lee, D. J.; Park, J. K.; Kim, H. T. *ChemSusChem* **2015**, *8*, 2496.

(42) Hartmann, P.; Bender, C. L.; Sann, J.; Dürr, A. K.; Jansen, M.; Janek, J.; Adelhelm, P. *Physical Chemistry Chemical Physics* **2013**, *15*, 11661.

(43) Xia, C.; Black, R.; Fernandes, R.; Adams, B.; Nazar, L. F. *Nature chemistry* **2015**, *7*, 496.

(44) Kumaresan, K.; Mikhaylik, Y.; White, R. E. *Journal of The Electrochemical Society* **2008**, *155*, A576.

(45) Waluś, S.; Barchasz, C.; Colin, J.-F.; Martin, J.-F.; Elkaïm, E.; Leprêtre, J.-C.; Alloin, F. *Chemical Communications* **2013**, *49*, 7899.

(46) Schneider, H.; Gollub, C.; Weiß, T.; Kulisch, J.; Leitner, K.; Schmidt, R.; Safont-Sempere, M. M.; Mikhaylik, Y.; Kelley, T.; Scordilis-Kelley, C. *Journal of The Electrochemical Society* **2014**, *161*, A1399.

(47) Busche, M. R.; Adelhelm, P.; Sommer, H.; Schneider, H.; Leitner, K.; Janek, J. *Journal of Power Sources* **2014**, *259*, 289.

(48) Mikhaylik, Y. V.; Akridge, J. R. *Journal of The Electrochemical Society* **2004**, *151*, A1969.

(49) Rauh, R.; Abraham, K.; Pearson, G.; Surprenant, J.; Brummer, S. *Journal of The Electrochemical Society* **1979**, *126*, 523.

(50) Chang, D.-R.; Lee, S.-H.; Kim, S.-W.; Kim, H.-T. *Journal of Power Sources* **2002**, *112*, 452.

(51) Wang, W.; Wang, Y.; Huang, Y.; Huang, C.; Yu, Z.; Zhang, H.; Wang, A.; Yuan, K. *Journal of Applied Electrochemistry* **2010**, *40*, 321.

(52) Kim, S.; Jung, Y.; Lim, H. S. *Electrochimica Acta* **2004**, *50*, 889.

(53) Zhang, S. S. *Journal of Power Sources* **2013**, *231*, 153.

(54) Gao, J.; Lowe, M. A.; Kiya, Y.; Abruña, H. c. D. *The Journal of Physical Chemistry C* **2011**, *115*, 25132.

(55) Aurbach, D. *Journal of Power Sources* **2000**, *89*, 206.

(56) Kim, S.; Jung, Y.; Park, S.-J. *Electrochimica Acta* **2007**, *52*, 2116.

(57) Barchasz, C.; Leprêtre, J.-C.; Patoux, S.; Alloin, F. *Electrochimica Acta* **2013**, *89*, 737.

(58) Mikhaylik, Y. V.; Kovalev, I.; Schock, R.; Kumaresan, K.; Xu, J.; Affinito, J. *ECS Transactions* **2010**, *25*, 23.

(59) Zhang, S. S. *Electrochimica Acta* **2012**, *70*, 344.

(60) Aurbach, D.; Pollak, E.; Elazari, R.; Salitra, G.; Kelley, C. S.; Affinito, J. *Journal of The Electrochemical Society* **2009**, *156*, A694.

(61) Suo, L.; Hu, Y.-S.; Li, H.; Armand, M.; Chen, L. *Nature Communications* **2013**, *4*, 1481.

(62) Cuisinier, M.; Cabelguen, P.-E.; Adams, B.; Garsuch, A.; Balasubramanian, M.; Nazar, L. *Energy & Environmental Science* **2014**, *7*, 2697.

(63) Wang, L.; Byon, H. R. *Journal of Power Sources* **2013**, *236*, 207.

(64) Adams, B. D.; Black, R.; Radtke, C.; Williams, Z.; Mehdi, B. L.; Browning, N. D.; Nazar, L. F. *ACS Nano* **2014**, *8*, 12483.

(65) McCloskey, B. D.; Valery, A.; Luntz, A. C.; Gowda, S. R.; Wallraff, G. M.; Garcia, J. M.; Mori, T.; Krupp, L. E. *The Journal of Physical Chemistry Letters* **2013**, *4*, 2989.

(66) Thotiyl, M. M. O.; Freunberger, S. A.; Peng, Z.; Chen, Y.; Liu, Z.; Bruce, P. G. *Nature Materials* **2013**, *12*, 1050.

(67) Hartmann, P.; Bender, C. L.; Vračar, M.; Dürr, A. K.; Garsuch, A.; Janek, J.; Adelhelm, P. *Nature Materials* **2013**, *12*, 228.

(68) McCloskey, B. D.; Garcia, J. M.; Luntz, A. C. *The Journal of Physical Chemistry Letters* **2014**, *5*, 1230.

(69) Li, Y.; Yadegari, H.; Li, X.; Banis, M. N.; Li, R.; Sun, X. *Chemical Communications* **2013**, *49*, 11731.

(70) Yadegari, H.; Li, Y.; Banis, M. N.; Li, X.; Wang, B.; Sun, Q.; Li, R.; Sham, T.-K.; Cui, X.; Sun, X. *Energy & Environmental Science* **2014**, *7*, 3747.

(71) Liu, W.; Sun, Q.; Yang, Y.; Xie, J.-Y.; Fu, Z.-W. *Chemical Communications* **2013**, *49*, 1951.

(72) Kang, S.; Mo, Y.; Ong, S. P.; Ceder, G. *Nano Letters* **2014**, *14*, 1016.

(73) McCloskey, B.; Bethune, D.; Shelby, R.; Mori, T.; Scheffler, R.; Speidel, A.; Sherwood, M.; Luntz, A. *The Journal of Physical Chemistry Letters* **2012**, *3*, 3043.

(74) Bender, C. L.; Hartmann, P.; Vračar, M.; Adelhelm, P.; Janek, J. *Advanced Energy Materials* **2014**, *4*.

(75) Oh, S. H.; Adams, B. D.; Lee, B.; Nazar, L. F. *Chemistry of Materials* **2015**, *27*, 2322.

(76) Meini, S.; Tsiouvaras, N.; Schwenke, K. U.; Piana, M.; Beyer, H.; Lange, L.; Gasteiger, H. A. *Physical Chemistry Chemical Physics* **2013**, *15*, 11478.

(77) Leskes, M.; Moore, A. J.; Goward, G. R.; Grey, C. P. *The Journal of Physical Chemistry C* **2013**, *117*, 26929.

(78) Ganapathy, S.; Adams, B. D.; Stenou, G.; Anastasaki, M. S.; Goubitz, K.; Miao, X.-F.; Nazar, L. F.; Wagemaker, M. *Journal of the American Chemical Society* **2014**, *136*, 16335.

(79) Schwenke, K. U.; Metzger, M.; Restle, T.; Piana, M.; Gasteiger, H. A. *Journal of The Electrochemical Society* **2015**, *162*, A573.

(80) McCloskey, B.; Speidel, A.; Scheffler, R.; Miller, D.; Viswanathan, V.; Hummelshøj, J.; Nørskov, J.; Luntz, A. *The Journal of Physical Chemistry Letters* **2012**, *3*, 997.

(81) Adams, B. D.; Black, R.; Williams, Z.; Fernandes, R.; Cuisinier, M.; Berg, E. J.; Novak, P.; Murphy, G. K.; Nazar, L. F. *Advanced Energy Materials* **2015**, *5*.

(82) Sharon, D.; Etacheri, V.; Garsuch, A.; Afri, M.; Frimer, A. A.; Aurbach, D. *The Journal of Physical Chemistry Letters* **2012**, *4*, 127.

(83) García, J. M.; Horn, H. W.; Rice, J. E. *The Journal of Physical Chemistry Letters* **2015**, *6*, 1795.

(84) Kwabi, D. G.; Batcho, T. P.; Amanchukwu, C. V.; Ortiz-Vitoriano, N.; Hammond, P.; Thompson, C. V.; Shao-Horn, Y. *The Journal of Physical Chemistry Letters* **2014**, *5*, 2850.

(85) Walker, W.; Giordani, V.; Uddin, J.; Bryantsev, V. S.; Chase, G. V.; Addison, D. *Journal of the American Chemical Society* **2013**, *135*, 2076.

(86) Das, S.; Højberg, J.; Knudsen, K. B.; Younesi, R.; Johansson, P.; Norby, P.; Vegge, T. *The Journal of Physical Chemistry C* **2015**, *119*, 18084.

(87) Kumar, N.; Radin, M. D.; Wood, B. C.; Ogitsu, T.; Siegel, D. J. *The Journal of Physical Chemistry C* **2015**, *119*, 9050.

(88) Bieker, G.; Winter, M.; Bieker, P. *Physical Chemistry Chemical Physics* **2015**, *17*, 8670.

(89) San Filippo Jr, J.; Chern, C.-I.; Valentine, J. S. *The Journal of Organic Chemistry* **1975**, *40*, 1678.

(90) Schwenke, K. U.; Meini, S.; Wu, X.; Gasteiger, H. A.; Piana, M. *Physical Chemistry Chemical Physics* **2013**, *15*, 11830.

(91) Xu, W.; Xu, K.; Viswanathan, V. V.; Towne, S. A.; Hardy, J. S.; Xiao, J.; Nie, Z.; Hu, D.; Wang, D.; Zhang, J.-G. *Journal of Power Sources* **2011**, *196*, 9631.

(92) Xu, K. *Chemical Reviews* **2004**, *104*, 4303.

(93) Balaish, M.; Kraytsberg, A.; Ein-Eli, Y. *Physical Chemistry Chemical Physics* **2014**, *16*, 2801.

(94) Lorenzola, T.; Lopez, B.; Giordano, M. *Journal of The Electrochemical Society* **1983**, *130*, 1359.

(95) Liang, C.; Wang, F.; Xu, Y.; Chen, J.; Liu, D.; Luo, Z. *New Journal of Chemistry* **2013**, *37*, 2568.

(96) Fulem, M.; Růžička, K.; Růžička, M. *Fluid Phase Equilibria* **2011**, *303*, 205.

(97) Xu, D.; Wang, Z.-l.; Xu, J.-j.; Zhang, L.-l.; Wang, L.-m.; Zhang, X.-b. *Chemical Communications* **2012**, *48*, 11674.

(98) Chen, Y.; Freunberger, S. A.; Peng, Z.; Bardé, F.; Bruce, P. G. *Journal of the American Chemical Society* **2012**, *134*, 7952.

(99) Bryantsev, V. S.; Giordani, V.; Walker, W.; Uddin, J.; Lee, I.; van Duin, A. C.; Chase, G. V.; Addison, D. *The Journal of Physical Chemistry C* **2013**, *117*, 11977.

(100) Geiculescu, O.; DesMarteau, D.; Creager, S.; Haik, O.; Hirshberg, D.; Shilina, Y.; Zinigrad, E.; Levi, M.; Aurbach, D.; Halalay, I. *Journal of Power Sources* **2016**, *307*, 519.

(101) Corey, E.; Barrette, E.-P.; Magriotis, P. A. *Tetrahedron Letters* **1985**, *26*, 5855.

(102) Itoh, O.; Iwakoshi, N.; Saitoh, T.; Katano, H.; Fujisawa, Y.; Hasegawa, Y.; Sugita, T.; Ichikawa, K. *Bulletin of the Chemical Society of Japan* **1982**, *55*, 177.

(103) Madsen, A. S.; Kristensen, H. M.; Lanz, G.; Olsen, C. A. *ChemMedChem* **2014**, *9*, 614.

(104) Cheon, S.-E.; Ko, K.-S.; Cho, J.-H.; Kim, S.-W.; Chin, E.-Y.; Kim, H.-T. *Journal of The Electrochemical Society* **2003**, *150*, A796.

(105) Scrosati, B.; Garche, J.; Tillmetz, W.; *Advances in Battery Technologies for Electric Vehicles* Elsevier Ltd.: Cambridge, UK: 2015.

(106) Rauh, R.; Shuker, F.; Marston, J.; Brummer, S. *Journal of Inorganic and Nuclear Chemistry* **1977**, *39*, 1761.

(107) Raiß, C.; Peppler, K.; Janek, J.; Adelhelm, P. *Carbon* **2014**, *79*, 245.

(108) Younesi, R.; Veith, G. M.; Johansson, P.; Edström, K.; Vegge, T. *Energy & Environmental Science* **2015**, *8*, 1905.

(109) Krossing, I.; Raabe, I. *Angewandte Chemie International Edition* **2004**, *43*, 2066.

(110) Kögel, J. F.; Linder, T.; Schröder, F. G.; Sundermeyer, J.; Goll, S. K.; Himmel, D.; Krossing, I.; Kütt, K.; Saame, J.; Leito, I. *Chemistry–A European Journal* **2015**, *21*, 5769.

(111) Krossing, I. *Chemistry–A European Journal* **2001**, *7*, 490.

(112) Tsujioka, S.; Nolan, B. G.; Takase, H.; Fauber, B. P.; Strauss, S. H. *Journal of The Electrochemical Society* **2004**, *151*, A1418.

(113) Parsons, R. *Handbook of electrochemical constants*; Academic Press, 1959.

(114) Xiong, S.; Xie, K.; Diao, Y.; Hong, X. *Journal of Power Sources* **2014**, *246*, 840.

(115) Cuisinier, M.; Hart, C.; Balasubramanian, M.; Garsuch, A.; Nazar, L. F. *Advanced Energy Materials* **2015**, *5*.

(116) Tasaki, K.; Goldberg, A.; Lian, J.-J.; Walker, M.; Timmons, A.; Harris, S. J. *Journal of The Electrochemical Society* **2009**, *156*, A1019.

Glossary

CV	Cyclic voltammogram
Diglyme	Diethyleneglycol dimethylether
DME	1,2-dimethoxyethane
DMDMB	2,3-dimethoxy-2,3-dimethyl butane
DMDMP	2,4-dimethoxy-2,4-dimethyl butane
DMTMP	2,4-dimethoxy-2,4-dimethyl pentane
DMT	N,N-dimethyl triflamide
DPT	N,N-dipropyl triflamide
ECC	Electrochemical-chemical
FTIR	Fourier transform infrared
GDL	Gas diffusion layer
Li-O_2	Lithium oxygen
Li-S	Lithium Sulphur
Na-O_2	Sodium oxygen
NMR	Nuclear magnetic resonance
OER	Oxygen evolution reaction
ORR	Oxygen reduction reaction
PC	Propylene carbonate
PTC	Phase transfer catalyst
TEGDME	Tetraethyleneglycol dimethyl ether
TMOA	Trimethyl orthoacetate
TMOB	Trimethyl orthobutyrate
TMOF	Trimethyl orthoformate

TMOP	Trimethyl orthopropionate
TMOV	Trimethyl orthovalerate